論文 / 著書情報
Article / Book Information

題目(和文)	熱帯域大都市ジャカルタの領域スケールから微気象スケールの気象観測的研究：季節変化、海風、CO2
Title(English)	Regional to Micrometeorological Observation in Tropical Megacity of Jakarta: Season, Sea Breeze, and CO2
著者(和文)	IDEWA GEDE Agung Junnaedhi
Author(English)	I Dewa Gede Junnaedhi
出典(和文)	学位:博士(工学), 学位授与機関:東京工業大学, 報告番号:甲第12569号, 授与年月日:2023年9月22日, 学位の種別:課程博士, 審査員:神田 学,木内 豪,中村 恭志,髙木 泰士,VARQUEZ ALVIN CHRIST,稲垣 厚至
Citation(English)	Degree:Doctor (Engineering), Conferring organization: Tokyo Institute of Technology, Report number:甲第12569号, Conferred date:2023/9/22, Degree Type:Course doctor, Examiner:,,,,,
学位種別(和文)	博士論文
Type(English)	Doctoral Thesis

Regional to Micrometeorological Observation in Tropical Megacity of Jakarta: Season, Sea Breeze, and CO_2

東京工業大学
Tokyo Institute of Technology

A DISSERTATION PRESENTED

BY

I DEWA GEDE AGUNG JUNNAEDHI

TO

THE DEPARTMENT OF TRANSDISCIPLINARY SCIENCE AND ENGINEERING

GLOBAL ENGINEERING FOR DEVELOPMENT, ENVIRONMENT, AND SOCIETY

IN PARTIAL FULFILMENT OF THE REQUIREMENTS

FOR THE DEGREE OF

DOCTOR OF ENGINEERING

TOKYO INSTITUTE OF TECHNOLOGY

TOKYO, JAPAN

SEPTEMBER 2023

ADVISOR

PROFESSOR MANABU KANDA (神田　学)

CO-ADVISOR

DR. ATSUSHI INAGAKI (稲垣　厚至)

INTERNAL COMMITTEES

PROFESSOR TSUYOSHI KINOUCHI (木内　豪)

DR. HIROSHI TAKAGI (高木　泰士)

DR. TAKASHI NAKAMURA (中村　恭志)

DR. ALVIN CHRISTOPHER GALANG VARQUEZ

Dedication

This works is dedicated to all curious people in the world who immersed themselves to reveal the state, dynamic and interaction of nature. This piece is just my two cent out of zillions that are required to understand the whole world.

Abstract

Regional to micrometeorological variation of atmospheric condition in Jakarta is analyzed using multi-year near-surface observations network. Emphasize is given to seasonal variation of sea breeze and CO_2 flux and concentration in urban area of Jakarta. It was found that the sea breeze in Jakarta started earlier, propagated more rapidly, and lasted for a shorter period during the rainy than dry season. Night-time cloud downwelling and variation of thermal properties across Jakarta are considered as the major factors in this seasonal discrepancy. The passage of sea breeze front in Jakarta will cause variance in east-west atmospheric boundary layer height, which may induce momentary increase in CO_2 concentration. In micrometeorological scale, sea and land breeze plays an important role in governing the CO_2 flux by modifying the source area, while CO_2 concentration heavily depends on boundary layer height variation. These results show strong inter-connection between various atmospheric scales in tropical megacity Jakarta.

抄録

複数年にわたる地表面近傍観測網を用いて、ジャカルタの大気環境について広域から微気象気候特性について解析した。ジャカルタの都市部における海風と CO_2 フラックス・濃度の季節変動について特に注目した。ジャカルタの海風は乾季よりも雨季の方が早く始まり、伝播速度が速く、持続時間が短いことが分かった。夜間の雲のダウンウェリングとジャカルタ全域の熱特性の変化が、この季節変化を生む主な要因と考えられる。ジャカルタにおける海風前線の通過は、東西の大気境界層の高さの変動を引き起こし、CO_2 濃度の瞬間的な上昇を引き起こす可能性がある。微気象スケールでは、海風と陸風の発生が CO_2 フラックスのソースエリアを大きく変化させ、CO_2 濃度が境界層の高さの変化に大きく依存することを示した。これらの結果は、熱帯の大都市ジャカルタにおける様々な大気スケール間の，強い相互関係を示している。

Acknowledgements

I would like to express my sincere gratitude to my supervisor Prof. Manabu Kanda for all his suggestions and continuous support in my brief learning period at this beloved institution. It has been a steep learning curve for me in this period of my life, but I always know who to look to at the end of the rope. I could not say enough gratitude to my second supervisor, Dr. Atsushi Inagaki, for giving me the opportunity to learn much more knowledge, especially in the world of atmospheric observation. Without his countless suggestions, help and support, I might not have finished this research work.

I would also like to thank my internal thesis committees: Prof. Tsuyoshi Kinouchi, Dr. Hiroshi Takagi, Dr. Takashi Nakamura, and Dr. Alvin Christopher Galang Varquez, for their constructive comments and suggestions for the improvement of my dissertation. I really appreciate their questions that come from a different perspective, which I found very insightful.

My study and research would not be accomplished without funding support from Beasiswa Unggulan Dosen Indonesia – Lembaga Pengelola Dana Pendidikan (BUDI - LPDP) Indonesia (The Indonesian Endowment Fund). For that I would like to express my deep gratitude.

Special thanks to Dr. Alvin Christopher Galang Varquez for his advice on research and non-research related things during my time at Tokyo Tech. My sincere gratitude also goes to Mr. Do Ngoc Khan for the help and assistance he gave me during my life as a student at Tokyo Tech. I also appreciated all the help I received from Mrs. Yuko Okamoto, especially that related to the administrative work.

My sincere thanks to my lab mates: Mr. Tasuku Watanabe, Mr. Alexandros Marios Makedonas, Mr. Hiroki Ryoga, and Mr. Harunari Soeda, for sharing the good, the best and the greatest learning period in the past couple of years. I also thank all members of Kanda Lab. and Alvin Lab.: Ms. Yuka Asai, Mr. Itthikorn Jittaveeroj (Korn), Mr. Chinchuthakun Worameth (Tan), Ms. Kirara Nomura, Mr. Emir Mendoza, Mr. Kosuke Akita, Ms. Shiho Ishigaki, Ms. Minori Fujimaki, Ms. Haruka Matsuta, Mr. Daichi Hirade, Mr. Mitsuna Sekiya, Mr. Jiang Congrong, Ms.

Jin Xiao, Ms. Liu Ying, Ms. Kaho Nakai, and Mr. Yoongsomporn Thanakrit (Bank), for many memorable experiences in the last year of my study.

My greatest gratitude to my family, my wife Made Santriyani and my two sons, Dewa Gede Hiro and Dewa Gede Tobi, for the love and support that they gave me to accomplish this work. Without them I would not have the strength and courage to finish this work. My gratitude also to my parents: Mr. I Dewa Gede Suta Dharma and Mrs. I Dewa Ayu Putu Seruni, my parents' in-law: Mr. I Wayan Subagia and Mrs. Ni Nengah Masni, and my sisters: I Dewa Ayu Sruti Andari and I Dewa Ayu Agung Trisna Lantari, for their support in my pursuit of knowledge. Last but not least, I would like to thank everyone that I could not mention in this page, for any help, assistance and support that I received to accomplish my study at Tokyo Institute of Technology. From the bottom of my heart, I would like to say, "Terima kasih banyak; Thank you so much; and どうもありがとうございました".

Table of Contents

List of Tables

List of Figures

List of Abbreviations

Abbreviation	Definition
ABL	Atmospheric boundary layer
ADC	Analog to digital conversion
AMS	American Meteorological Society
AWS	Automatic weather station
BLR	Boundary layer radar
BMKG	Badan Meteorologi Klimatologi dan Geofisika
BPS	Badan Pusat Statistik
CBN	Cibinong
CC-BY-3.0	Creative Commons Attribution 3.0
CC-BY-3.0-IGO	Creative Commons Attribution 3.0 International Governed Organization
CC-BY-NC-SA	Creative Commons Attribution Non-commercial Share-alike
CC-BY-SA	Creative Commons Attribution Share-alike
CGK	Cengkareng or code name for Soekarno-Hatta International Airport Jakarta
CO	Carbon monoxide
CO_2	Carbon dioxide
COVID-19	Corona virus disease 2019
Cu	Cumulus cloud
DKI Jakarta	Daerah Khusus Ibukota Jakarta
E	East
EC	Eddy covariance
ECMWF	European Centre for Medium-range Weather Forecast
ENE	East-northeast
ENSO	El Nino Southern Oscillation
ERA5	5^{th} generation ECMWF atmospheric reanalysis

ESE	East-southeast
FNL	Final analysis
GHG	Greenhouse gas
GPM	Global Precipitation Measurement
IMERG	Integrated Multi-satellite Retrievals for GPM
IPCC	Inter-governmental Panel on Climate Change
JCH	Temporary observation site at Jakarta City Hall
JRA-55	Japanese 55-year Reanalysis
KHB	Kelvin-Helmholtz billow
KKP	Observation site at Kementrian Kelautan dan Perikanan
LLH	Observation site at Laboratorium Lingkungan Hidup
LST	Land surface temperature
LT/LST	Local time/Local standard time
MAD	Median absolute deviation
MC	Maritime Continents
MERRA	Modern Era Retrospective analysis for Research and Applications
ML	Mixed layer
N	North
NE	Northeast
NNE	North-northeast
NNW	North-northwest
NW	Northwest
OBS	Observation
ODbL	OpenDatabase License
OSM	OpenStreet Map
PAR	Photo-synthetically active region
PM	Particulate Matter
QGIS	Quantum Geographic Information System
RHS	Right hand side
RL	Residual layer
RMS	Root mean square

S	South
SBC	Sea breeze circulation
SBD	Sea breeze day
SBF	Sea breeze front
SBG	Sea breeze gravity current
SBH	Sea breeze head
SBL	Stable boundary layer
SE	Southeast
SEA	Southeast Asia
SSE	South-southeast
SST	Sea surface temperature
SSW	South-southwest
STMKG	Sekolah Tinggi Meteorologi Klimatologi dan Geofisika
SW	Southwest
Sc	Stratocumulus cloud
TIBL	Thermal internal boundary layer
UHI	Urban heat island
UMEP	Urban Multi-scale Environmental Predictor
UN DESA	United Nation Department of Economic and Social Affairs
UTC	Universal Time Coordinated
UV	Ultraviolet
W	West
WHOI CDR	Woods Hole Oceanographic Institute Climate Data Record
WNW	West-northwest
WPL	Webb-Pearman-Leuning
WRF	Weather Research and Forecast
WSW	West-southwest
ppm	Part per million
tr1	Seasonal transition 1, from rainy to dry season
tr2	Seasonal transition 2, from dry to rainy season

List of Symbols

Symbol	Definition	Unit
$\lvert\cdots\rvert$	Absolute value of respective variable	same as variable's unit
$\overline{\cdots}$	Mean or average of respective variable	same as variable's unit
$\langle\cdots\rangle$	Median of respective variable	same as variable's unit
C_{CO_2}	Concentration of CO_2	ppm
F_{CO_2}	Flux of CO_2	mg m^{-2} s^{-1}
F_x	Flux of arbitrary mass scalar x	mg m^{-2} s^{-1}
H_{BL}	Boundary layer height	m or km
L_d	Downward longwave radiation	W m^{-2} s^{-1}
L_u	Upward longwave radiation	W m^{-2} s^{-1}
Q_F	Anthropogenic heat	W m^{-2} s^{-1}
Q_H	Latent heat flux	W m^{-2} s^{-1}
Q_H	Sensible heat flux	W m^{-2} s^{-1}
R_L	Net longwave radiation, equal to $L_d - L_u$	W m^{-2} s^{-1}
R_N	Net radiation, equal to $R_S + R_L$	W m^{-2} s^{-1}
R_S	Net shortwave radiation, equal to $S_d - S_u$	W m^{-2} s^{-1}
S_d	Downward shortwave radiation	W m^{-2} s^{-1}
S_u	Upward shortwave radiation	W m^{-2} s^{-1}
T_s	Sonic temperature	K or °C
V_{SBF}	Sea breeze propagation speed	m s^{-1}
V_d	Sea breeze gravity current densimetric speed	m s^{-1}
V_g	Ambient flow speed	m s^{-1}
m_c	Molar mass of CO_2, approximately to 44.01 g mol^{-1}	g mol^{-1}
m_d	Molar mass of dry air, approximately to 28.97 g mol^{-1}	g mol^{-1}
m_v	Molar mass of water vapor, approximately to 18.01 g mol^{-1}	g mol^{-1}
q_v	Specific humidity	kg kg^{-1}
s_c	Mixing ratio of CO_2	kg kg^{-1}
u_*	Friction velocity	m s^{-1}

z_0	Roughness length	m
z_d	Displacement height	m
z_m	Measurement height	m
θ_v	Virtual potential temperature	K or °C
λ_f	Frontal area index	unitless
λ_p	Planar area index	unitless
ρ_1	Density of lighter land-air mass	kg m^{-3}
ρ_2	Density of denser marine-air-mass	kg m^{-3}
ρ_a	Density of air, or otherwise stated as molar density	kg m^{-3} or mol m^{-3}
ρ_c	Molar density of CO_2	mol m^{-3}
ρ_d	Molar density of dry air	mol m^{-3}
ρ_v	Molar density of water vapor	mol m^{-3}
L	Obukhov length	m
P-corr	Pearson correlation	unitless
RH2	Relative humidity at 2-m height from the surface	%
T2	Air temperature at 2-m height from the surface	K or °C
U	Mean zonal wind speed	m s^{-1}
V	Mean meridional wind speed	m s^{-1}
W	Mean vertical wind speed	m s^{-1}
WS	Wind speed	m s^{-1}
WS10	Wind speed at 10-m height from the surface	m s^{-1}
h	Sea breeze gravity current or depth	m
ΔQ_A	Net storage addition or subtraction by advection	W m^{-2} s^{-1}
ΔQ_S	Net heat storage	W m^{-2} s^{-1}
$\dots'$	Fluctuation part of respective variable	same as variable's unit
RH	Relative humidity	%
T	Absolute air temperature	K or °C
g	Gravity acceleration, approximately 9.8 m s^{-2}	m s^{-2}
k	Internal Froude number of gravity current	unitless
u, v, w	wind component along X, Y, and Z axis	m s^{-1}
z	Effective height ($z_m - z_d$) or generic height	m
ζ	Surface layer stability parameter, equal to z/L	unitless
θ	Potential temperature	K or °C
κ	von Karman constant, approximately 0.4	unitless

λ	Latent heat of evaporation	J kg^{-1}
ΔT	Temperature difference between two air masses	K

Chapter 1 Introduction

Atmospheric dynamic is a superposition of various scale phenomena (Orlanski, 1975), which interact and influenced by each other and creating a non-linear conditions, that may or may not repeat their past history exactly (Lorenz, 1963). Larger scale meteorological phenomena tend to drive smaller scale phenomena through energy transfer and feature effects. On the other hand, smaller scale phenomena may trigger larger phenomena, or through aggregation become the cause of such large phenomena. Global warming is a good example of this process. While it was well known that global warming might be the cause of increasingly extreme weather events, the root of global warming itself is the excessive release of greenhouse gases (GHG)(Hansen *et al.*, 1998), such as CO_2 and methane, which happen in localized area. These gases are then transferred by small scale process, that is the turbulence, into the upper region of atmosphere, then distributed and aggregated by the larger circulation. The global aggregation effect of these gases will create a barrier to the outgoing longwave radiation from surface, hence increasing global surface temperature which is known as global warming. To mitigate the effect of global warming, as well as other severe meteorological events, it is important to observe various states of the atmosphere, from the biggest scale, down to the smallest scale possible. This will enable us to keep track of the atmospheric condition and study its dynamic, hence predict or project its future state.

In the lowest part of the atmosphere, in the so called atmospheric boundary layer (ABL) where surface condition highly influence the atmospheric flows (Stull, 1988), the interaction between regional sizes (macro-scales) and micro-scale meteorological phenomena is mostly prominent. In fact, day-to-day weather which we perceive is mostly controlled by this regional-to-micro-scale interaction inside the ABL (Stull, 1988; Holton, 2004). Hence, any change in the surface conditions will modify this interaction, and eventually change the daily weather conditions that once we knew. Rapid change in surface conditions mostly occurs in cities or urban areas. Big cities and especially megacities, are the most rapidly changed surface area in the world (Liu *et al.*, 2014), as well as the geographical pinnacles of energy consumption and the associated GHG emissions (Grubler *et al.*, 2012; Seto *et al.*, 2014). Urbanization, where more people will live in the cities or urban areas (United Nations, 2018a), will propel city's

surface change and energy consumption (Grimm *et al.*, 2008). Hence, the atmospheric condition in such areas is expected to evolve faster than the rest of the world, not only affecting its inhabitants, but also contributing to global climatic change. In those cities, as the local ABL will immediately adapt to the surface changes, the effect of urbanization might become more dominant than the effect of global warming (Khanh *et al.*, 2023). Again, this will stress the importance of monitoring, reporting, and analyzing the atmospheric condition of these urban areas to understand the complex interaction between various scales of atmospheric phenomena. The results of these activities will support us in formulating mitigation and or adaptation strategies to reduce the bad effects of such rapid surface change.

1.1 Motivation

In the near future, tropical cities are predicted to lead the world's urban growth. Figure 1.1 highlight the population and growth rate of Asia and African cities, based on World Urbanization Prospect (United Nations, 2018a). It is also predicted that many of these cities will grow into megacities, metropolitan urban areas with more than 10 million population. With increased population, these cities, especially the megacities, will become the major producers of GHGs, other pollutants and anthropogenic heat. That being said, these cities will make more contribution to the global warming (Roth, 2007; United Nations, 2018a, 2018b). At the same time, these cities might become more severely impacted by global warming. In addition to that, the effect of urbanization itself might also amplify the global warming (Khanh *et al.*, 2023). In the past few decades, total warming in the tropical cities could reach an average of 1 °C. Among them, tropical-monsoonal cities experienced the highest among other tropical cities (Marcotullio *et al.*, 2021).

The ability to cope with the severe consequences of global warming and urbanization effect will heavily depend on the understanding of physical and dynamical atmospheric processes in these respective cities. Mitigation against adverse atmospheric phenomena that comes with urbanization is usually based on studies of the urban atmospheric condition. Many of the mitigation policies were based on atmospheric models which were developed based on observational studies. Understanding the physical and dynamical processes of atmosphere and its variations in city scales will be beneficial for validating and improving these models. Combined with improved model skill, knowledge of full scale atmospheric condition, from regional to micro-scale, will provide policymakers with an effective mitigation strategy, as well as important information for communities and stakeholders towards addressing environmental

problems in changing urban environments (Duren and Miller, 2012; IPCC, 2014). Special attention should be given to megacities as they emit more GHGs, pollutants, and heat, thus producing a more significant impact to the environment. Since the megacities tends to change more rapidly, it is necessary to prioritizing the observation to establish measurement baseline and provide a robust verification for future change (Gurjar and Lelieveld, 2005; Duren and Miller, 2012).

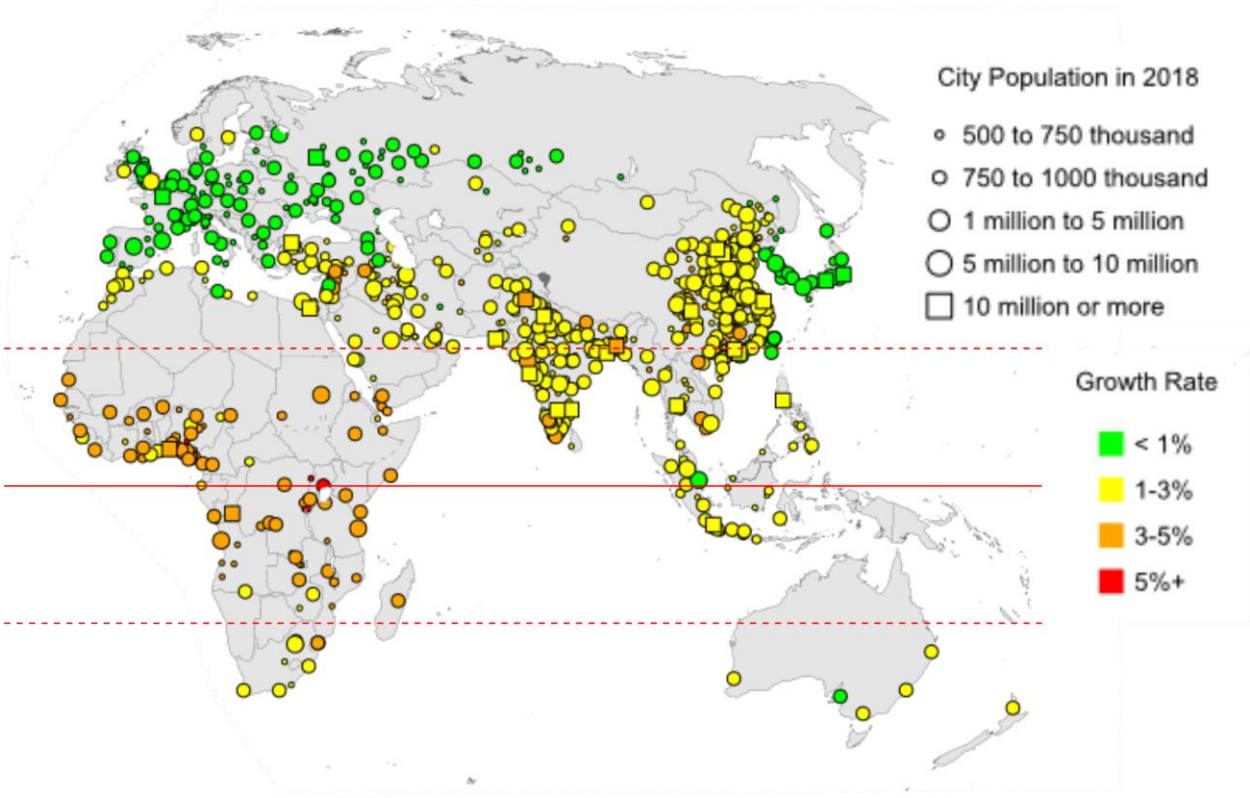

Figure 1.1 City population and growth rate map based on UN DESA World Urbanization Prospect (United Nations, 2018a) for Europa, Asia, Africa and Australia. The solid-red line shows the equator, while dashed-red lines denote the boundary of tropical region. Modified from image published by UN DESA (2018) which is licensed under Creative Commons CC-BY-3.0-IGO license.

Unfortunately, compared to many cities and megacities in the mid-latitude, datasets and studies on urban atmospheric condition in the tropical cities or megacities are still very limited. Many atmospheric models have not been checked against tropical datasets, and the empirical sub-models and constants are biased towards conditions of mid-latitude where dataset are abundant. Hence, only rudimentary understanding of physical processes in the tropical atmosphere is available (Gurjar and Lelieveld, 2005; Roth, 2007; Roth *et al.*, 2017). As an example of the case, in around 70 studies on the urban carbon dioxide (CO_2) exchange studies, only less than 5 studies were conducted in tropical areas (Velasco and Roth, 2010; Grimmond

and Christen, 2012; Matthews and Schume, 2022). Even for historical climate dataset, tropical areas, especially in Southeast Asia (SEA), are still majorly under-represented (Page *et al.*, 2004). Such under-representation will compromise our ability to monitor climate variability and change, especially regarding climate extremes.

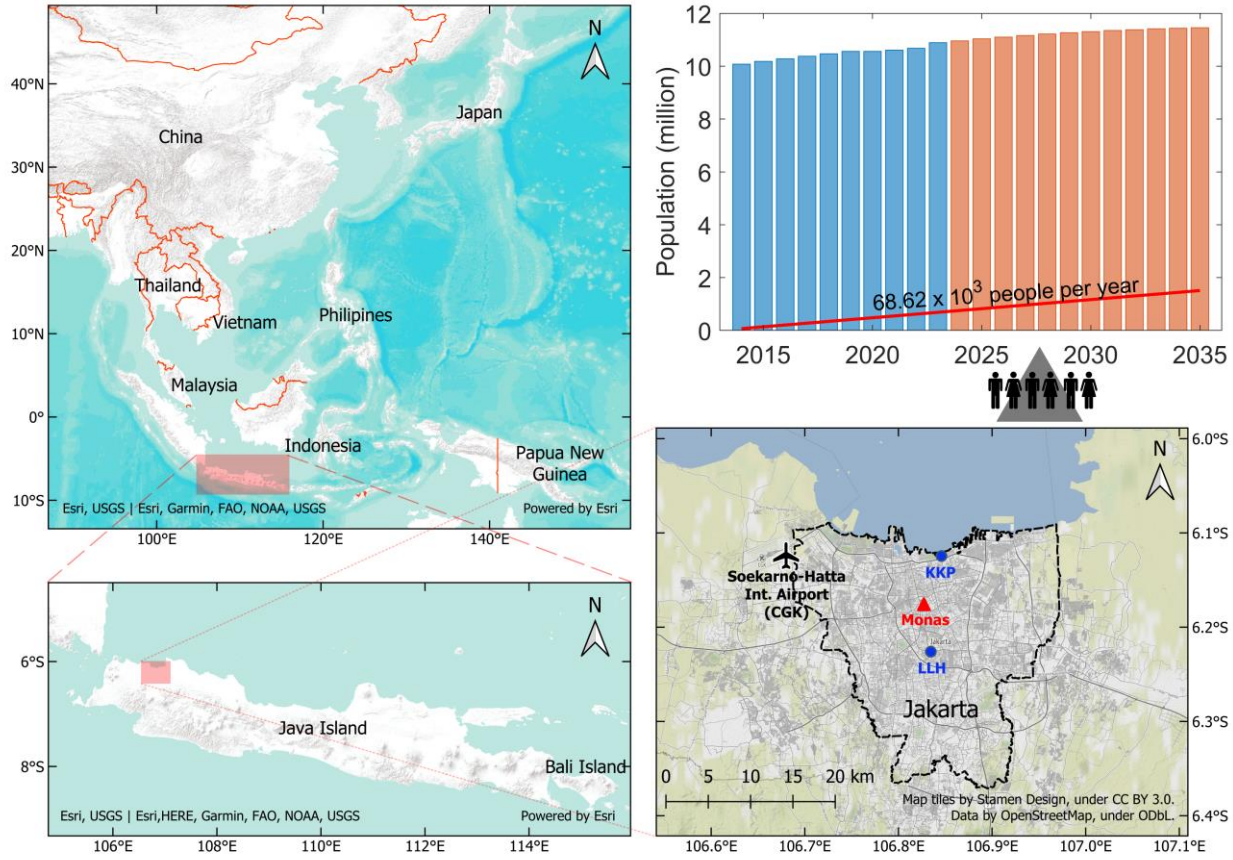

Figure 1.2 Map of Southeast Asia (SEA) extended to Papua New Guinea, Japan, and China (upper-left); map of Java Island (bottom-left); Map of Jakarta and surrounding sub-urban area (bottom-right); and bar plot of annual population in Jakarta based on data from BPS Provinsi DKI Jakarta (2023) (top-right). The red triangle on map of Jakarta shows the landmark of Jakarta, the National Monument (Monas), while blue circles denote the location of observation sites which dataset used in this study. Blue bar on population plot indicates existing population, while red bar indicates the population projection.

Unlike other tropical areas, tropical areas in SEA possess unique traits that cannot be found in another equatorial region (see Figure 1.2 upper-left). Rather than fully covered by sea or continent, the tropical area of SEA is consisting of thousands of island separated by relatively narrow seas, hence it was named as Maritime Continent (MC) by Ramage (1968). This uniqueness is causing the area to become geographical hot-spots for large scale convective activities that is thought to drive global climate (Ramage, 1968; Neale and Slingo, 2003; Yamanaka *et al.*, 2018). These convective activities were driven by diurnal circulation,

particularly sea breeze circulation, thus making this circulation as the most important variability over MC (Qian, 2008; Wu *et al.*, 2009; Qian *et al.*, 2012; Yamanaka, 2016; Katsumata *et al.*, 2018; Yamanaka *et al.*, 2018; Ruppert and Zhang, 2019). Thus, sea breeze circulation in tropical MC possesses a strong teleconnection to global climate and plays important role in distribution of heat, moisture, and other scalars such as CO_2, particulate matters (PM) and other air pollutants, through global atmospheric circulation.

Jakarta is one of the megacities inside the MC which served as capital city of Indonesia. Jakarta is situated on the northern coast of Java, one of the most densely populated island in the world (Figure 1.2 bottom-left). Like many other coastal cities in western MC, Jakarta's weather and climate is mainly driven by the Asia-Australian Monsoon system and diurnal circulation of sea and land breeze (Hamada *et al.*, 2002; Yamanaka, 2016; Katsumata *et al.*, 2018). Like many other tropical cities, it undergoes rapid urbanization; and as a monsoonal tropical city it potentially in higher risk for climate related hazard (Marcotullio *et al.*, 2021). Currently, Jakarta is home to more than 10 million people (BPS Provinsi DKI Jakarta, 2023). This number might be an underestimation as many of its citizens were not registered. In addition to that, there are several million more people that were commuting from the neighboring sub-urban area into the city area to do work or go to school. With the growth rate of 68 thousand people per year (see Figure 1.2 upper-right), the number of populations in Jakarta is rapidly increasing. Rapid urbanization in recent years has changed the city landscapes and energy balance which may result in adverse effects to its inhabitants. From bottom-up perspective, this will also increase Jakarta contribution to global climate change, which in-turn amplifying the already adverse effects of urbanization.

In recent years, Jakarta have seen more frequent severe-high-intensity rain during rainy season (Trilaksono *et al.*, 2011; Yulihastin *et al.*, 2020; Siswanto *et al.*, 2022). On the other hand, during dry season bad air quality is increasingly occurs (Dinas Lingkungan Hidup DKI Jakarta, 2017; Wati and Nasution, 2018; Lestari *et al.*, 2022). It was also observed that intensity of morning rainfall in rainy season is increased, while in other seasons late afternoon rainfall peak is delayed (Siswanto *et al.*, 2016). These suggest a hypothesis that these events might be related to seasonal variation of diurnal circulation (sea/land breeze) and variation in turbulence transport of energy and other scalars. These variations might also further be modified by urbanization, thus suggesting the necessity to conduct urban atmospheric study in the scale smaller than diurnal timescale. As illustrated in Figure 1.3, various-scale phenomena govern the weather in Jakarta, with monsoon playing important role as background conditions, while under the ABL diurnal circulation and turbulent transfer dominating the atmospheric condition.

However, there are only limited studies on urban atmospheric dynamics conducted in Jakarta with scale smaller than diurnal timescale. Limited high-temporal-resolution data availability hinders researchers from studying such smaller scales variability. Furthermore, the urban micro-meteorological phenomena might be an uncharted territory in meteorological studies in Jakarta. Study on turbulent characteristic or flux exchange, such as heat and CO_2 exchange, has never been reported.

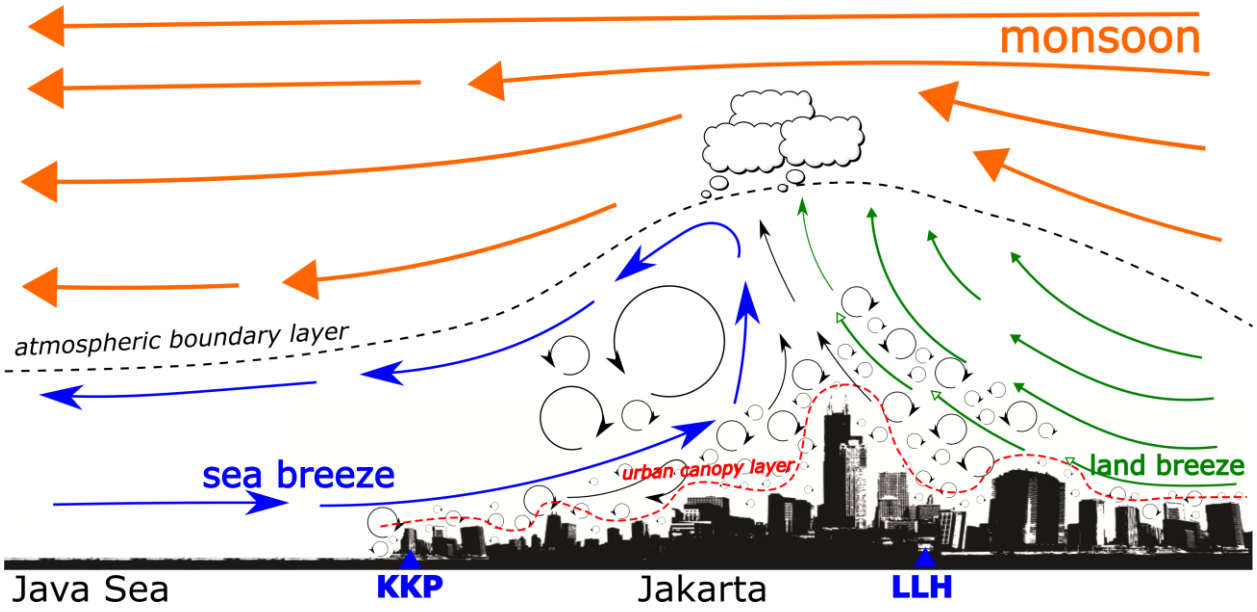

Figure 1.3 Illustration of various scale atmospheric phenomena that govern the meteorological condition in Jakarta. The blue triangle symbols with KKP and LLH code mark the relative position of observation sites which dataset is used in this study. See text in Chapter 3 for the abbreviations. The buildings and symbols only serve as illustrative purpose and do not represent the actual buildings, position, or distance. For actual locations, please refer to the observation map in Chapter 3.

Within the framework of global mitigation and local adaptation to climate change, an intensive, high-temporal-resolution urban atmospheric observation campaign has been conducted in Jakarta since 2017 (Junnaedhi *et al.*, 2018). The locations of the observation are indicated on Figure 1.2 bottom-right. By utilizing fast-response sensors, such as ultrasonic anemometer and gas analyzer, this observation campaign presents an opportunity to conduct investigation into diurnal scale variation and micro-scale turbulent flux exchange, especially CO_2 flux exchange, in Jakarta. The multi-year time span of the observation period also provides adequate data to conduct analysis on seasonal changes. Thus, this study is motivated by, and implemented on this observational campaign with the main goal to better understand the urban atmosphere condition in tropical megacity Jakarta.

This study might not be the first study that covers sea breeze in Jakarta, but it's definitely one that heavily based on intensive observation campaign. In terms of urban micrometeorological studies, this study might be the first attempt to study the urban CO_2 flux exchange in Jakarta. Thus, it is hoped that this study will become measurement baseline for micro-scale atmospheric variation in Jakarta and serve as invaluable reference for future urban micrometeorological studies in Jakarta or generally in Indonesia.

1.2 Objectives and importance of the study

The main objective of this study is to understand various-scale variations of atmospheric conditions in Jakarta based on mostly, but not limited to, atmospheric measurement data that has been acquired through the intensive, multi-year observation campaign. This main objective is further separated into 3 specific objectives which focused on the meso-scale diurnal circulation of sea breeze and micro-scale exchange of CO_2 in Jakarta.

The first specific objective of this study is to investigate Jakarta's sea breeze variation in conjunction with seasonal transition and analyze possible mechanism behind it. Previous researches have confirm the existence and significance of sea breeze over Jakarta (Hadi *et al.*, 2000, 2002; Araki *et al.*, 2006; Ferdiansyah *et al.*, 2020), however none of them were addressing its seasonal variation. The unique configuration of two inline observation sites as illustrated in Figure 1.1 allows us to estimate the propagation speed of sea breeze over the city. This objective also aimed to confirm whether the city's existence has significant impact on sea breeze variation. Previous research indicated that urban heat island (UHI) circulation over Jakarta may slow down sea breeze advancement inland (Ferdiansyah *et al.*, 2020). However, the usage of satellite derived cloud lines to identify sea breeze and limited number of sea breeze day samples might not be adequate to analyze variation in sea breeze propagation. The current investigations use a direct observation approach over a longer period, hence a larger number of sea breeze day samples. Thus, it may be more viable to analyze variation in sea breeze propagation. The result of these investigations could be used as foundation to study the connection between sea breeze and a late afternoon rainfall peak or bad air quality as discussed previously. In the future projection of Jakarta's urban climate, sea breeze might be significantly altered (Darmanto *et al.*, 2019), hence having baseline of current seasonal variation of sea breeze will be valuable as reference to isolate the effect of climate change and urbanization.

The second specific objective is to gain more complete knowledge on sea breeze structure in Jakarta in relation to its geomorphological settings, which could not be covered by

limited surface observations. For this purpose, an atmospheric model will be employed to simulate typical sea breeze conditions in Jakarta. The observation data will serve as validation to the model simulation. Since the sea breeze also depends on topographic and geomorphologic features of the coast, it is important to get insight into how these localized features affect the sea breeze in Jakarta. Furthermore, sea breeze propagation could modify the boundary layer (Hadi *et al.*, 2000; Miller *et al.*, 2003), hence it may affect the turbulent transport over the city during its passage. Thus, knowledge of this modification might be important for analyzing turbulent transport and pollution concentration.

The third specific objective of this research is to analyze the micrometeorological variation of CO_2 flux and concentration in the urban area of Jakarta and assess the influence of meso-scale variability such as sea breeze in CO_2 variation. Since the report on urban CO_2 studies for tropical megacities is very limited, it is expected that this analysis will become a contribution to global urban CO_2 studies as a representative of tropical megacities. As not much is known about atmospheric chemistry in the tropics, where much of the world population growth occurs, the study of atmospheric CO_2 flux from tropical megacities like Jakarta will have special significance in the studies of global CO_2 exchange which drive climate change (Gurjar and Lelieveld, 2005; Duren and Miller, 2012). Furthermore, this micrometeorological study might be the first report on CO_2 exchange in Jakarta, thus could potentially become foundation for subsequent micrometeorological research in Jakarta.

1.3 Scopes of the study

This dissertation with the title "Regional to Micrometeorological Observation in Tropical Megacity of Jakarta: Season, Sea Breeze, and CO_2" comprise six (6) chapters. The chapter title and a brief description of each chapter will be given in the following text.

Chapter 1: Introduction. This first chapter introduces the facts, issues and opportunities that become the background and motivation for conducting this study. The objectives of this study, as well as the importance of this study, were presented in this chapter. Lastly, this chapter also described the scope of the dissertation report.

Chapter 2: Theoretical Background. This chapter presents various knowledge on atmospheric or meteorological studies which serves as foundation for the analyses conducted in the next chapters. This chapter covers the related topics on atmospheric structure, meteorological phenomena scales, the atmospheric boundary layer, sea breeze and its interaction with urban areas, and CO_2 flux exchange in urban areas. The theoretical background

presented in this chapter is complementary to the specific subjects covered in the following chapters.

Chapter 3: Chapter 3 Seasonal Variation of Sea Breeze in Jakarta. The third chapter presents investigation results on seasonal variation of sea breeze using multi-year data from 2-point surface observation in Jakarta. The first part of this chapter describes the observation sites, data acquisition and processing, and the method to define sea breeze passage timing. In the subsequent part, the definition of seasonal transition, the seasonal variation of sea breeze, and impact of the Jakarta city existence is discussed. The chapter ends with a summary and conclusion.

Chapter 4: Structure of Boundary Layer during Sea Breeze. This chapter mainly discusses modification of boundary layer by sea breeze propagation based on numerical model simulation using Weather Research and Forecasting (WRF) model. The first part describes the sea breeze cases that are simulated, followed by model configuration, and model initialization. Next part discusses the validation of model results using observation conducted in Jakarta. The structure of boundary layer during sea breeze event is discussed in the following part, along with its implication to CO_2 concentration. This chapter is closed by a concluding remark.

Chapter 5: Diurnal Variation of CO_2 in Urban Jakarta. The fifth chapter presents the results of multi-year CO_2 observation in urban core area of Jakarta. This chapter includes the observation settings, data processing, results presentation, and discussion. General diurnal pattern of CO_2 flux and concentration is mainly discussed, along with its long-term variation. Effect of large-scale social restrictions during COVID-19 pandemic on $_{CO2}$ condition in Jakarta also discussed. General results from this chapter are summarized in the last part of this chapter.

Chapter 6: Concluding Remark. This chapter combined and summarized all study results from previous chapter and highlighting the research findings of this study. This chapter is closed with future research directions that will be taken as the continuation of this study.

This specific study only covers parts of the main objective that was stated in the previous part. As described in the scope of the last chapter, there are future research directions that will be pursued as the continuation of this study. That being said, the scope that covered by this study is expected to become the foundation of those future studies.

1.4 Summary

Many cities in the tropical-monsoonal areas undergo rapid urbanization which changed their landscapes radically. Several of them will also be developed into megacities. In the near

future, many of these cities will become major contributors to GHGs, pollutant and anthropogenic heat, which drives global climate change. At the same time, these cities will be more severely impacted by global climate change. The ability to cope with global climate change and urbanization effects will heavily depend on understanding of the physical and dynamical atmospheric processes in the city, which will be invaluable for the formulation of mitigation strategies and policies. However, in many of these cities, dataset and urban atmospheric studies are still very limited and sometimes only cover macro-scales processes.

Jakarta is the prime example of a tropical-monsoonal megacity that undergoes rapid urbanization, thus potentially contribute to-, and at the same time, severely affected by-, the climate change. Recent evidence suggests that urbanization may have affected the main atmospheric circulation in Jakarta, that is the sea breeze. Urbanization in Jakarta may also contribute to higher release of pollutants and GHGs, such as CO_2, resulting in air quality problems. However, atmospheric studies in Jakarta were still largely focused on monsoon or larger scale variability, with less or no study focusing on sea breeze variation and smaller scale processes like turbulent transport.

This study is an attempt to extend knowledge on urban atmospheric variabilities in Jakarta with emphasis on sea breeze variation and structure, and CO_2 flux exchange. The study is mainly based on multi-year surface observation in Jakarta, which utilizes a combination of fast-response and slow-response sensors. The study also employs high-resolution meso-scale modeling to complement the observation. While the grand aim is to better understand urban atmospheric condition in Jakarta, the objectives of this study are limited to three (3) objectives which are, 1) investigate the sea breeze seasonal variation and impact of the city to the variation; 2) describe the typical structure of sea breeze in Jakarta; and 3) analyze the diurnal pattern of CO_2 flux and concentration in Jakarta and the possible influence of the diurnal sea/land breeze circulation. The three objectives will be reported in the subsequent separated chapters, alongside introduction, background theory, and a summary in the last chapter. This study is hoped to become a base for subsequent urban atmospheric studies in Jakarta, as well as a contribution that represent tropical megacities to the global urban climate studies.

Chapter 2 Theoretical Background

Atmosphere is the air layer covering the Earth. Compared to the Earth's radius, which is approximately 6,371 km, the atmosphere is considered very thin, only a few hundred kilometers. Based on its thermal profile, the atmosphere can be divided into four layers, which are troposphere, stratosphere, mesosphere, and thermosphere (Ahrens, 2001; Stull, 2020). The interface between these layers is named tropopause, stratopause, and mesopause, respectively. The profile of density, pressure, speed of sound, and temperature for each layer can be seen in Figure 2.1. The thickness of the atmosphere (edge of thermosphere) is roughly between 120 to 500 km. Above the thermosphere, called the exosphere, air molecules were still existing, although very limited and easily escaped into outer space.

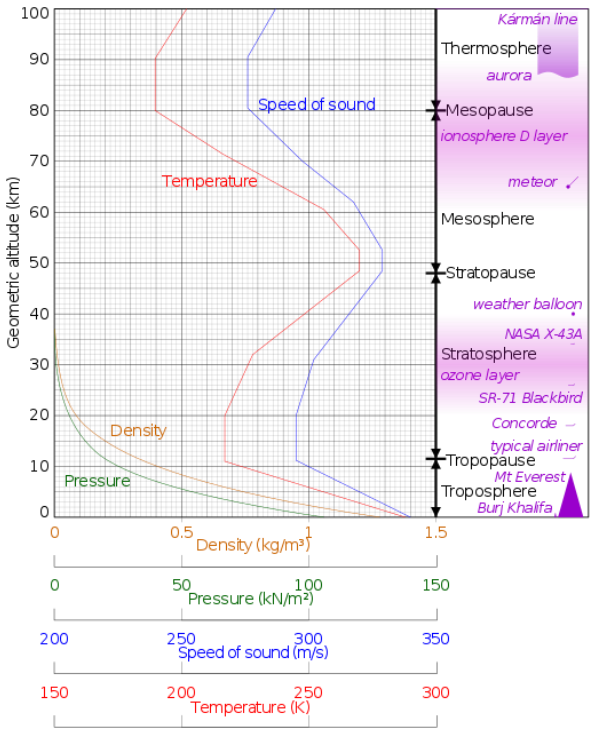

Figure 2.1 Vertical profiles of atmospheric density, pressure, speed of sound and temperature based on 1962 U.S. Standard Atmosphere (left), and atmospheric layers based on temperature profile (right). Image was retrieved from Wikipedia (2023) which is shared under Creative Commons CC-BY-SA 3.0 license.

From a human perspective, the most important layer of atmosphere is the lowest layer, the troposphere, where most of weather and climate processes take place. In this layer, pressure, density, speed of sound and temperature decrease rapidly with altitude (Figure 2.1). However, more than 90% of the air molecules were contained in the troposphere, even though it was only around 12 km in height (Ahrens, 2001; Stull, 2020). Above 50% of the air molecules are confined below 5.5 km (at pressure level around 500 hPa); way lower than the highest peak on Earth, Mount Everest. The troposphere receives heat from the surface; hence its temperature decreases with height. However, decrease in pressure with height also reduce air temperature adiabatically, thus further decrease air temperature with height. This profile of temperature decrease in troposphere is also known as lapse rate, with the standard atmosphere value around 0.65 ℃ per 100 m. In the troposphere, various atmospheric or meteorological phenomena occur, and it also comes in various spatial and time scales. The superposition and interaction of these phenomena defines the weather, hence the climate which is the average values of weather in a longer period.

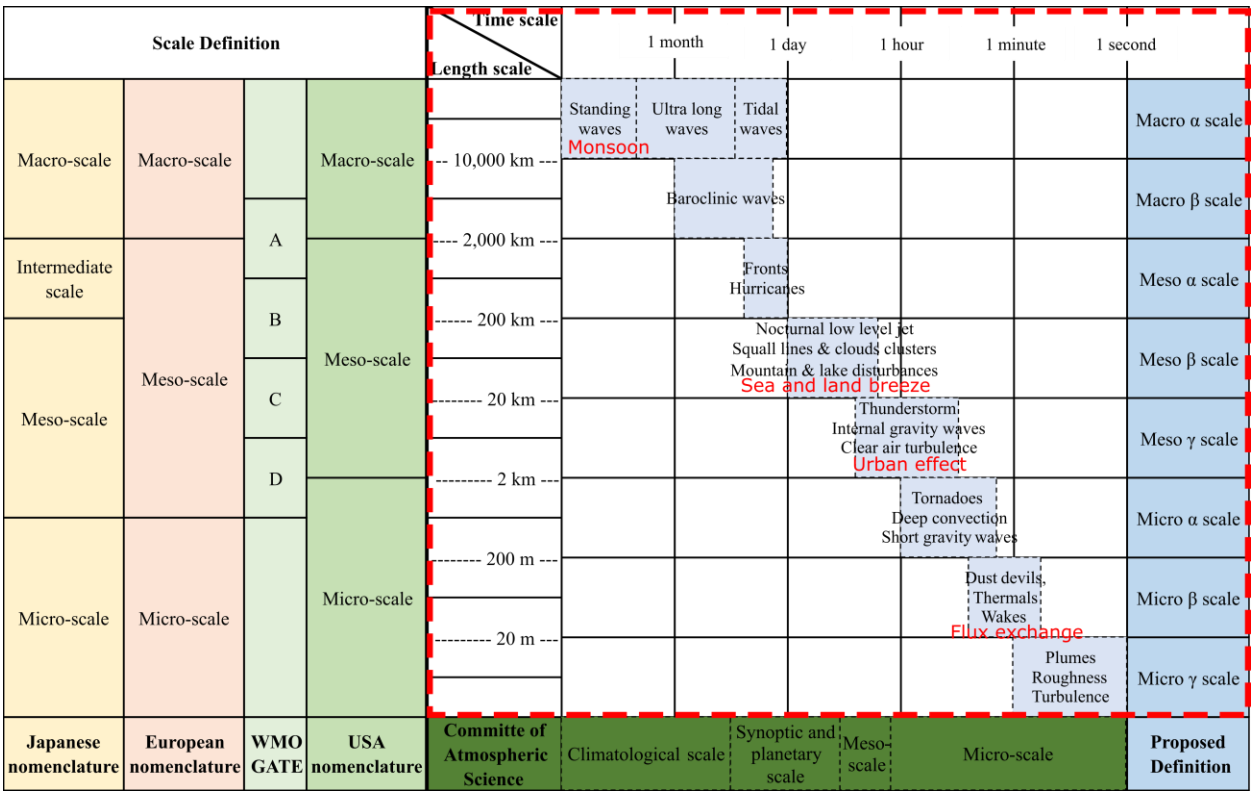

Figure 2.2 Spatial and time scales of atmospheric phenomena as proposed by Orlanski, (1975) in red-dashed box, in comparison with scales from various institutions. Image was reproduced and modified from Orlanski (1975) which available through the 'fair use' policy of © copyright AMS under U.S. Copyright Act (17 U.S. Code § 107).

To better understand the atmospheric physic and dynamic, researchers usually focus on certain scales of atmospheric movement and screened-out the other scales, or completely neglect it if it's much smaller than the scale of interest (Holton, 2004). In meteorology, scale analysis is important to isolate certain phenomena to study it in more detail, or to simplify the governing equations of atmospheric models which tailored to predict certain scale of atmospheric conditions. Before 1975, many institutions around the world define the meteorological scale in bulk, from micro-, meso-, to macro-scale, based on mostly spatial scale of the phenomena. However, due to lack of adequate observational data, many meteorological phenomena whose spatial and temporal scales are intermediate between those categories are still undefined. Due to surge of interest in the urban environment and in severe storm weather condition, Orlanski (1975) proposed more detail spatio-temporal scales to cover more wide range of meteorological phenomena (Figure 2.2). Large and long-time variations such as seasonal change and monsoon falls to macro α scale, while diurnal circulation such as sea and land breeze is considered as meso β scale. Smaller size phenomena, but span half-day, such as urban effects or UHI, is still part of meso-scale, precisely meso γ scale. However, anything smaller and shorter in period than that will fall under micro-scale categories, which includes tornadoes and deep convection (micro α scale), thermals and wakes (micro β scale), up to roughness effect and turbulence (micro γ scale). While Orlanski's definition is widely accepted and adapted, many meteorologists still use several scale terms, such as synoptic or regional scale which is used to collectively define the macro-scale and larger-longer scales phenomena like monsoon, ENSO, global cell circulations and other planetary waves.

In vertical sense, each scale also has an upper limit. Most macro-scales and meso α scale phenomena could span in the entire troposphere, some even reach the stratosphere. For example, the monsoon circulation; its low level flow could reach 10 to 14 km, while its return flows fills up the rest of the troposphere (Trenberth *et al.*, 2000; Kottayil *et al.*, 2020). However, meso β scales or smaller phenomena usually contains inside the lowest part of troposphere, in the so-called atmospheric boundary layer (ABL). In fact, most of weather conditions were triggered by condition in the ABL, where heat, moisture and scalars from the surface is mixed and transferred upward by turbulence, thus controlling the state of lower troposphere (Stull, 1988, 2020). The ABL and atmospheric phenomena in the ABL will be discussed briefly in the next sub-section.

2.1 The atmospheric boundary layer and its atmospheric phenomena

The Earth's surface is the bottom boundary of the atmospheric flows. As with any flows interfacing with a surface, it will create two unequally flow region; the thin boundary layer close to the surface and the undisturbed outer layer (Schlichting and Gersten, 2016). These two flow regions divide the troposphere into the atmospheric boundary layer (ABL) at the bottom, and the free atmosphere (FA) for the rest of troposphere (Figure 2.3). The ABL is the lowest part of the troposphere that is directly influenced by earth's surface conditions, and actively responds to surface forcings with timescale of about an hour or less (Stull, 1988). The FA is the layer where inertial force of macro-scale phenomena dominates. Even so, the activities of the ABL below it could produce clouds in this layer such as cumulus (Cu) or stratocumulus (Sc) cloud. The border between ABL and FA is characterized by temperature inversion which effectively blocks any transport from ABL into FA, hence called capping inversion.

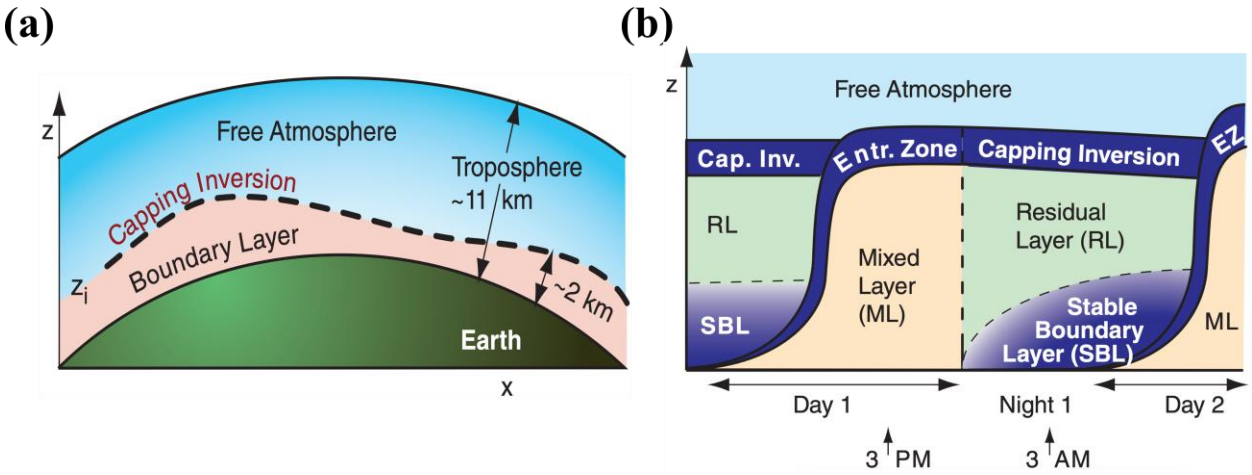

Figure 2.3 The location of atmospheric boundary layer (ABL) relative to troposphere (a) and day-to-day evolution of over land ABL during fair weather condition. Color shades are used to differentiate the ABL sub-layers which is associated with its non-local stability condition: tan for unstable, green for neutral, and dark blue for stable condition. Images were taken from Stull (2020) which is shared under a CC-BY-NC-SA 4.0 license.

The turbulent transport and mixing process inside ABL will modify the height of ABL diurnally, between 100 m to 3000 m (Stull, 1988, 2020; Garratt, 1994). The surface forcings, which include frictional drag, heat transfer, and evapotranspiration, will modify the structure of the ABL. Diurnal evolution of ABL is shown in Figure 2.3 b (after Stull, 2020). In the daytime, heat transfer

from surface which receive energy from the sun will create non-local unstable layer and turbulent transfer will effectively mix the air, creating the mixed layer (ML). During daytime, the capping inversion layer could also entrain dry air from FA into the ABL hence become the entrain zone. The height of ABL in daytime could reach between 1000 to 3000 m. Once the sun's energy is no longer available during nighttime, the surface will gradually draw heat from the atmosphere, collapsing the ML and creating stable layers of air, thus the boundary layer is confined inside the stable boundary layer (SBL). The remnant of ML above SBL which still has the residue of turbulent air is called residual layer (RL). The height of ABL during nighttime could be reduced to only 100 m or less, depending on the surface temperature. The vertical distribution of scalars emanating from the surface, such as heat, moisture, GHGs, pollutant and any other gas traces, are effectively regulated by the ABL (Garratt, 1994; Seibert *et al.*, 2000; Miao *et al.*, 2019). On the other hand, since the ABL height is influenced by the surface condition, any change in the surface will be reflected into the ABL, hence re-arrange the vertical distribution of scalars. External forcings from circulation in the ABL also plays an important role in modifying ABL height.

Seasonal change, as well as macro-scale circulation like monsoon, have shown to affect the ABL height (e.g., Raman *et al.*, 1990; Sugimoto *et al.*, 2000; Seidel *et al.*, 2012; Sandeep *et al.*, 2014; Guo *et al.*, 2016). This modification could be direct through surface modification, e.g., cooling or wetting the surface, or indirect via altercation of smaller scale meteorological phenomena like the diurnal circulations. Meso-scale, diurnal circulations, such as sea and land breeze, lake breeze, and mountain and valley breeze, are usually contained inside the ABL. However their presence could also modify the internal structure of ABL. Sea breeze especially, can modify ABL height significantly by dissolving the already developed ABL and replaced it with the internal boundary layer of the sea breeze (Garratt, 1994; Hadi *et al.*, 2000; Talbot *et al.*, 2007). Coupling between macro-scale and meso-scale circulation under the ABL is the fundamental driver of weather and climate systems in many parts of the world, including the tropical Maritime Continent (MC) of Southeast Asia. In fact, monsoon and sea breeze, are the most important variables influencing the MC climate (Yamanaka *et al.*, 2018). Both circulation patterns are basically driven by variation in solar forcing, differs only in the time scale. They arise as a consequence of the annual march of the sun and Earth's rotation, respectively (Nitta and Sekine, 1994; Yang and Slingo, 2001; Qian *et al.*, 2010; Yamanaka, 2016).

The ABL is highly influenced by the surface condition, hence radical surface modification will affect the ABL height significantly. In urban area where surface condition is rougher, and heat release is more intense due to man-made materials, increased surface area, and higher anthropogenic heat release, the ABL height is found to be higher than in the rural area (Barlow, 2014; Oke *et al.*, 2017). Since many cities and urban areas, especially megacities, are built in the coastal region, the combined influences of seasonal change, sea breeze, and urban effect maybe the ultimate factor that define the day-to-day weather condition and air quality of the areas (Barlow, 2014; Oke *et al.*, 2017; Miao *et al.*, 2019). Thus, understanding the interaction between these elements could become the key to better predict the weather condition or to improve the air quality of those areas. In the context of this study which focused on meteorological condition of coastal megacity of Jakarta, it is important to have background knowledge on the sea breeze and its interaction with urban areas. In the next sub-section, the sea breeze and its interaction with urban areas will be elaborated briefly.

2.2 Sea breeze and its interaction with urban areas

Sea breeze is a shallow layer of cool and moist marine air that moves inland as a response to local scale pressure difference between sea and land during daytime (Miller *et al.*, 2003). The idealized schematic of sea breeze is depicted in Figure 2.4. The sea breeze itself is part of a mesoscale circulation with landward flow at bottom part, rising flow inland, seaward flow in the upper part, and sinking air over sea at several kilometers from the shore (see blue-dashed line in Figure 2.4). The bottom part of the circulation is a gravity-driven current, namely sea breeze gravity current (SBG), that is generated by density difference between sea and land due to temperature contrast between them (Simpson and Britter, 1979, 1980; Chiba, 1993; Reible *et al.*, 1993; Finkele *et al.*, 1995). To conserve the momentum, a backward (seaward) flow will form on the top of the gravity current, and an offshore subsidence occurs far in the sea (not shown). The leading edge of the gravity current, that is the interface between marine-air-mass and land-air-mass, is known as sea breeze front (SBF). The top of SBF, which is elongated backward due to backward flow, is called the sea breeze head (SBH). Due to strong convergence and forced convection, cumulus clouds (Cu) often form on top of SBH, making a lateral line of shallow clouds which moves with the SBF as it propagates inland (Stull, 1988; Miller *et al.*, 2003; Ferdiansyah *et*

al., 2020). The strong shear between the gravity current flow and the backward flow behind the SBH often creates the Kelvin-Helmholtz instability. In the presence of clouds, this instability could be seen in peculiar form known as Kelvin-Helmholtz billows (KHB). Propagation of SBG over land areas will change the structure of boundary layer. As shown in Figure 2.4, passage of SBF will diffuse the pre-existing boundary layer due to mixing with colder air and gradually replace it with much lower thermal internal boundary layer (TIBL) which form inside SBG (Stull, 1988; Hadi *et al.*, 2000; Prabha *et al.*, 2002; Miller *et al.*, 2003; Ribeiro *et al.*, 2018). The pre-existing boundary layer might remain but decoupled from the TIBL by the remaining cool marine air above the TIBL. Thus, sea breeze passage could potentially reduce the mixing length of pollutants and other trace gases (Miller *et al.*, 2003).

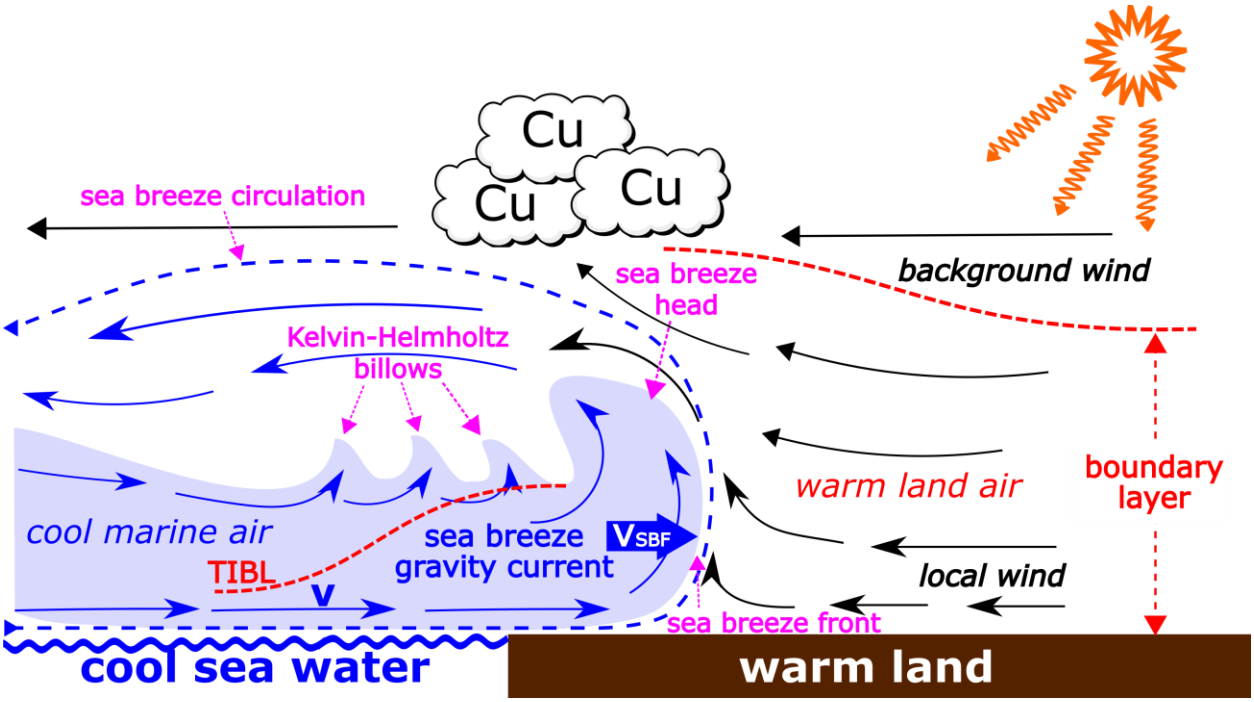

Figure 2.4 Idealized schematic of sea breeze circulation depicting advancement of sea breeze gravity current (blue shade) from the sea into the land. Boundary layer height is denoted by red-dashed line, which transitioning into thermal internal boundary layer (TIBL) inside the sea breeze. The schematic is re-interpreted and composed based on description and illustration from various sources (e.g., Lyons, 1982; Stull, 1988; Miller *et al.*, 2003).

The propagation speed of sea breeze is particularly important as it could define the rate changes of ABL height, the advection of pollutants, the rigorousness of the inland thunderstorm, or the strength of orographic forcings (Kitada, 1987; Garratt, 1994; Prabha *et al.*, 2002; Miller *et al.*, 2003; Wu *et al.*, 2009; Robinson *et al.*, 2011; Birch *et al.*, 2015; Ribeiro *et al.*, 2018). Sea

breeze propagation speed could be inferred from the movement speed of the SBF, hence denoted as V_{SBF}. The sea breeze propagation speed (V_{SBF}) is different from the sea breeze wind speed (V) that is observed at some point along the sea breeze path (see Figure 2.4). The V_{SBF} is the speed at which the entire SBG progress inland, while V is the wind speed inside the SBG. The SBF is characterized by sharp changes in wind direction, humidity, and temperature, hence these changes can be used to detect the SBF passage, then used to calculate the V_{SBF} (Hadi *et al.*, 2002; Jayakrishnan *et al.*, 2021; Reddy *et al.*, 2021).

As sea breeze is a form of gravity-driven current (Simpson, 1969; Simpson and Britter, 1979), and the characteristic propagation speed, otherwise known as densimetric speed (V_d), of such current is proportional to

$$V_d = k\sqrt{\frac{\rho_2 - \rho_1}{\rho_1} gh} = k\sqrt{\frac{\Delta\rho}{\rho_1} gh.} \qquad (2.1)$$

In above equation, ρ_1 [kg m^{-3}] is density of lighter land-air mass, ρ_2 [kg m^{-3}] is the density of denser marine-air-mass, and g [9.8 m s^{-2}] is gravity acceleration. Depth of the gravity current or denser air h [m] could be assumed as a function of ABL height (refer to Figure 2.4). The constant k is the internal Froude number, which is the ratio between inertial force and buoyancy force. In reality, this value is not constant as it assumed, but varies with the geographical setup of the sea breeze area (Simpson and Britter, 1980; Miller *et al.*, 2003). Since density is inversely proportional to temperature (T), equation (2.1) could also be rearranged as

$$V_d = k\sqrt{\frac{\Delta T}{T} gh,} \qquad (2.2)$$

where ΔT [K] is temperature difference between land-air mass and marine-air-mass, while T [K] is absolute temperature of the denser air-mass (Simpson, 1969; Schoenberger, 1984; Miller *et al.*, 2003). Densimetric speed could be considered as propagation speed of dense air mass into lighter ambient air in the absence of opposing flow. The existence of flow in the ambient air (V_g) will reduce or increase the gravity-current propagation as depicted by local wind in Figure 2.4. This local wind would depend on the geographical and geomorphological setup of the sea breeze domains. Most often, this local wind is the opposing land breeze flow, but in other conditions it could be caused by cross-shore geostrophic wind component resulting from synoptic scale pressure gradient. In the case of Jakarta, the local wind is probably the land breeze that is enhanced by the

mountain wind that comes from the Gede-Pangrango mountain range in the southern areas of Jakarta (approximately 50 – 60 km from Jakarta). But in other regions, this local wind could be representation of dessert wind, or continental breeze, or just mountain wind if the mountain is adjacent to the sea. In some situations, the opposing flow might not exist at all, or the flow is really weak (under 0.1 m/s) due to homogeneous temperature distribution at night. That is why, the term used to name this sea breeze opposing wind is local wind. Based on correlation between laboratory experiment and atmospheric data, Simpson and Britter (1980) estimate that the opposing flow will reduce the densimetric speed of sea breeze by 3/5 of its strength. They also found that best estimate of k is approximately 0.87. Thus, a rough estimate of sea breeze propagation speed (V_{SBF}) is given by:

$$V_{SBF} = 0.87\sqrt{\frac{\Delta T}{T} gh} - 0.59V_g. \qquad (2.3)$$

In the absence of opposing flow, hence $V_{SBF} = V_d$, sea breeze propagation speed is ranged between 1 – 5 m s^{-1} (Stull, 1988). It is clear from equation (2.3) that sea breeze gravity current will be initiated when there is a positive temperature difference between air over land and air over sea (ΔT). Inversely, sea breeze current will cease-out when temperature over land is lower than temperature over sea, i.e., ΔT become negative. Time between sea breeze onset and cessation is sea breeze duration, which will depend on how long positive ΔT is maintained.

Seasonal variation in land-sea air temperature difference and background wind will induce variation in sea breeze (Gilliam *et al.*, 2004; Azorin-Molina *et al.,* 2011; Grau *et al.,* 2021; Shen *et al.*, 2021). Variation in sea breeze onset, cessation, and duration were observed in the monsoonal region of the eastern Indian (Reddy *et al.,* 2021). In the tropical MC, specifically over the eastern coast of the Malay Peninsula, the seasonal change in cloudiness is the most important factor that affect sea breeze onset and strength (Jayakrishnan *et al.,* 2021). Seasonal variation of sea breeze can also be induced by the physical settings of sea breeze path (Miller *et al.,* 2003; Gilliam *et al.,* 2004). One important of such physical setting is the existence of city or urban area.

Urban area development and urbanization could modify the sea breeze frequency and characteristics, although this modification may be varied between cities. In Shanghai for example, increased urban roughness and decreased solar radiation by anthropogenic aerosol are assumed to cause reduction of summer sea breeze frequency and wind speed (Shen *et al.,* 2019). In Adelaide, however, temperature increase and urban heat island (UHI) due to urbanization are considered as

the cause of increase in sea breeze maximum wind speed and sea breeze earlier onset, notably during summer and autumn (Masouleh *et al.*, 2019). Urban heat island (UHI) circulation, a phenomena commonly occurs in large cities, may interact with sea breeze and modify its characteristics (Yoshikado and Kondo, 1989; Cenedese and Monti, 2003; Freitas *et al.*, 2007; Hu and Xue, 2016; Ribeiro *et al.*, 2018; Hu *et al.*, 2022). Due to this interaction, seasonal difference in urban heat island (UHI) intensity, could potentially alter the sea breeze onset and propagation speed (Yoshikado, 1992; Wang *et al.*, 2019). Such seasonal differences in UHI-intensity in MC's tropical city has been demonstrated through extensive observation in Singapore (Chow and Roth, 2006; Roth *et al.*, 2022). Their result shows consistently higher UHI intensity during dry season compared to rainy season. Thus, it is importance to consider the urban influences into the seasonal variation of sea breeze.

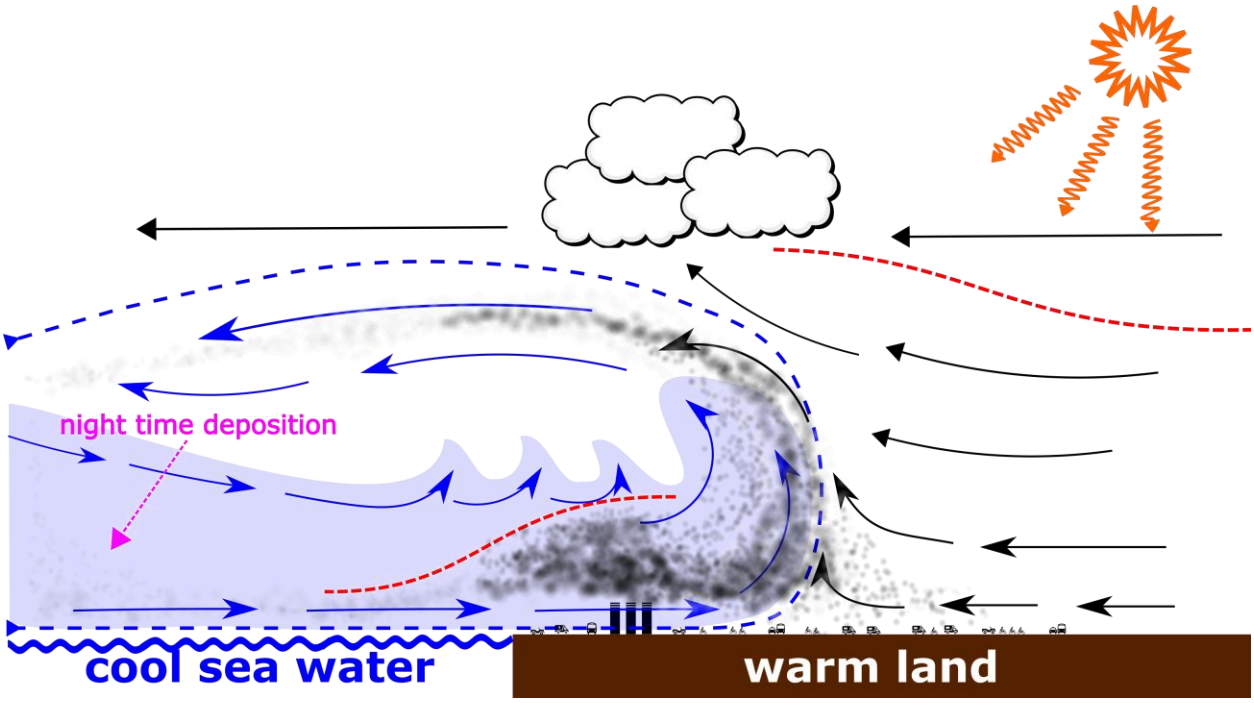

Figure 2.5 Schematic illustration on impact of sea breeze to pollutant distribution over coastal urban areas.

Interaction between sea breeze with megacity such as Jakarta, could be very complex, yet very influential to the local atmospheric condition and the sea breeze itself (Yoshikado and Kondo, 1989; Freitas *et al.*, 2007; Kanda, 2007; Ribeiro *et al.*, 2018). There are many forward forcings and feedback mechanism in this interaction which make it non-linear and unique across places. Kanda *et al.*, (2001) shows that combination between sea breezes convergence and urban heat

island (UHI), a common phenomenon found in megacities, increases the generation of low-level clouds. On the other hand, sea breeze could force and control ventilation mechanism over the city which potentially mitigate the UHI effects (Ribeiro *et al.*, 2018; He *et al.*, 2020). Study by Ferdiansyah *et al.* (2020) found that, there were cases where sea breeze intrusion is delayed over the urban core area of Jakarta. There is a possibility that in the future, the state of sea breeze circulation in rapidly developing cities will be much different than current conditions, thus altering the city's weather and climate altogether.

In urban areas, sea breeze is also known to modify pollutants and trace gases transport, either horizontal or vertical, and affect their concentration. As illustrated in Figure 2.5, the SBF passage could increase pollutant and gases concentration via upward convergence or hygroscopic growth by moister marine air (Takashima *et al.*, 2019). The pollutants that carried upward by SBF will be transported offshore by the backward flow, but then recirculated again onshore by SBG in the following day, effectively becoming additional source to pollutants concentration (Anthes, 1978; Talbot *et al.*, 2007; Arrillaga *et al.*, 2018). The low-height TIBL generated by sea breeze could trapped pollutants emitted from the surface, while the sea breeze wind transport it inland (Talbot *et al.*, 2007). These complex meteorological transport processes could be better understood by observing a passive tracer such as CO_2 (Arrillaga *et al.*, 2018; Lin *et al.*, 2018). CO_2 is a remarkable passive tracer which is not only important as a representation of pollutants, but also as a proxy of micro-scale turbulent condition as well as anthropogenic activities in urban areas. Since nowadays urban areas is considered as one of the main contributors to global CO_2 emissions, research on urban CO_2 dynamics become more and more important (Velasco and Roth, 2010; Duren and Miller, 2012; Roth *et al.*, 2017). In the next subsection, theory and references on urban CO_2 studies will be presented briefly.

2.3 The urban CO_2 flux and concentrations

CO_2 is regarded as the most prominent greenhouse gas (GHG) that contributes to global climate change (Hansen *et al.*, 1998). While CO_2 is naturally produced by organism respiration system and volcanic activities, recent CO_2 production is largely contributed by anthropogenic energy consumption. Record of CO_2 concentrations have shown an increasing trend in the last few decades (Keeling *et al.*, 2001), which is linked to energy consumption, especially energy from

fossil fuel (Canadell *et al.*, 2007; Friedlingstein *et al.*, 2019). Based on global final energy consumption, the contribution of urban areas to the world CO_2 emission is approximated more than 70% (Seto *et al.*, 2014). Thus, cities or urban areas can be considered as the main source of CO_2 emission (Velasco and Roth, 2010; Schwandner *et al.*, 2017).

Net amount of urban CO_2 emissions could be inferred directly from measurement of its vertical flux. Flux is the transfer rate of quantity, in mass or energy, across a unit area per unit time (Stull, 1988; Aubinet *et al.*, 2012; Foken *et al.*, 2012; Burba, 2013). The flux of quantity across a horizontal plane is a function of the velocity of the air (e.g., w), the density of the air (ρ_a) and the relative amount of the quantity (e.g., mixing ratio s) that is being transferred (Figure 2.6a). Positive value of flux indicates that the atmosphere is gaining quantity, while negative sign indicates the atmosphere is losing quantity.

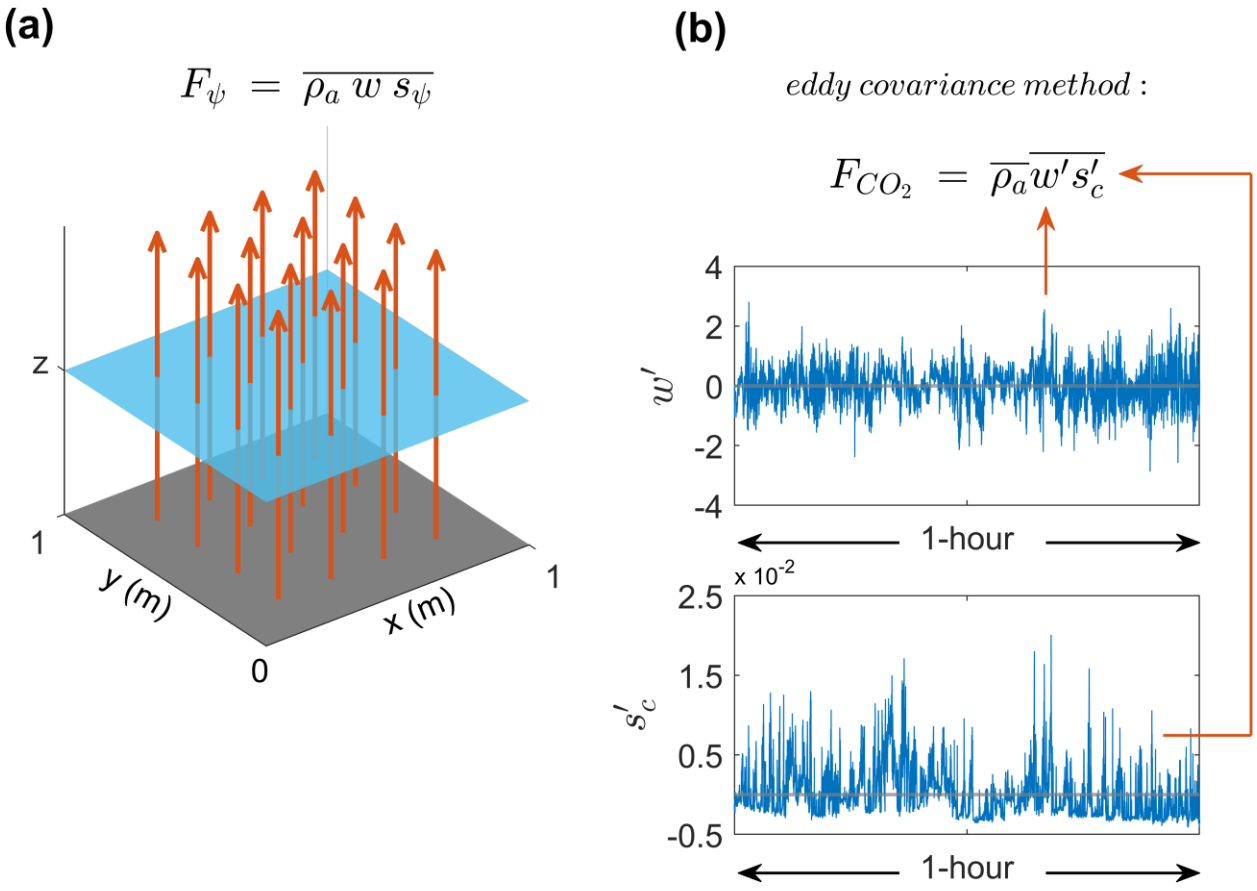

Figure 2.6 Illustration of vertical flux as transfer rate of quantity across a unit area per unit time (a); and (b) illustration of eddy covariance method to estimate CO_2 vertical turbulent flux from 1-hour fast fluctuations of vertical wind (w')and mixing ratio of CO_2 (s'_c).

Given a pair measurement of vertical wind speed (w) in m s^{-1} and mixing ratio of CO_2 (s_c) in kg kg^{-1}, the flux of CO_2 (F_{CO_2}) can be calculated as:

$$F_{CO_2} = \overline{\rho_a \, w \, s_c} \qquad (2.4),$$

where ρ_a is the density of air in kg m^{-3} and overbar denotes time average of variables under it. For any arbitrary variable ψ, one can separate the mean and turbulent (fluctuation) parts using the Reynolds decomposition (Stull, 1988):

$$\Psi = \bar{\Psi} + \Psi' \qquad (2.5),$$

where

$$\bar{\Psi} = \frac{1}{n}\sum_{i=1}^{n} \Psi_i \qquad (2.6)$$

is the mean of ψ; and ψ' is the instantaneous fluctuation or turbulent part of ψ. Hence, applying Reynolds decomposition to equation (2.5) will result in:

$$F_{CO_2} = \overline{(\overline{\rho_a} + \rho'_a)(\overline{w} + w')(\overline{s_c} + s'_c)} \qquad (2.7).$$

Expanding the above equation yield:

$$F_{CO_2} = \overline{\overline{\rho_a}\overline{w}\overline{s_c}} + \overline{\overline{\rho_a}\overline{w}s'_c} + \overline{\overline{\rho_a}w'\overline{s_c}} + \overline{\overline{\rho_a}w's'_c} + \overline{\rho'_a\overline{w}\overline{s_c}} + \overline{\overline{w}\rho'_a s'_c} + \overline{\rho'_a w'\overline{s_c}} + \overline{\rho'_a w's'_c}$$

$$I \qquad II \qquad III \qquad IV \qquad V \qquad VI \qquad VII \qquad VIII \qquad (2.8).$$

Based on Reynolds rule of averaging, terms II, III, and V are equal to zero as they contained averages of fluctuations. Term VIII could be ignored since density fluctuation is very small and as a third order moment it could be assumed negligible. Flux density of dry air is zero such as,

$$\overline{w\,\rho_a} = \overline{w'\,\rho'_a} + \overline{w}\overline{\rho_a} = 0 \qquad (2.9),$$

hence mean vertical wind could be calculated as

$$\overline{w} = \frac{\overline{-w'\,\rho'_a}}{\overline{\rho_a}} \qquad (2.10).$$

Substituting equation (2.10) into term I yield:

$$\overline{\rho_a}\,\overline{w}\,\overline{s_c} = -\overline{\rho'_a\,w'\overline{s_c}} \qquad (2.11),$$

which is the negative form of term VII. This will make term I and term VII cancel out from each other and vanish. Substituting again equation (2.10) into term VI will produce a fourth order moment which is almost equal to zero as:

$$\overline{\overline{w}\,\rho'_a\,s'_c} = -\frac{1}{\overline{\rho_d}}\overline{w'\,\rho'_a\,\rho'_a\,s'_c} \approx 0 \qquad (2.12).$$

The only term left from equation (2.8) is term IV. Thus, within the assumption of dry air and the third and fourth order term is negligible, F_{CO_2} can be considered approximately equal to:

$$F_{CO_2} \approx \overline{\rho_a}\,\overline{w's'_c} \qquad (2.13).$$

Equation (2.13) is the basic form to calculate flux of any quantity, including heat, moisture, GHGs, and other scalars. This method is known as eddy covariance (EC) method as it uses the covariance of fluctuating (eddy) components of *w* and the quantity that is measured, as illustrated in Figure 2.6b. The EC method is considered as the only method to directly measure flux exchange between surface and atmosphere, hence often regarded as standard referenced measurement (Aubinet *et al.*, 2012; Foken *et al.*, 2012; Baldocchi, 2020).

The CO_2 flux estimation using EC method will require measurement using a set of fast response sensors to measure velocity and CO_2, such as ultrasonic anemometer and open-path gas analyzer (Foken *et al.*, 2012; Burba, 2013). However, open-path gas analyzer usually measured molar density of CO_2 (ρ_c), in mol m^{-3}, rather than its mixing ratio, thus equation 2.13 should be modified to use the molar density. Using relationship of (see Webb *et al.*, 1980):

$$s'_c = \left(\frac{\rho_c}{\rho_a}\right)' = \frac{\rho'_c}{\rho_a} - \frac{\rho'_a}{{\rho_a}^2}\rho'_a \qquad (2.14),$$

where ρ_a here is molar density of air in mol m^{-3}, and then substitute it to equation (2.13), we will get:

$$F_{CO_2} \approx \overline{w'\rho'_c} + \overline{w}\,\overline{\rho_c} \qquad (2.15).$$

One problem that arise from the usage of molar density measurement from open-path gas analyzer is, its value will change with the change of temperature as it will change the sampling volume (Massman, 2005; Burba, 2013). Following the work of Webb *et al.* (1980), under the assumption of dry air, the second term on the right-hand side (RHS) of equation (2.15) can be expanded using equation (2.10) and Boussinesq approximation to yield:

$$F_{CO_2} \approx \overline{w'\rho'_c} + \frac{\overline{\rho_c}}{\bar{T}}\,\overline{w'T'} \qquad (2.16),$$

where $\bar{T}$ and T' are the mean and fluctuation of air temperature. Equation (2.16) implies that CO_2 flux is influenced by the kinematic sensible heat flux ($\overline{w'T'}$). As the sensible heat flux increases, the atmosphere will be gaining more CO_2 from the surface. However, the assumption of dry atmosphere could not be applied in most fields. Instead, the real atmosphere is mostly moist and the density of water vapor (ρ_v) is much lighter than dry air, hence its existence will increase the

buoyancy of the air. For that, expansion of equation (2.10) should account for partial pressure of water vapor and the gas law for moist air should be applied. Elaborating on these term, Webb *et al.* (1980) expands equation (2.15) into

$$F_{CO_2} = \overline{w'\rho'_c} + \left[\frac{m_d}{m_v}\frac{\overline{\rho_c}}{\overline{\rho_d}}\overline{w'\rho'_v}\right] + \left[\left(1 + \frac{m_d}{m_v}\frac{\overline{\rho_v}}{\overline{\rho_d}}\right)\frac{\overline{\rho_c}}{\overline{T}}\overline{w'T'}\right} \quad (2.17),$$

where ρ_d is the molar density of dry air, with value around 42.285 g mol^{-1}; ρ_v is the molar density of water vapor; and $m_d = 28.97\ g\ mol^{-1}$ and $m_v = 18.02\ g\ mol^{-1}$ are the molar mass of dry air and water vapor, respectively. The second and third RHS terms on equation (2.17) is known as WPL terms, after Webb *et al.*, (1980). Equation (2.17) shows that in order to correctly calculate F_{CO_2} using open-path gas analyzer will require simultaneous measurements of temperature and moisture fluctuations. That is why CO_2 gas analyzer usually also measures water vapor (H_2O) molar density and its installed with ultrasonic anemometer to get flow velocity fluctuation as well as air temperature fluctuation (Foken *et al.*, 2012; Burba, 2013).

The usage of ultrasonic anemometer to measure temperature will require another correction since the temperature measured is sonic temperature (T_s), which close to virtual temperature (T_s). To get the absolute temperature (T), (Schotanus *et al.*, 1983) propose correction as follows:

$$T = [T_s/(1 + 0.51\ q_v)] \quad (2.18),$$

where q_v is the specific humidity, which could be calculated as:

$$q_v = \frac{m_v\rho_v}{(m_d\rho_d + m_v\rho_v)} = \frac{1}{\left(\frac{m_d\rho_d}{m_v\rho_v} + 1\right)} \quad (2.19).$$

Based on equation (2.18), correction of kinematic sensible heat flux when using sonic temperature is derived by Dijk *et al.* (2004) as follows:

$$\overline{w'T'} = \overline{w'T_s'} - 0.51\overline{s_v}\overline{w'T_s'} - 0.51\overline{T_s}\overline{w'q_v'} \quad (2.20).$$

To get the actual sensible heat flux (Q_H), we can multiply the kinematic sensible heat flux with mean density of air ($\overline{\rho_a}$) in kg m^{-3}, and specific heat of air (c_p), which has a value of 1004 J kg^{-1} K^{-1}, as the following:

$$Q_H = \overline{\rho_a}c_p\overline{w'T'} \quad (2.21).$$

Since the gas analyzer also measuring water vapor fluctuation, we could also obtain the latent heat flux (Q_L) using the relationship:

$$Q_L = \lambda E = \lambda\left[\left(1 + \frac{m_d}{m_v}\frac{\overline{\rho_v}}{\overline{\rho_d}}\right)\left(\overline{w'\rho'_v} + \frac{\overline{\rho_v}}{\overline{T}}\overline{w'T'}\right)\right] \quad (2.22),$$

where is λ latent heat of evaporation in J kg^{-1}, which could be assumed constant or more precisely determined using empirical function of T. Obtaining the sensible and latent heat flux values, along with CO_2 flux would be beneficial in assessing the relationship between CO_2 emission and energy balance, especially in the presence of net radiation data. Many urban CO_2 studies usually coupled with energy balance observation (Grimmond *et al.*, 2004; Moriwaki and Kanda, 2004; Ao *et al.*, 2016; Roth *et al.*, 2017; Hong *et al.*, 2020).

While the EC method is a popular method of measuring CO_2 fluxes, it remains challenging to implement it in the urban area. Finding representative measurement site and acquiring permission for installment may pose a challenge in conducting measuring CO_2 flux using EC method. As consequences, many urban CO_2 measurement is forced to be conducted in any available infrastructure. Since urban canopies heterogeneities will limit the validity of flux measurement in local or even microscale area, care should be given in assessing the land cover and urban aerodynamic parameters surrounding the observation infrastructure (Aubinet *et al.*, 2012; Feigenwinter *et al.*, 2012; Ao *et al.*, 2016; Matthews and Schume, 2022). Several methods are available to estimate the urban aerodynamic parameters, either using anemometric or morphometric methods (Grimmond *et al.*, 1998; Grimmond and Oke, 1999a; Kanda *et al.*, 2013; Kent *et al.*, 2017). In the case of single height measurements of wind field, morphometric methods are the only option. Evaluation by Kent *et al.*, (2017) reveal that there is an agreement between anemometric method and morphometric methods that consider maximum height variability in urban environments, such as Kanda *et al.* (2013) method. This result also implies that CO_2 sensor may need to be located higher than roughness elements to provide a local-scale or city-scale representation, otherwise selective fetch direction could be applied to remove invalid measurement.

In conjunction with the urban aerodynamic parameters and fetch direction, analysis of urban CO_2 exchange with EC method should also carefully consider the source area of the flux, otherwise known as flux footprint. Flux source area or flux footprint is the area where majority of the flux is coming from (see Figure 2.7). This area usually elongated toward upwind direction, with maximum fetch usually found a few tenth meter in front of sensor location (Kljun *et al.*, 2004). The footprint could be estimated using several available footprint estimation models (e.g., Hsieh *et al.*, 2000; Kormann and Meixner, 2001; Kljun *et al.*, 2015; Wang *et al.*, 2018). It should be noted that most of these models assumed a flat and smooth homogeneous surface, and are not suited for heterogenous urban surface, thus an underestimation should be expected (Velasco and

Roth, 2010). The source area will change following the prevailing wind speed and direction, hence estimating it for the whole measurement period and combined the results into climatological footprint would be useful for the flux analysis (Kljun *et al.*, 2015; Schmutz *et al.*, 2016; Roth *et al.*, 2017). Many of climatological footprint over urban areas shows that urban CO_2 flux measurement using EC methods typically provides estimates at micro (neighborhood) or local (district) scale, rather than city scale (Matthews and Schume, 2022).

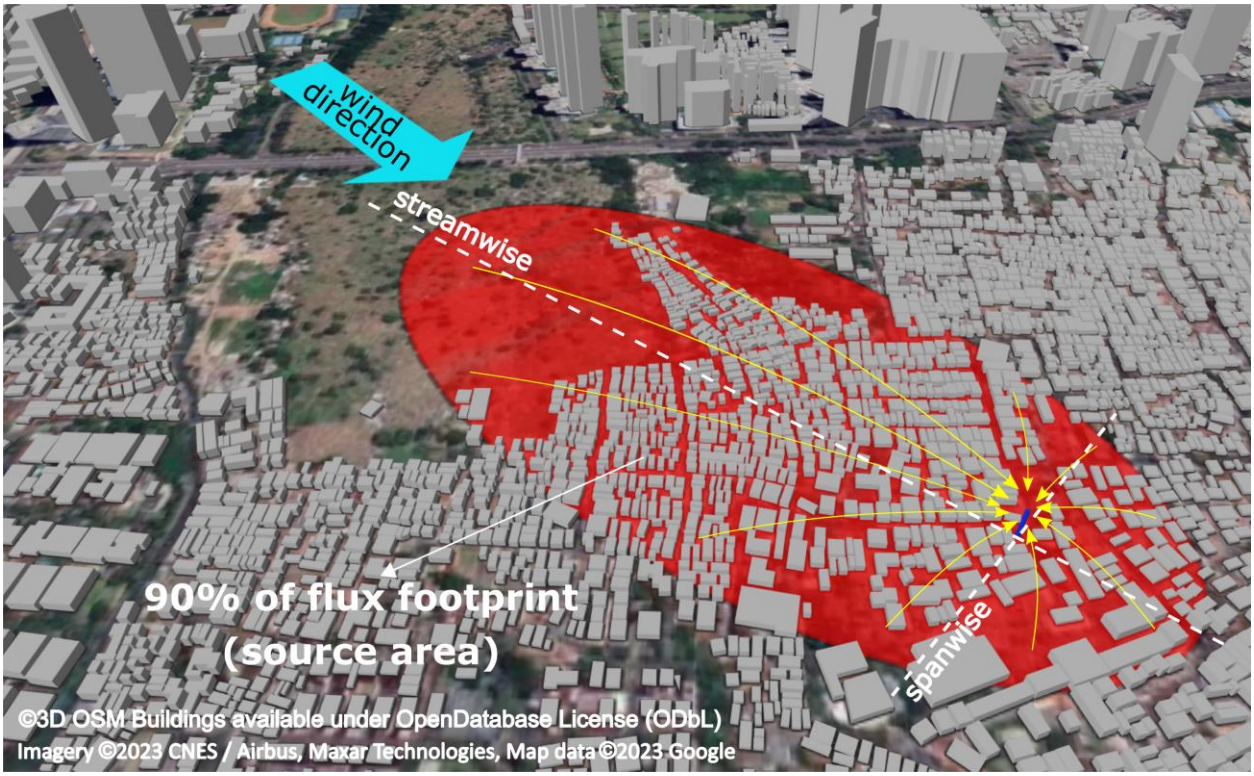

Figure 2.7 Illustration of flux footprint over urban area where flux is measured at the blue tower. Red shaded area comprises the majority (90 %) of flux source area. The footprint is not based on actual modelling and serves for illustration purposes, but the map and buildings are actual data provided by entities as written on the attributions. Base map uses satellite imagery from Google which is available with attribution under specific terms and conditions; and buildings data is obtained from OpenStreet Map (OSM) Building which licensed under OpenDatabase License (ODbL).

While cities and urban areas do not represent an ideal surface for measuring CO_2 flux using EC methods, many researchers have found that the method is still applicable as long as the measurement, data processing and analysis is conducted according to well-known principal, best practices, and guidelines that have been created by the research community (Dijk *et al.*, 2004; Lee *et al.*, 2005; Mauder and Foken, 2006; Aubinet *et al.*, 2012; Foken *et al.*, 2012; Burba, 2013;

Fratini and Mauder, 2014; Vitale *et al.*, 2020). CO_2 flux measurement with EC method therefore become an important way to understand urban CO_2 emissions and to formulate strategies in reducing its impact. As remarkably pointed out by Christen, (2014), such in-situ measurement of GHGs inside urban atmosphere could be used to compare and verify top-down inventories of GHGs or bottom-up models; to asses land cover change effect and local to regional scale feedback of urban emissions; and to provide monitoring of emission trend and its impact, as well as metric to assess the efficiency of policy measures.

2.4 Summary

The atmosphere is a thin layer of air, in comparison to Earth's radius, that is vital for life on Earth. Even so, only the lowest 5% of its height, in the so-called troposphere layer, is dominant in determining the conditions that we perceived. Inside the troposphere layer, superposition of various scales atmospheric phenomena drives the weather and climate. While the upper troposphere is dominated by macro-scale phenomena, the lowest part is a mixed of macro- to micro-scale phenomena due to the influence of Earth's surface. This surface-influenced-layer is called the atmospheric boundary layer (ABL) and it evolved diurnally.

Many meso-scale, diurnal circulations were contained and influenced the condition inside the ABL. One of such circulation is sea breeze circulation which is a dominant circulation over coastal area. Since many urban areas, cities, and megacities were built over coastal area, interaction between sea breeze and urban effect is inevitable. Sea breeze could provide fresh and cool air for urban areas but could also reduce the ABL height and promotes pollutant concentration. At the same time, urban areas its urbanization processes will modify the atmospheric energy balance and induce variations in sea breeze characteristics. These dynamics would affect the daily weather and air quality conditions over the coastal urban areas, as well as influencing the vertical micro-scale transport of heat, moisture, greenhouse gases (GHGs) and other scalars. These vertical transport processes will define the contribution of those urban areas to global climate change, which in the end will return to amplify the adverse effects of urbanization itself.

To understand urban atmospheric dynamics, as well as tracking the GHGs contribution, measuring urban GHGs emission such as CO_2 is necessary. Research projects to study the CO_2 exchange in urban atmosphere have been conducted in various cities across the globe. Many of those research projects employ the eddy covariance method to estimate the urban CO_2 emission

from a set of fast response wind and gas sensors. While this method undoubtedly provides the most accurate estimation of urban CO_2 emissions, careful consideration, preparation, implementation, and data processing should be carried out before analyzing and applying the results for policy formulation. Nevertheless, understanding the whole spectrum of meteorological phenomena of vulnerable areas, such as urban areas, is important to formulating strategies in adapting and mitigating the impacts of radical change that happen in such areas. Thus, knowledge of urban atmospheric environments should always be updated.

Chapter 3 Seasonal Variation of Sea Breeze in Jakarta

Due to the complexity of the interaction between various scale atmospheric phenomena, it is necessary to first understand how larger scale process affect the smaller one (top-down processes), before analyzing the opposite (bottom-up processes). Larger scale process, such as monsoon, which govern Jakarta's seasonal transition (Hamada *et al.*, 2002; Chang *et al.*, 2005b; Yoden *et al.*, 2016) might control the sea breeze over the city. This control will have direct consequences to the interaction of sea breeze with smaller phenomena like UHI and turbulent flux exchange. Thus, it is important to understand how seasonal transition affects the sea breeze in Jakarta.

3.1 Introduction

Atmospheric conditions in Jakarta, Indonesia, which is the largest megacity in the MC, are strongly influenced by the sea breeze in both the dry and rainy seasons. During the dry season, the sea breeze is the main driver of aerosol and pollutant transport (Pinandito *et al.*, 2001; Sofyan *et al.*, 2007), whereas during the rainy season, the sea breeze may trigger afternoon precipitating clouds, especially in southern Jakarta (Renggono *et al.*, 2001). Observations have suggested that sea and land breeze circulation are the main drivers of the meridional migration of diurnal rainfall between Jakarta coastal and southern inland areas (Mori et al., 2018). On the other hand, urban area and urban development in Jakarta may change the sea breeze. A recent study suggests that the UHI may be causing the delay of sea breeze propagation over Jakarta (Ferdiansyah et al., 2020), and such change could affect the timing and strength of convective storm (Robinson *et al.*, 2013). Numerical simulation by Argüeso *et al.* (2016) has shown that existence of the city of Jakarta will enhance sea breeze circulations, increase near-surface moisture flux convergence, and lead to an increase of precipitation.

Due to the importance of sea breeze for Jakarta, it is necessary to understand how it varies over the seasons and whether the city affects this variation. A boundary-layer radar (BLR) study

conducted in Serpong, a suburb of Jakarta, showed that a clear sea breeze signal is usually found during the dry season, but not in the rainy season (Hadi et al., 2002). They also show that sea breeze intrusion occurred earlier on cloudy days, however the mechanism was not investigated. Using the same dataset, a later study observed sea breeze circulation during the rainy season, especially when the prevailing winds were weak (Araki et al., 2006). Although seasonal variation in sea breeze intensity has been discussed, seasonal variation in sea breeze onset, duration, and propagation has not yet been studied in Jakarta; such an analysis requires long-term observations collected at multiple locations.

The objective of this study was to extend our knowledge of sea breeze characteristics in Jakarta, focusing on its seasonal variation of onset, duration, and propagation speed. Using a multi-year dataset obtained from two near-surface observation stations in Jakarta, we examined the effects of seasonal transition on the sea breeze and explored the potential underlying mechanism. This study is the first to observe sea breeze characteristics within the urban area of Jakarta. Our findings will provide a foundation for future studies on interactions between the sea breeze and climate change and/or urbanisation in Jakarta. Microclimate changes observed in Jakarta (Siswanto *et al.*, 2022) may also influence the sea breeze (Darmanto *et al.*, 2019); therefore, knowledge about seasonal sea breeze variation will be important for isolating the effects of climate change and urbanisation, thus improving the accuracy of future analyses.

3.2 Material and methods

The main dataset used in this study comprised near-surface observations conducted at two sites in urban areas of Jakarta. Jakarta is located on the northern coast of western Java Island (Figure 3.1). Along its northern side, its width is the same as that of Jakarta Bay (~30 km), whereas its southern side has a width of only ~13 km. The distance from Jakarta Bay to the southern border is ~30 km. Jakarta is situated in a relatively flat area, with a mountain range ~50 km to the south having a maximum height of 3,000 m a.s.l. (Mt. Gede-Pangrango). The main dataset was used to characterise the sea breeze and analysed to obtain the seasonal variation in sea breeze onset, duration, and propagation speed. Several freely available datasets also used for the analysis.

3.2.1 Two points near-surface observations for sea breeze study

Meteorological observations were conducted at two sites in Jakarta (Figure 3.1a). The sites were selected for ease of sea breeze propagation measurement. The first observation site is a coastal area ~450 m from the Jakarta coast. The instruments were placed on top of a building owned by Badan Riset Kelautan dan Perikanan–Kementrian Kelautan dan Perikanan (KKP), hereinafter KKP. There are many residential houses to the east of the site, a highway to the south, and a recreational area to the west (Figure 3.1a, inset). The KKP building is 18 m in height, which is higher than most surrounding structures, except for an apartment building to the north-northwest. All instruments were mounted on 2-m steel poles, as shown in Figure 3.1b.

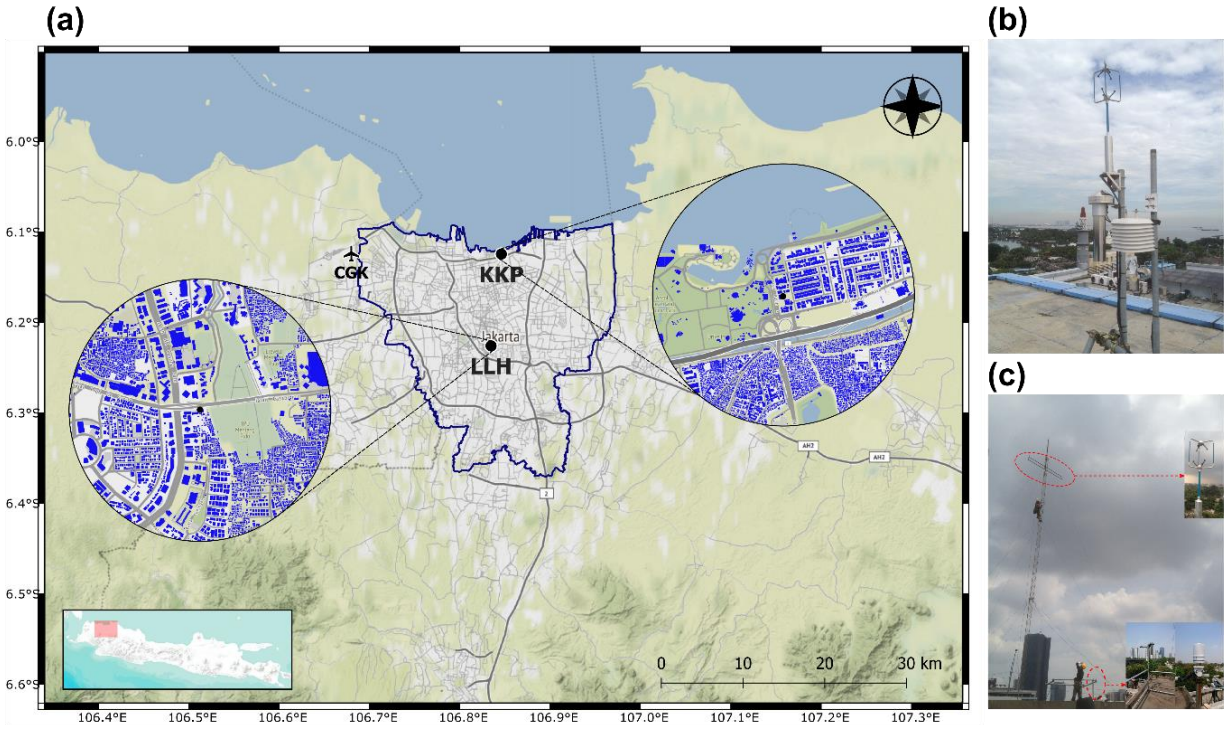

Figure 3.1 (a) Map of Jakarta, Indonesia showing observation sites. Photographs of the observation instruments used at the (b) Badan Riset Kelautan dan Perikanan–Kementrian Kelautan dan Perikanan (KKP) and (c) and Laboratorium Lingkungan Hidup (LLH) buildings. A sounding station at Soekarno–Hatta International Airport (CGK) is indicated by the plane symbol; the blue perimeter line indicates the Jakarta city administrative boundary. Blue patches in circular insets indicate building footprints within a 1-km radius of the observation sites. Rectangular inset shows a map of Java Island indicating the position of the study area. Map tiles by Stamen Design, under CC-BY-3.0 with data from OpenStreetMap, under ODbL. Photograph courtesy of Dr. Atsushi Inagaki.

The second site is in the business district in the urban core of Jakarta, 11.26 km to the south

of the KKP building. Instruments were placed on top of a building owned by Laboratorium Lingkungan Hidup (LLH), Jakarta City Government, hereinafter LLH. The LLH building has a height of 22 m, which is extended by a 10-m lattice tower. There is a large cemetery to the east of the park, and many tall buildings to the north and southwest. Wind and radiation measurement instruments were mounted on the lattice tower at a height 7.3 m above the rooftop, and other instruments were mounted at the base of the tower (Figure 3.1c). A detailed description of the site is provided in Table 3-1. Because the instruments were mounted on the tops of buildings, it could be considered that the observations are within the urban roughness sublayer (Oke *et al.*, 2017).

Table 3-1 Descriptions of the observation sites.

Description	KKP	LLH
Building height	18 m	22 m
Terrain elevation	2.9 m	13.6 m
Site surrounding	Coastal area, ±450 m from sea, with large recreational area with dense vegetation in NW to SW direction. Building base higher than surrounding canopy, except for one building in the north.	Business district in urban core area, with many tall buildings in N and SW direction. There is a large cemetery in NNE to SSE direction with sparse vegetation.
Instruments and measurement height (z_m)	ultrasonic anemometer: 21 m temperature/humidity gauge:20 m	ultrasonic anemometer: 29.3 m net radiometer: 29.3 m temperature/humidity gauge: 23 m automatic weather station: 23 m
Displacement height (z_d)	13.5 m	12.8 m

*) Darmanto et al. (2017)

The main instruments used at both sites were ultrasonic anemometers and temperature/humidity gauges (Figure 3.1b, c). A net radiometer and automatic weather station (AWS) were also installed on the LLH building. The main purpose of the AWS was to obtain rainfall data for ultrasonic anemometer screening. Measurements were mainly logged at a sampling rate of 10 Hz, whereas the net radiometer and AWS logged measurements at 1- and 5-min intervals, respectively. Detail specification of the instruments is presented in Appendix A.

Observations were conducted from March 2017 to October 2021, except for net radiometer measurements, which started in January 2019. Data were not obtained continuously throughout the observation period; they could not be obtained during several periods due to errors or technical problems. At the LLH building, no data were obtained for nearly 5 months, from June to October 2020. Approximately 45 months of data were obtained for the analysis.

3.2.2 Observation data screening and processing

The average of each observed variable was used for the analysis. Averaged 1-h variables were mainly analysed, with 10-min averages used to identify sea breeze intrusion and cessation. Prior to averaging, observation data from the main instruments were subjected to pre-processing. Thresholds of ± 25 m s^{-1}, 278.15–318.15 K, and 0–100% were used to detect non-physical wind speed components (*U*, *V*, *W*), air temperature (*T*), and relative humidity (*RH*), respectively. Anomalously high or low measurements within very short periods, i.e. spikes, were detected using the median absolute deviation (MAD) algorithm (Mauder et al., 2013). Observation sample x_i is considered a spike if:

$$|x_i| > \left|\langle x\rangle \pm \frac{7 \times MAD}{0.6745}\right| \quad (3.1),$$

where $\langle x\rangle$ symbolizing the median of x and

$$MAD = \langle|x_i - \langle x\rangle|\rangle \quad (3.2).$$

Erroneous measurements were replaced with values linearly interpolated from adjacent measurements, or with average values of non-erroneous measurements, depending on the number of consecutive erroneous measurements. If the proportion of erroneous measurements exceeded 60% of the total sample window, the average value was discarded. Because ultrasonic anemometers are highly sensitive to rain, variables were "screened" using AWS rainfall intensity data, at a threshold of ≥ 1 mm/h. The total amount of data that was removed by the rainfall-threshold is 5.2% at KKP and 6.1% at LLH. After processing and screening, from all 1-hourly mean values between 1st March 2017 00:00 and 31st October 2021 23:00, usable data acquired is 82.5% and 74.3% from KKP and LLH sites respectively.

Although average values were the main focus, wind fluctuations (u', v', w') and sonic temperature fluctuation (T_s') were also used to calculate sensible heat flux (Q_H) and stability parameter (ζ). Sensible heat flux is calculated as follows:

$$Q_H = \rho c_p \overline{w' T_s'}\,, \qquad (3.3)$$

where ρ is the air density, c_p is the specific heat of air at constant pressure, and $\overline{w' T_s'}$ is the covariance of w' and T_s' (Stull, 1988). The stability parameter is calculated from effective height (z) and Obukhov length (L) as folows:

$$\zeta = \frac{z}{L} = \frac{(z_m - z_d)}{\left[\frac{\bar{T}_s u_*^3}{\kappa g \overline{w' T_s'}}\right]} \qquad (3.4)$$

where is z_m measurement height, z_d is displacement height, κ is von Karman constant (0.4), and u_* is friction velocity, which is estimated using:

$$u_* = \sqrt[4]{\left(\overline{u'w'}\right)^2 + \left(\overline{v'w'}\right)^2}\,. \qquad (3.5)$$

The displacement height (z_d) is obtained from estimation by Darmanto *et al.* (2017). The value of z_m and z_d are tabulated in Table 3-1.

3.2.3 Additional datasets

To support the analyses, several openly available datasets also retrieved. Sounding data observed by Badan Meteorologi Klimatologi and Geofisika (BMKG) at Soekarno-Hatta International Airport (CGK) were acquired via the University of Wyoming weather website (https://weather.uwyo.edu/upperair/sounding.html). Sounding data were available only at 00:00 and 12:00 UTC (07:00 and 19:00 LT, respectively), and only mandatory levels were retrieved. A climatological rainfall dataset (Global Precipitation Measurement [GPM] IMERG Level 3) was obtained (Huffman *et al.*, 2019). This dataset has a 0.1° spatial resolution and 30-min time interval. A global 3-hourly sea surface temperature (SST) dataset was acquired from the Woods Hole Oceanographic Institution (WHOI) Climate Data Record (CDR) (Clayson *et al.*, 2016). This SST dataset have a spatial resolution of 0.25° or approximately 25 km in the tropical area (assuming 1° ≈ 111 km). The SST dataset is available from January 1988 until present time, however for this research its only collected since January 2017. Temperature at 2-m and boundary-layer height estimates were retrieved from the ERA5 reanalysis dataset, which has a spatial resolution of 30 km and temporal resolution of 1 h (Hersbach *et al.*, 2020). Additional 2-m temperature from AWS observation at Cibinong (CBN), 30 km south of LLH, also acquired from cooperation between Institut Teknologi Bandung and Durham University. It's a limited dataset, with time span between 2018 to 2020. This dataset is not freely available but could be acquired upon request.

3.3 Results

A monthly–diurnal composite of zonal wind speed (U) observed at the KKP and LLH buildings showed strong annual variation, shifting between positive (westerly) and negative (easterly) every year, with the direction remaining consistent at the diurnal scale (Figure 3.2a, b). The zonal wind component was dominated by easterlies From May to September, and by westerlies from December to March. During seasonal transition periods, zonal wind tended to be weaker and daily wind directions became less consistent. Sounding observations at CGK confirmed this shift (Figure 3.2c, d). Sounding data also indicated diurnal zonal wind consistency in the morning (07:00 LT) and evening (19:00 LT). Similar patterns were observed in both lower-level (10:00 hPa) and upper-level (850 hPa) sounding, indicating consistent zonal wind directions throughout the boundary layer height (H_{bl}). Sounding data indicated the magnitude of observed near-surface zonal winds were consistent with lower-level sounding. However, higher-level sounding was seen at higher magnitudes, following the logarithmic boundary-layer wind profile (Stull, 1988; Arya, 2001).

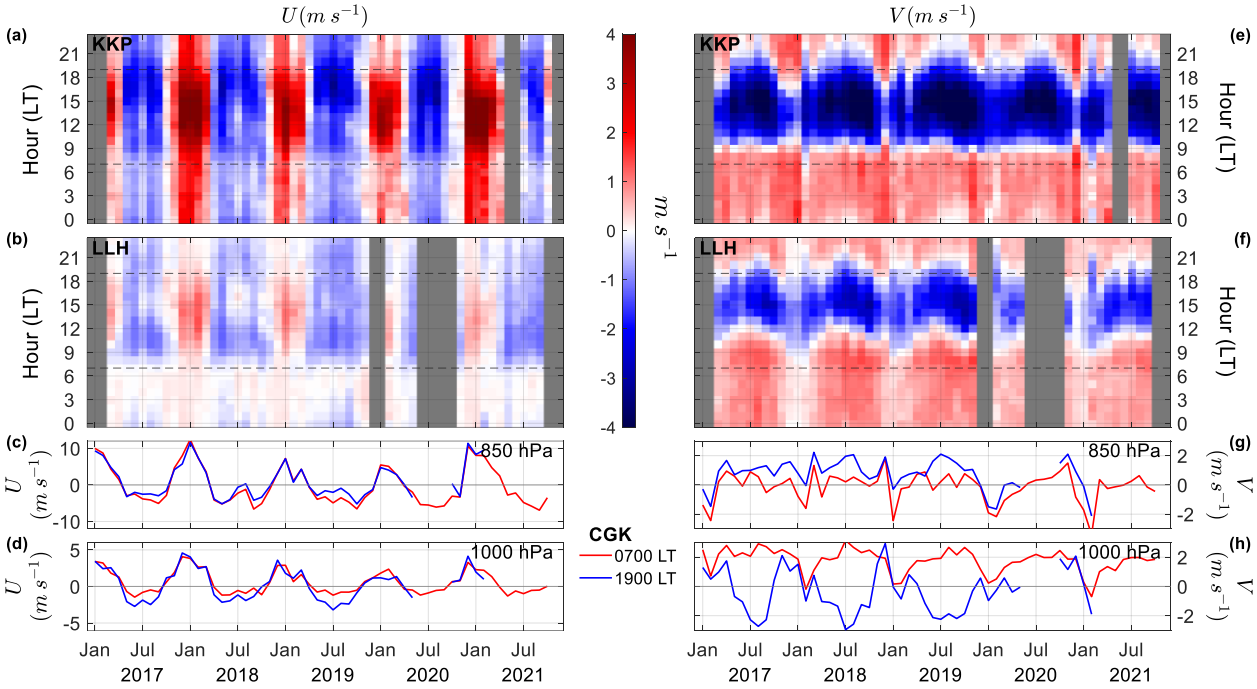

Figure 3.2 Monthly diurnal composite zonal wind (U) and meridional (V) wind speed (m s^{-1}) data observed at the (a, e) KKP and (b, f) LLH buildings. Monthly averaged U and V data obtained from sounding observations at CGK for (c and g) 850 hPa and (d and h) 1,000 hPa. Grey shading in (a, b, e, and f) indicates missing data. Horizontal dashed lines indicate sounding measurement times. Red and blue lines indicate sounding observations at 07:00 and 19:00 LT, respectively.

Although they were dominated by annual signals, near-surface zonal winds observed at the KKP and LLH buildings also exhibited diurnal variation. Zonal wind magnitudes were stronger during the daytime and weaker at night, consistent with the diurnal variation of near-surface wind speed observed by other researcher (e.g., Crawford and Hudson, 1973; Fajber *et al.*, 2014; Jiménez *et al.*, 2016). Stronger daytime near-surface winds were caused by rapid, efficient momentum transfer from aloft by the convectively unstable boundary layer, whereas the more stable night-time boundary layer will reduced downward momentum transport, hence resulting in slower near-surface winds (Arya, 2001; Fajber *et al.*, 2014; Jiménez *et al.*, 2016). The diurnal change in boundary layer stability condition is confirmed from stability parameter (ζ). The average value of ζ on both sites during daytime is ranged from -1 to -12.34, indicating a very-unstable to extremely-unstable condition (Sorbjan and Grachev, 2010; Cantero *et al.*, 2022). Meanwhile during night-time, average ζ is ranged from -0.2 to 5.3, indicating a weakly-unstable to extremely-stable condition.

By contrast, the meridional wind component ($\bar{v}$) exhibited a strong diurnal cycle (Figure 3.2e, f). Diurnal shifts between positive (southerly) and negative (northerly) values of V occurred throughout the observation period, indicating sea and land breeze circulation, respectively. Compared to KKP, southerly to northerly shifts at the LLH building occurred later, and the periods of northerly (sea breeze) winds were shorter, strongly suggesting that the sea breeze propagates from north (KKP) to south (LLH). Sounding observations also provide evidence of these circulation patterns (Figure 3.2g, h). Meridional wind sounding at 07:00 LT showed dominant southerly winds at the lower level (1000 hPa), with weak winds at the upper level (850 hPa), indicating a shallow land breeze. Conversely, sounding observations at 19:00 LT indicated dominant northerly winds at the lower level and southerlies at the upper level, clearly indicating the sea breeze and its return flow aloft (anti-sea breeze), as also described in previous studies (Hadi et al., 2000; Hadi et al., 2002; Araki et al., 2006). Sounding data from December to February do not appear to show similar sea breeze circulation patterns, likely due to the shorter sea breeze duration (Figure 3.2e). Because Jakarta is situated on the northern side of Java Island, wind decomposition into its zonal and meridional components can be used to separate annual and diurnal circulation patterns. The zonal wind can be used to identify seasonal changes, and meridional wind to identify the sea breeze.

3.3.1 Determination of seasonal transition

Over the MC, seasons are typically categorised as dry or rainy according to the rainfall pattern (Tanaka, 1994; Hamada *et al.*, 2002; Chang *et al.*, 2005b). Transitions between the dry and rainy seasons are mainly driven by the monsoon regime change between the Asian winter (Australian summer) monsoon and Asian summer (Australian winter) monsoon (Chang *et al.*, 2005b; Belgaman *et al.*, 2017). Within the Southern Hemisphere MC, including Jakarta, the Asian winter monsoon carries considerably more moisture from the eastern Indian Ocean and northern MC, mainly the South China Sea (Suwarman *et al.*, 2013), thus inducing more rainfall over this area. Conversely, the Asian summer monsoon carries less moisture and produces less rainfall. Thus, the Asian winter monsoon regime is regarded as the rainy season, and the Asian summer monsoon as the dry season.

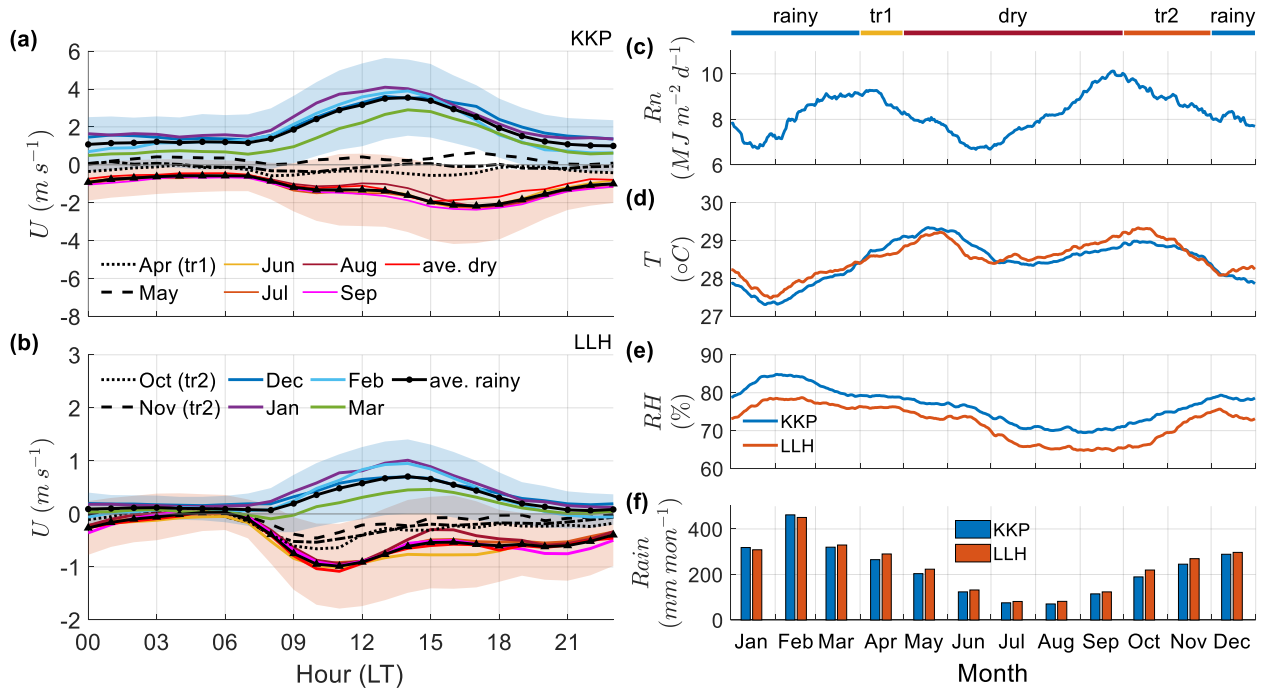

Figure 3.3 (Left) Diurnal time series of monthly averaged zonal wind speed (*U*) observed at the (a) KKP and (b) LLH buildings. Black lines with triangles (red shading) and circles (blue shading) indicate mean and standard deviation values during the dry and rainy periods, respectively. (Right) Multi-year (c) mean daily total net radiation, (d) daily average temperature, and (e) relative humidity (*RH*) measured at the (blue) KKP and (red) LLH buildings, and monthly accumulated rainfall obtained from the Global Precipitation Measurement (GPM) dataset. For image clarity, data were smoothed using a 31-day moving average filter. GPM data were averaged around each site using a 9-point average. Seasonal periods based on zonal wind are indicated at the top of the right panel.

Because the dry and rainy seasons are mainly defined in terms of rainfall, they vary among geographic locations, even within relatively short distances (Hamada *et al.*, 2002; Chang *et al.*, 2005b; Moron *et al.*, 2009; Ferijal *et al.*, 2022). Based on pentad (5-day) rainfall variation, Jakarta's climatology has been classified as A-I, which is dominated by an annual cycle and a rainy season from September to February (Hamada et al., 2002). However, when using this classification system, rainy season length varies among stations in Jakarta. For example, at coastal stations such as Tanjung Priok, the rainy season typically persists for 3 months (December–March), whereas at Halim, an inland station roughly 17 km from Tanjung Priok, the rainy season lasts for 5 months (November–April). To study the sea breeze, which can extend up to 80 km inland, a more robust definition of seasonal length is required.

In this study, the strong annual variation exhibited by zonal winds is used as a parameter to determine the lengths of seasonal periods in Jakarta. A diurnal time series of monthly averaged *U* observed at both sites shows clear seasonal separation (Figure 3.3a, b). A diurnal pattern characterised by dominant easterlies was observed from May to September, whereas the opposite pattern was observed from December to March. The transition periods, i.e., April, October, and November, are clearly distinguished by low winds throughout the day. By clustering these diurnal *U* patterns, the seasons in Jakarta are separated into a dry season from May to September and rainy season from December to March. Although this seasonal separation was based on wind data, the terms "dry" and "rainy" were retained because they are typically used to distinguish seasons in this region. In this study, the transition from the rainy to dry season in April is referred to as transition 1 (tr1), and that from the rainy to dry season in October or November is referred to as transition 2 (tr2).

The atmospheric conditions for several seasonal periods are shown in Figure 3.3c–f. The maximum daily total net radiation energy (R_N) occurred during the late dry season (September), with a second peak in April (Figure 3.3c). Minimum R_N values were observed in January during the rainy season and June during the dry season. The maximum and minimum R_N values appeared to follow the equinox and solstice, respectively. Annual daily mean *T* showed a similar pattern to R_N, but with a clear lag (Figure 3.3d). Peaks of *T* were observed in May (dry season) and October (tr2), whereas the minimum *T* values were observed in late January and July, following a net radiation minimum in June. Although the net radiation minima were similar in magnitude, minimum *T* values during the rainy season were much lower than in the dry season. This suggests

that another *T* regulatory mechanism, such as cold air advection, may dominate during the rainy season (Chang et al., 2005a). In tropical Jakarta, high *RH* values of > 60% were observed throughout the year (Figure 3.3e). The lowest *RH* values occurred in the last 3 months of the dry season (July–September), whereas the maxima occurred at the peak of the rainy season, from late January to early February. Maximum and minimum rainfall amounts were observed in February and July–September, respectively. Applying the wind-based seasonal period thresholds to the GPM rainfall data, we found that the monthly rainfall in Jakarta was < 200 mm/month during the dry season and > 300 mm/month during the rainy season.

3.3.2 Meridional wind variation and sea breeze identification

The seasonal mean meridional wind data shown in Figure 3.4a, b suggest that sea breeze circulation was dominant in both seasons. A northerly to southerly shift before noon and southerly to northerly shift after sunset were clearly observed at both sites. Hadi et al. (2002) argued that daytime enhancement of low-level northerlies during the rainy season was unlikely to have been caused by the sea breeze due to a lack of obvious land–sea temperature differences and subdued seaward return flow. However, a comparison of *T* at KKP and sea surface temperature (SST) near Jakarta (Figure 3.4c) showed that daytime land–sea temperature differences occurred in both seasons. While over land *T* shows significant variation between dry and rainy season, SST during both seasons does not differs significantly; thus, seasonal sea breeze variation in Jakarta might be primarily affected by temperature dynamics over land rather than over the sea.

The difference between diurnal change of surface temperature between rainy and dry season could also be seen from time-latitude plot (Hovmoller plot) of 2-m temperature from ERA5 dataset (Figure 3.5 a, b). Albeit the ERA5 dataset has quite low spatial resolution (~30 km), it shows that on average, there is a more than 4 ℃ difference between daytime and nighttime temperature over land, while only less than 1 ℃ difference over the sea. In the daytime, the air over land area is 2 to 4 ℃ higher than the air over the sea, hence driving the sea breeze regardless rainy or dry season. In nighttime, the situation is opposite, over land air temperature is colder than over the sea, thus the air flow from land to sea, creating the land breeze. It is important to note that, the ERA5 dataset has a quite low resolution. One grid of ERA5 could cover the entire Jakarta city (see Figure 3.5c), thus the effect of the city existence and finer detail on the sub-urban and rural area might not be represented very well. The 2-m temperature also does not account for potential pressure difference

between the sea or coastal area with higher ground elevation in the south like the Mt. Gede-Pangrango areas, which is more than 3000 m above the sea level. Up to 50 km from the coast however, this pressure difference might be negligible since the area is very flat. Hence, it might be not suitable to assess the strength of the sea or land breeze. Nevertheless, this dataset could give us general insight on the air temperature dynamic over the land and sea around Jakarta, while the strength of the sea and land breeze will be discussed based on the strength of meridional wind speed.

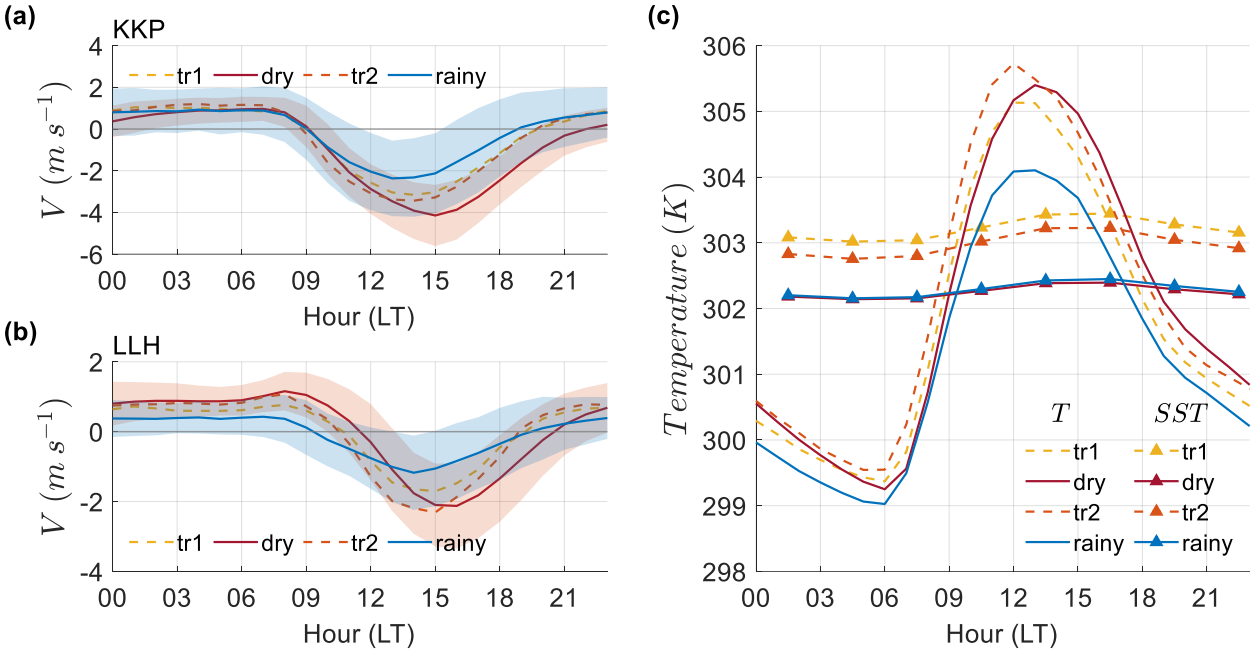

Figure 3.4 Seasonal average hourly meridional wind speed (*V*) observed at the (a) KKP and (b) LLH buildings, and seasonal average air temperature (*T*) at KKP and sea surface temperature (*SST*) on the Java Sea, north of Jakarta. Red and blue shading in (a, b) indicate standard deviations of *V* during the dry and rainy seasons, respectively.

The diurnal variation in peak northerly wind between seasons is shown in Figure 3.4a, b. The peak magnitude of northerly wind differed significantly between the dry and rainy seasons, whereas that during the dry season was nearly double that in the rainy season. We can also observe seasonal variation in the time of peak northerly wind, which occurred at approximately 13:00 LT in the rainy season and approximately 15:00 LT in the dry season at KKP. A similar transition was observed at LLH, but with a 1-h lag. These findings are in contrast with those of a previous study showing that the timing of the peak northerly anomaly did not vary seasonally (Araki et al., 2006).

nother striking feature revealed by comparing Figure 3.4a, b with Figure 3.2e, f is a clear discrepancy in the southerly to northerly shift between KKP and LLH. This shift occurred at approximately 09:00 LT at KKP, whereas its timing varied seasonally at LLH. At LLH, the shift occurred earlier in the rainy season than the dry season, suggesting seasonal variation in the V_{SBF}. The positioning of the KKP and LLH sites allowed us to estimate this parameter using the intrusion time and distance between sites.

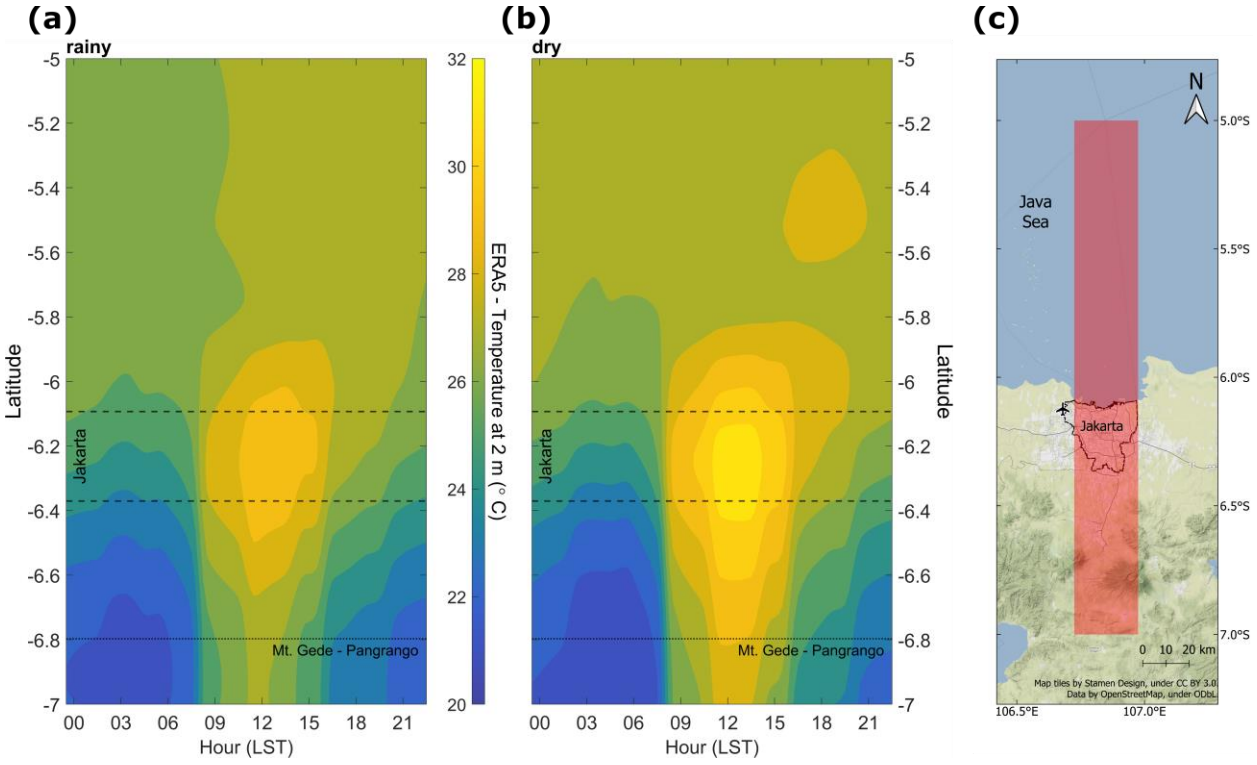

Figure 3.5 Time-latitude plot (Hovmoller plot) of 2-m temperature (T2m) from ERA5 dataset for rainy season (a), dry season (b), and the coverage map of the ERA5 grid for the plot (c). Width of the coverage in (c) is equal to 1-grid of ERA5 dataset, which is approximately 30 km.

To further investigate sea breeze seasonal variation, a dataset of selected sea breeze occurrences or sea breeze days is constructed. Sea breezes were identified based on front intrusions at each site. Front intrusion onset was indicated by a sharp change in meridional wind direction, accompanied by a rapid increase in humidity. Similar methods have been used in several previous studies (e.g. Hadi et al., 2002; Ferdiansyah et al., 2020; Jayakrishnan et al., 2021; Reddy et al., 2021). Because the Jakarta coastline runs in the east–west direction, it can be assumed that the sea breeze mainly blows from north (sea) to south (land). Hence, by decomposing the wind vector and

retaining the meridional wind component (V), it could be assumed that the sea breeze signal is isolated. To further screened out the influence of monsoon from the meridional wind, its daily mean is extracted, leaving only its fluctuation. The positive to negative shifts in the meridional wind fluctuation (V) is used to identify the onset of sea breeze intrusion, and the opposite shift to identify sea breeze cessation. The identification process is further refined by using the abrupt increase in relative humidity (RH) to clear-cut when the intrusion time of sea breeze occurs. If the meridional wind shift is detected but not followed by rapid increased in humidity, then it will not be considered as sea breeze signal. This step is necessary to ensure that only the sea breeze signal is retained and discard doubtful cases where the wind shift might be caused by other phenomena (Sumner, 1977).

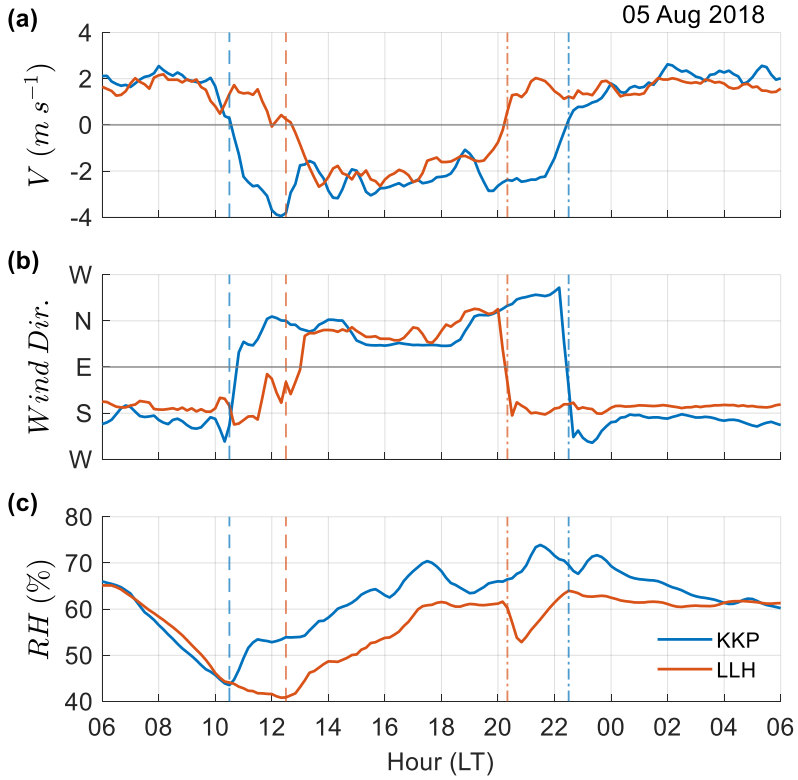

Figure 3.6 Example of 10-min averaged (a) V, (b) wind direction, and (c) RH observed at (blue) KKP and (red) LLH on August 5, 2018. Plots are smoothed using a 30-min moving average window. Vertical blue and red dashed lines indicate sea breeze intrusion times at KKP and LLH, respectively.

The calculated a daily 10-min average time series of the observation data is used to obtain a clearer understanding of the timing of sea breeze intrusion and cessation. Because significant

temperature drops were not typically observed during sea breeze intrusion in Jakarta, only V, wind direction, and RH were used for sea breeze identification. A representative daily time series of these factors for 5 August, 2018 are shown in Figure 3.6, where sea breeze intrusion occurred at approximately 10:30 LT (12:30 LT) at KKP (LLH) and sea breeze cessation occurred at approximately 20:10 LT (20:20 LT) at LLH (KKP). These thresholds were identified using a semi-automatic process for all available data; we applied a simple change detection algorithm followed by manual correction.

For V_{SBF} estimation, intrusion times for both sites were required; therefore, only days satisfying this requirement were retained in the dataset. Days with sea breeze intrusion detected at both sites were retained as sea breeze days; all other days were considered non-sea breeze days. For each sea breeze day, the cessation time at both sites was also identified. The cessation time of sea breeze is also regarded as the intrusion time of land breeze at each site. The sea breeze cessation time was identified only from V shifts because most data showed no obvious humidity changes during these periods. This might have reduced the accuracy of cessation time estimations; however, as most of the data indicate sharp wind direction shifts, as shown in Figure 3.6b, it is considered that the results are valid.

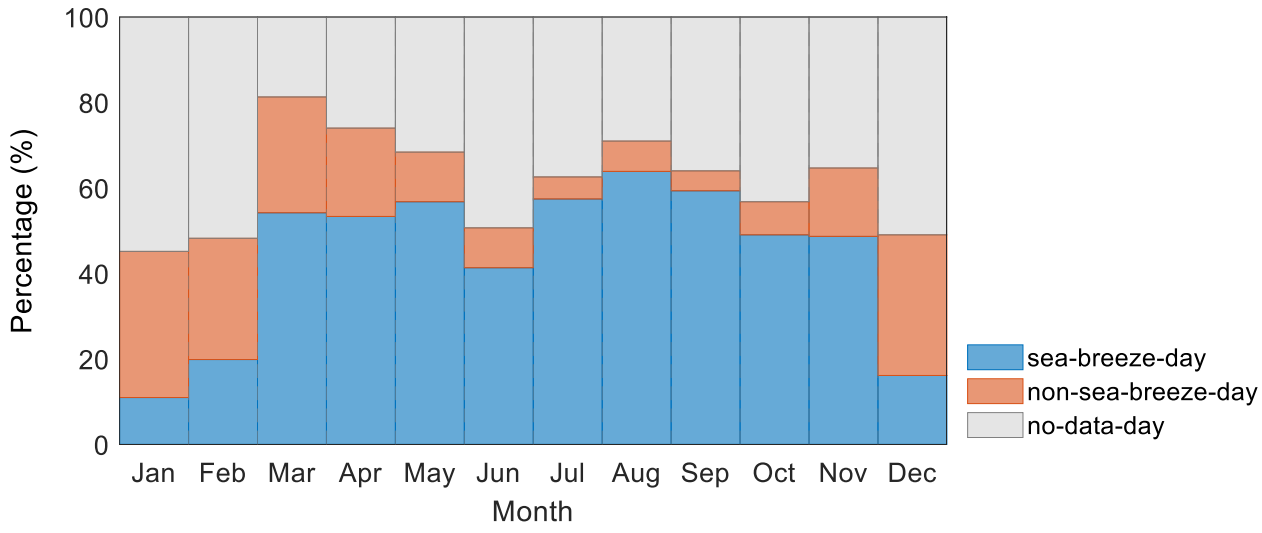

Figure 3.7 Monthly percentages of sea breeze days, non-sea breeze days, and days with no data from January 2017 to December 2021.

Among 1,121 days with available data throughout the observation period, 810 sea breeze days were identified. The percentages of sea breeze and non-sea breeze days are shown in Figure

3.7 Most sea breeze days occurred between March and November, consistent with the findings of previous studies (Hadi et al., 2002; Araki et al., 2006). Fewer sea breeze days were identified during December, January, and February. Araki et al. (2006) found that the sea breeze signal was less clear, but nevertheless distinguishable, during this period, especially on days with weak prevailing winds. Data were unavailable for many days during this period due to rainfall screening; thus, the number of sea breeze days was underestimated.

3.3.3 Seasonal variation in sea breeze

The monthly distribution of sea breeze intrusion times at both sites in Jakarta is shown in Figure 3.8. At KKP, sea breezes arrived earlier in the rainy season, and at tr2, than in the dry season and at tr1. If the sea breeze intrusion at KKP represents the sea breeze onset at Jakarta, then the sea breeze occurs faster in the rainy than dry season, although the earliest occurrence was in October (tr2). The interquartile range of sea breeze intrusion time shows fluctuation of approximately 0.5–1 h around the median value. The seasonal average intrusion time is provided in Table 3-2 and indicates an approximately 30-min difference in sea breeze onset between the rainy and dry seasons. This difference impacts sea breeze intrusion at LLH, where it arrives later during the dry season.

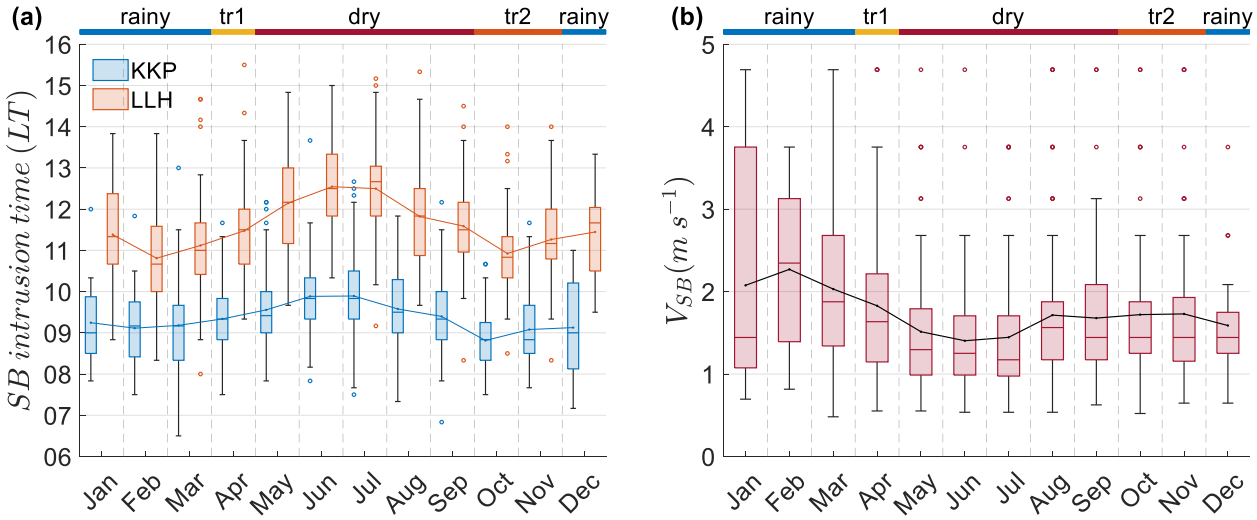

Figure 3.8 (a) Boxplot of sea breeze intrusion times at KKP and LLH and (b) sea breeze propagation speed (V_{SBF}). Dotted lines represent mean values for each month. Seasonal periods are indicated at the top of each plot.

Table 3-2 also shows the seasonal averages of sea breeze cessation time and duration. In this study, sea breeze duration was defined as the time difference between sea breeze cessation and intrusion at KKP, which was found to vary seasonally. At KKP, the cessation time was typically 19:00–19:30 LT, except in the dry season, when the sea breeze started late, but lasted until 21:00, i.e., for a longer duration (> 11 h) than in the rainy season (< 10 h).

The late sea breeze arrival at LLH during the dry season was caused by both late onset and lower propagation speed. The slowest sea breeze propagation was observed from May to July, and the fastest was in February (Figure 3.8). During the dry season, the average V_{SBF} was approximately 1.56 m s^{-1}, similar to previous observations based on satellite-derived cloud lines (Ferdiansyah et al., 2020). V_{SBF} was 0.55 m s^{-1} slower in the dry than rainy season (Table 3-2). The interquartile range of V_{SBF} also suggested that V_{SBF} tended to be higher during the rainy season.

Table 3-2 Seasonal averages of sea breeze characteristics observed in Jakarta.

Characteristic		tr1	dry	tr2	rainy
Avg. intrusion time (LT)	KKP	9:20	9:40	9:00	9:10
	LLH	11:30	12:10	11:10	11:10
Avg. cessation time (LT)	KKP	19:30	21:00	19:30	19:00
	LLH	18:50	19:30	18:20	17:40
Avg. duration (hour)		10.18 ± 2.2	11.30 ± 2.7	10.50 ± 2.6	9.80 ± 3.0
Avg. propagation speed (m s^{-1})		1.83 ± 0.9	1.56 ± 0.8	1.72 ± 0.8	2.01 ± 1.0

3.4 Discussion

3.4.1 Sea breeze onset

Based on equation (2.2), sea breeze onset depends on the rate at which positive ΔT between land and sea develops. Earlier sea breeze onset during the rainy season is likely caused by an earlier shift of ΔT, as clearly shown by the temperature difference between LLH and KKP (ΔTLLH–KKP) (Figure 3.9). The change from negative to positive ΔT occurred at approximately 07:30 LT in the rainy season but at approximately 09:30 LT in the dry season. A previous model simulation showed that sea breeze onset is sensitive to prior surface energy conditions (Junnaedhi *et al.*,

2021); thus, seasonal sea breeze variation can be explained using a surface energy budget. According to Oke *et al.* (2017), the surface energy budget over an urban area volume is defined as follows:

$$R_N + Q_F = Q_H + Q_L + \Delta Q_S + \Delta Q_A, \qquad (3.6)$$

where Q_H and Q_L are the sensible and latent heat flux, respectively, to or from the air, ΔQ_S is the change in above ground energy storage within the urban volume, which represents the heat capacity of all canopy elements, and ΔQ_A is the net energy added to or subtracted from the volume by advection. On the left-hand side of equation (3.6), Q_F is the anthropogenic heat flux, which is the heat released within the volume by human activities, and R_N is the net radiation at the surface, which is the sum of net shortwave (R_S) and net longwave (R_L) radiation, calculated as follows:

$$R_N = R_S + R_L = S_d - S_u + L_d - L_u, \qquad (3.7)$$

where S and L are shortwave and longwave radiation, respectively, and subscripts u and d are the upward and downward radiation components, respectively.

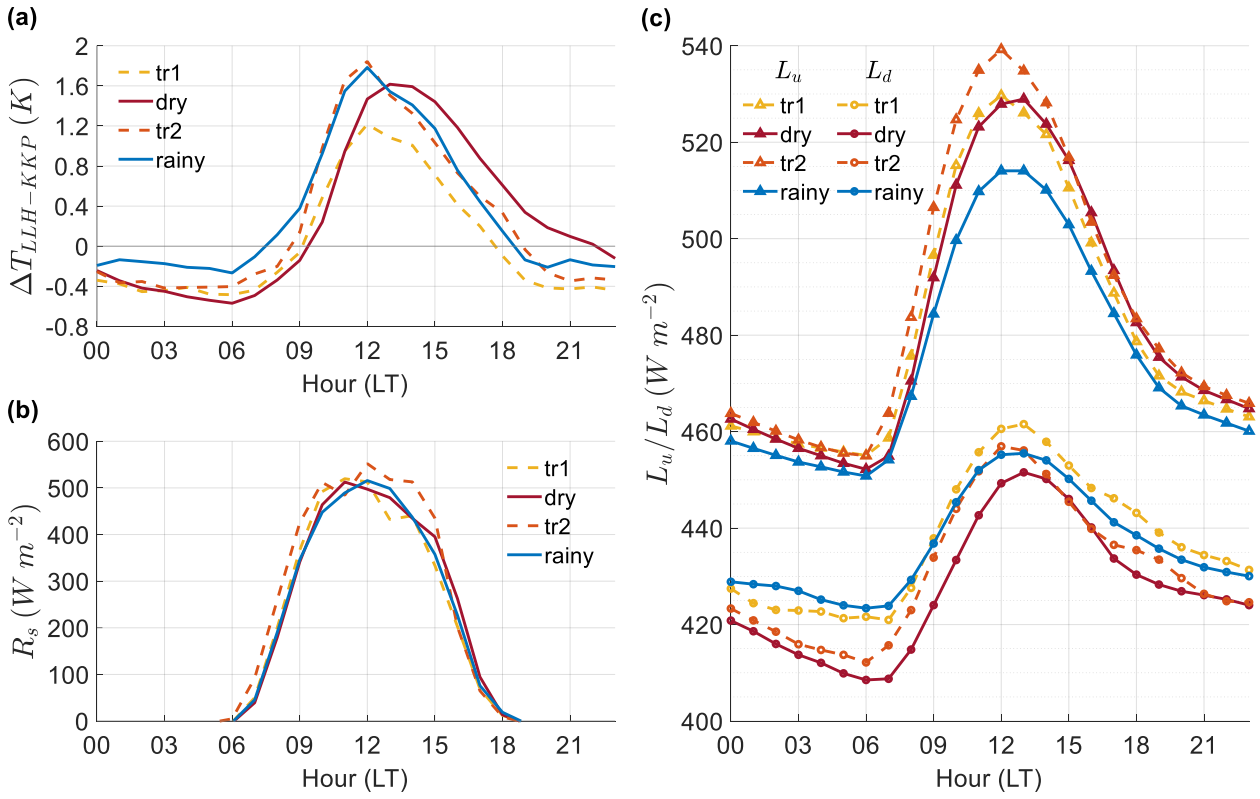

Figure 3.9 (a) Seasonal average hourly temperature differences between observations taken at LLH and KKP ($\Delta T_{LLH-KKP}$). (b) Net shortwave radiation (R_s) and (c) upward and downward components of longwave radiation (L_u and L_d) at LLH.

In the morning, prior to sea breeze onset, R_S observations in Jakarta showed no significant difference between the dry and rainy seasons (Figure 3.9b). Assuming little seasonal variation in anthropogenic heat production at this hour, discrepancies in $\Delta T_{LLH–KKP}$ may be attributed to variation in R_L during early morning before the sun rises. Downward longwave radiation (L_d) was higher in the rainy than dry season, whereas upward longwave radiation (L_u) showed slight variation between seasons (Figure 3.9c). This indicates that downward influx was more prominent than surface cooling prior to sea breeze onset. Downward radiative longwave influx, i.e. downwelling, is mainly derived from clouds (Arya, 2001). These cloud usually form in the afternoon and move offshore via the land breeze (Mori *et al.,* 2018), or may develop close to shore due to land breeze and monsoon convergence (Wu *et al.,* 2007). Early morning cross-shore clouds that scatter across the city can reduce temperature differences by distributing heat between the coast and inland areas, which induces a positive ΔT more rapidly when shortwave radiation (*Rs*) is available, ultimately causing earlier sea breeze onset.

By contrast, post-midnight ΔT values were more negative during the dry than rainy season as illustrated in Figure 3.10. More negative ΔT values indicate inhomogeneous cooling rates between coastal and inland areas. Between 00:00 and 06:00 LT, the average observed temperature dropped by 1.2 and 1.5 K at KKP and LLH, respectively. Dryer surfaces cause more intense radiative cooling during the night over inland areas, whereas coastal areas are warmer due to the proximity to the sea. If few or no clouds are available to distribute heat, strong negative cross-shore temperature differences occur before sunrise, such that more time is required for a similar amount of *Rs* (Figure 3.9) to overcome negative ΔT, thus delaying sea breeze onset.

To further analyse the effect of clouds downwelling on the sea breeze onset, its necessary to check the horizontal temperature gradient along the sea breeze path (north-south direction), before and after sea breeze onset. First it should be noted that the SST in Jakarta's offshore, which acquired from Woods Hole Oceanographic Institution (WHOI) Climate Data Record (CDR) (Clayson *et al.,* 2016), is not varied significantly across season. As depicted in Figure 3.10a, the SST shows overlapping lines between dry and rainy season. Hence, the SST difference between dry and rainy season is considered negligible. Due to the thermal properties of large water bodies, the near surface air temperature over sea usually more homogeneous and less varying (Pielke, 1981). Based on study by Feng *et al.* (2018), the average near surface air temperature in tropical

areas is 2.5 K lower than its SST and its follows the SST quite well. Thus, it could be assumed that the air temperature above the sea near Jakarta would also not vary across dry and rainy season.

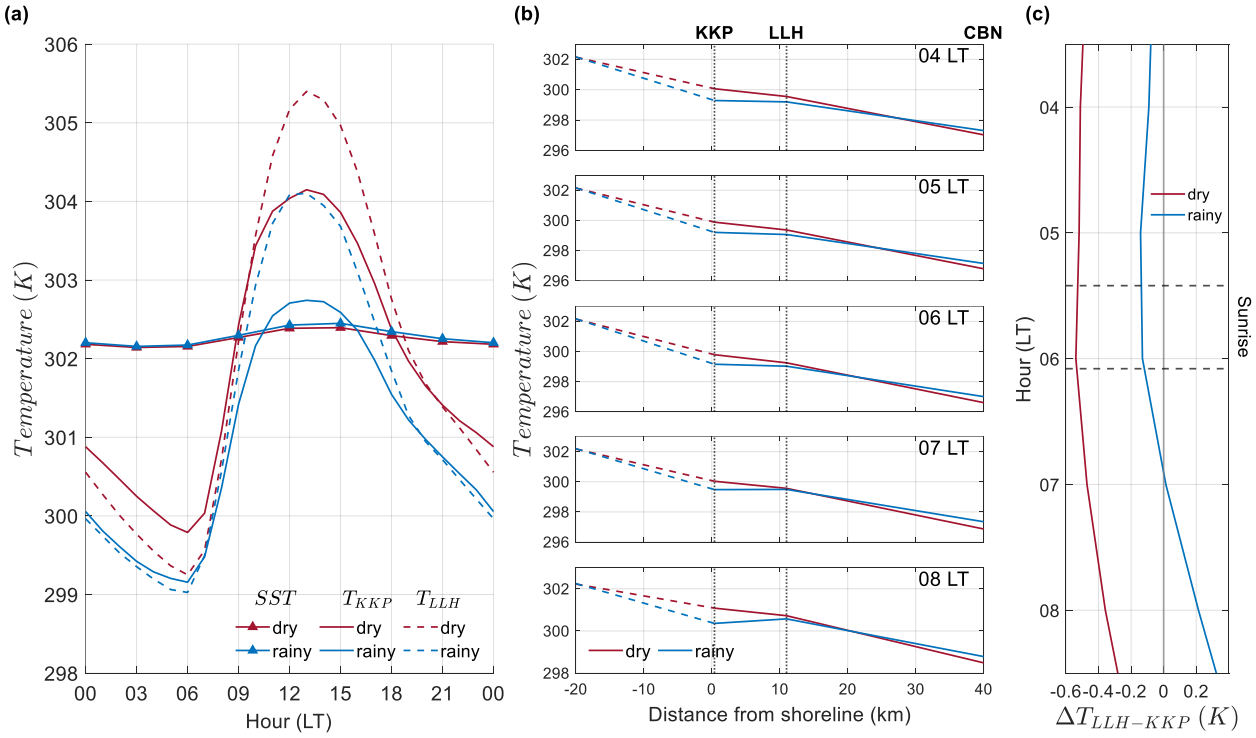

Figure 3.10 (a) Diurnal comparison between seasonal averaged SST and air temperature at KKP and LLH; (b) horizontal near surface temperature profile in north-south direction from observation at KKP, LLH and additional observation at Cibinong (CBN) between 04 LT and 08 LT; and (c) temperature difference between LLH and KKP ($\Delta T_{LLH-KKP}$) during same period as in (b).

Combining the estimation of air temperature over sea and the observed air temperature at KKP, LLH and an additional temperature observation at Cibinong (CBN), around 30 km south of LLH, the horizontal profile of near surface air temperature across Jakarta is presented in Figure 3.10b. From Figure 3.10b, it can be seen that before sunrise there is always a temperature gradient over the land with lower temperature inland and higher temperatures over the coastal area. This gradient occurs because inland areas cools faster than coastal area due to its vicinity to a large water bodies (Pielke, 1981; Stull, 1988). Over coastal Jakarta, temperatures during rainy season are always lower by 0.4 to 0.8 K with standard uncertainty of ±0.03 K, compared to dry season. However, over inland areas (CBN), the temperatures are always higher by 0.2 to 0.5 K with standard uncertainty of ±0.25 K. It is important to note that there is a significant difference in the

uncertainty of these values. This difference comes from the different instruments used at each site. Measurements in Jakarta (KKP and LLH) are conducted using Vaisala HMP155, which has an average accuracy of 0.2 K, at 10 Hz sampling rate or in other words sampled every tenth of a second (detail specification of instruments can be found on Table A1 in Appendix A). Since the mean temperature value is calculated from an hour of measurement, the number of samples is around 36000. With the samples maximum standard deviation is around 4.85 K from the mean value, the maximum standard uncertainty (Bell, 2001) of temperature measurement in these two sites are very low, only less than ±0.03 K at 95% level of confidence. On the other hand, temperature measurement at Cibinong (CBN) is measured using Atmos41 weather station which has lower accuracy at 0.42 K and output interval every 5 minute although internally sampled every 10 second. The maximum standard uncertainty of this measurement at 95% level of confidence is ±0.25 K, which is much higher than measurements at KKP and LLH. Nevertheless, the measurement at CBN is still useful for providing relative comparison of mean temperature between inland and coastal area of Jakarta.

In the dry season the temperature gradient is higher because of higher coastal temperature and lower inland temperature. On the contrary, the gradient in rainy season is less due to heat distribution by clouds downwelling across the land area. However, the clouds are not evenly distributed across the land. In the early morning, most of the clouds were concentrated over central and southern Jakarta after it marched meridionally from coastal areas (see Figure 6 in Mori et al., 2018). There were also less clouds in the coastal areas. After sunrise, the cloud concentration over Jakarta disappears, except for some thin clouds over the coastal areas. Thus, the temperature distribution by downwelling might not be homogeneous through land areas but concentrated over Jakarta central and south area. As seen in Figure 3.10b, the temperature gradient between LLH and KKP is 'flatter' during the rainy season than during the dry season.

Difference between the dry and rainy season can be clearly seen from temperature difference between LLH and KKP ($\Delta T_{LLH–KKP}$) presented in Figure 3.10c. The $\Delta T_{LLH–KKP}$ during dry season (red line) is more negative than during rainy season (blue line). After the sunrise, which usually occur around 05:30 – 06:00 LT, overland temperature increases. Just around 1.5-hour after sunrise, $\Delta T_{LLH–KKP}$ during rainy season already become positive, while $\Delta T_{LLH–KKP}$ during dry season is still negative. This will cause the sea breeze to start earlier in the rainy season than dry season.

3.4.2 Sea breeze propagation speed

Seasonal variation in V_{SBF} peaked during the rainy season (February) and reached a minimum in the dry season (June) (Figure 3.8b). To assess seasonal variation in V_{SBF}, we used equation (2.3) to estimate V_{SBF} from $\Delta T_{LLH–KKP}$ using V measured at LLH as V_g, and estimated h using the H_{bl} from the ERA5 dataset. Then, V_{SBF} was estimated 30 min after sea breeze intrusion at KKP, under the assumption that temperature at KKP during this time can be used to represent sea breeze gravity current temperature and the front was still located between KKP and LLH. These estimated V_{SBF} values were termed $V_{SBF(est)}$, and those obtained from detected meridional wind and humidity changes were termed $V_{SBF(obs)}$.

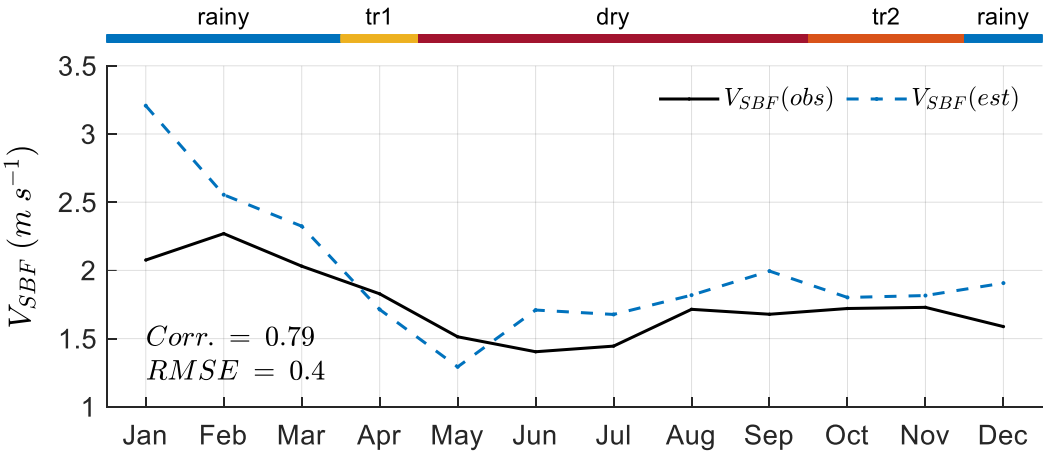

Figure 3.11 Monthly composite of observed ($V_{SBF(obs)}$) and estimated ($V_{SBF(est)}$) sea breeze front propagation speed.

Direct comparison of $V_{SBF(est)}$ and $V_{SBF(obs)}$ on a daily basis does not yield a clear relationship due to various factors not reflected in the V_{SBF} estimation, which assumes homogeneous density of both the sea breeze current and ambient air; however, density actually varies across the respective air masses. Another influential factor is the use of surface-level variables, which are prone to the effects of super adiabatic-layer and surface-layer turbulence (Reible *et al.*, 1993). The magnitude of $V_{SBF(est)}$ is also sensitive to sea breeze depth (h). To match the magnitude of $V_{SBF(obs)}$, we determined an optimum h value of 0.75 H_{bl}. Despite these, however, monthly composite of $V_{SBF(est)}$ and $V_{SBF(obs)}$ showed remarkably similar patterns (Figure 3.11), with higher propagation speed during the rainy season and lower speed during the dry season and transition periods. This demonstrates that equation (2.3) is still applicable for estimating the V_{SBF} at monthly and seasonal

time scales.

The separation of components in equation (2.3) clearly confirms the dependence of V_{SBF} on the temperature difference (Figure 3.12a), as $\Delta T/T$ is clearly higher in the rainy season than during other periods, such that the V_d (first term) is also higher. This result corresponds well with the observed V_{SBF} values (Figures 3.8b and 3.11). In the dry season, $\Delta T/T$ was significantly lower; therefore, V_{SBF} was also lower. However, observed and estimated V_{SBF} also increased slightly in August and September, respectively, which was attributed to higher h (Figure 3.12b). Seasonal variation in h showed the opposite trend to $\Delta T/T$. As temperature is higher during the dry season (Figure 3.3d), H_{bl} was also higher; therefore, sea breeze depth was greater. Although seasonal variation in h varied significantly, it did not significantly affect the seasonal variation of $V_{SBF(est)}$. The seasonal pattern of $V_{SBF(est)}$ was still greatly affected by the temperature difference.

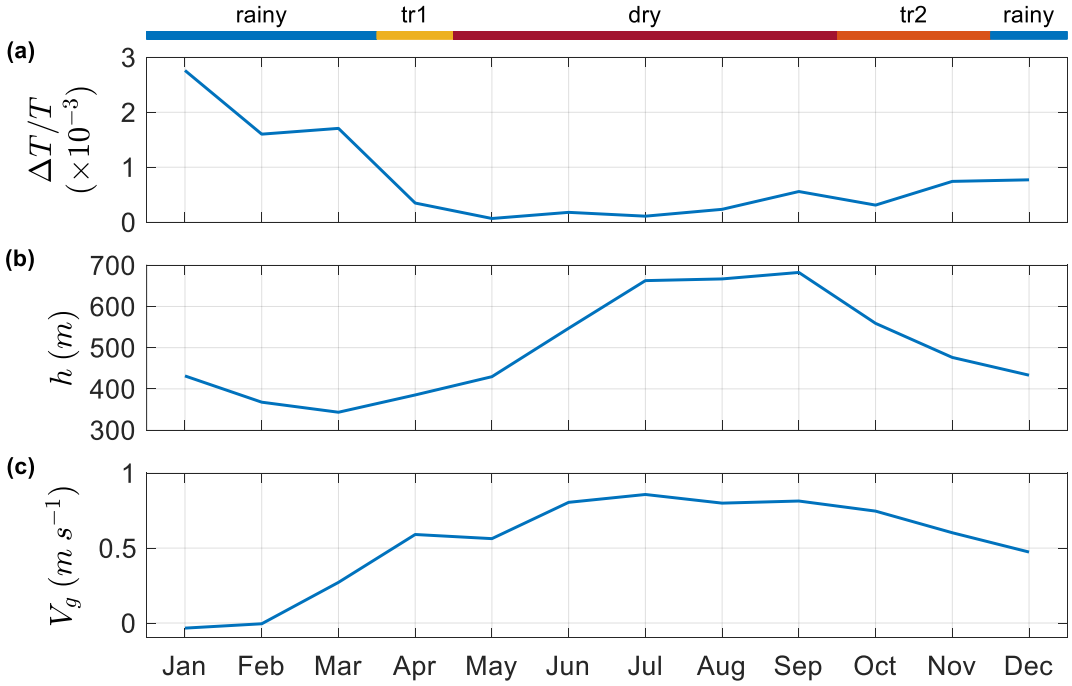

Figure 3.12 Monthly composite of (a) normalised temperature difference ($\Delta T/T$), (b) sea breeze depth (h), and (c) opposing flow (V_g), which were used to calculate $V_{SBF(est)}$ according to equation (2.3).

The opposing flow (V_g), i.e. the land breeze, was also driven by negative ΔT during the previous night. As shown in Figure 3.11c, the opposing flow was weaker in the rainy than dry season; thus, the SBF moved faster in the rainy season. In January and February, the opposing flow was negligible; thus, the V_{SBF} was equal to the V_d. Post-midnight heat distribution via cloud

downwelling in the rainy season caused less negative ΔT and weakened the land breeze, whereas more negative ΔT in the dry season produced stronger opposing flow, which reduced the V_{SBF}. These findings confirm that overland temperature difference is the main factor governing sea breeze seasonality in Jakarta.

3.4.3 Sea breeze duration

Longer sea breeze duration in the dry season was caused by prolonged positive ΔT during the night (Figure 3.9a). After dawn, positive ΔT was maintained by higher sensible heat release in the urban core area compared to the coast (Figure 3.13a and b). At KKP, Q_H dropped rapidly below 20 W m^{-1} after 18:00 LT, whereas at LLH, Q_H remained higher than at KKP until 22:00 LT. This discrepancy maintained the temperature differences between the urban core and coast, which ultimately prolonged sea breeze flow. In the rainy season, Q_H at both sites dropped to a similar value around sunset, such that positive ΔT was no longer sustained and the sea breeze flow ceased.

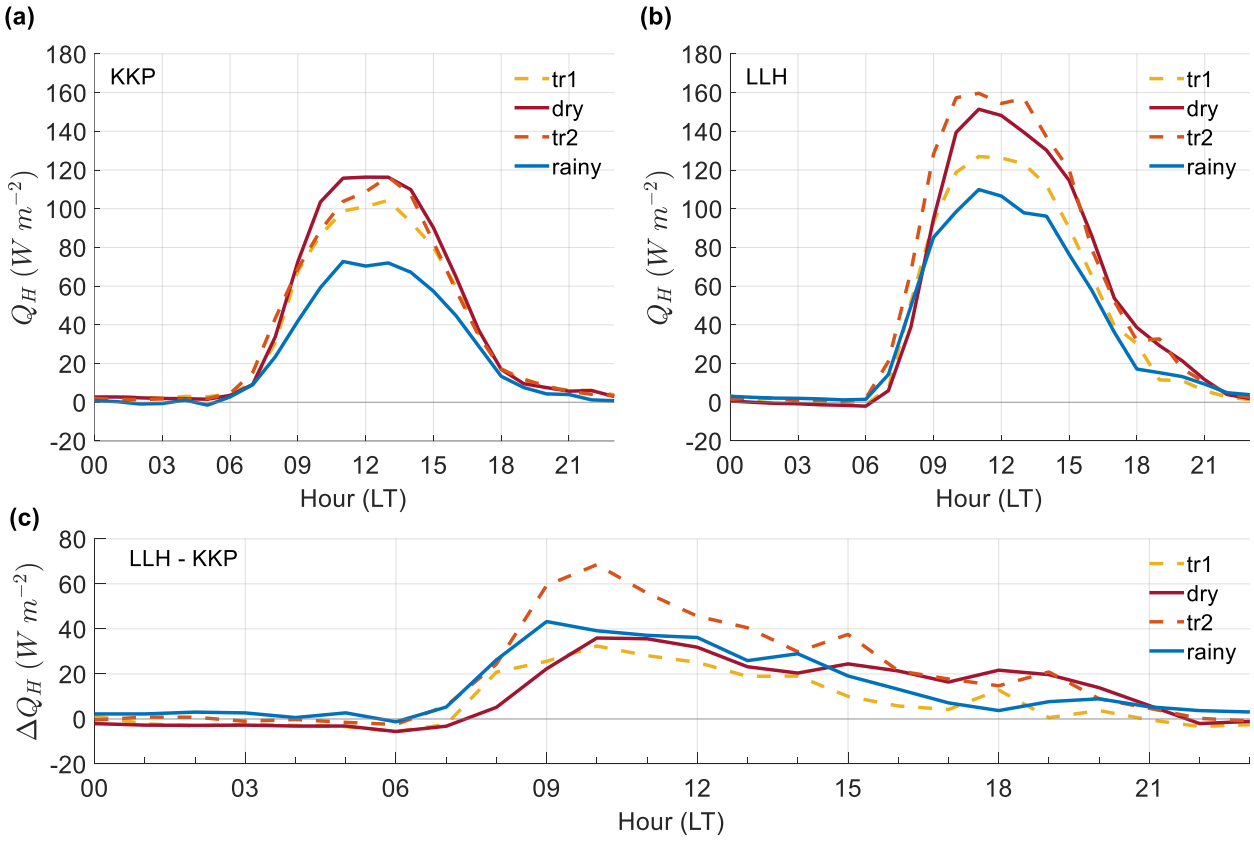

Figure 3.13 Seasonal average of hourly sensible heat flux (Q_H) observed at (a) KKP and (b) LLH, and (c) seasonal Q_H difference between LLH and KKP.

In the absence of incoming *Rs*, night-time heat release is mainly derived from the energy storage (ΔQ_S) term in equation (3.6). In the dry season, longer sensible heat release in LLH was caused by the higher thermal inertia of urban surfaces, due to the urban volume could store more energy during the daytime and release it over a longer period during the night (Grimmond and Oke, 1999b; Oke *et al.*, 2017). Conversely, coastal Jakarta has less thermal inertia, as it mainly comprises residential and recreational areas, whereas the larger vegetated areas and proximity to the sea significantly suppress the night-time Q_H release in preference for Q_L release. Thus, night-time sensible heat (Q_H) release over coastal Jakarta did not differ significantly among seasons (Figure 3.13a), demonstrating that urban areas can alter sea breeze duration, particularly during the dry season. During the rainy season, rainfall, which usually occurs from afternoon until midnight (Renggono *et al.*, 2001), wets urban surfaces such that Q_L release is preferable to Q_H release. Thus, night-time Q_H release over the urban area is reduced and positive ΔT values are dispersed, such that the sea breeze effectively ceases at earlier time. This seasonal discrepancy in duration may indicate significant effect of urban area of Jakarta to the seasonality of sea breeze.

3.4.4 Influence of urban area to seasonal sea breeze variation

While V_{SBF} estimation using equation (2.3) confirm that temperature difference overland and strength of opposing flow are the main factor in sea breeze seasonality, it did not consider many realistic physical settings and urban properties that influence sea breeze, such as topography, coastal orientation, surface friction, surface heating and urban heat island (UHI) circulation. Exclusion of such factors is causing the $V_{SBF(est)}$ to tend to be overestimate the $V_{SBF(obs)}$. Among the aforementioned factors, topography and coastal orientation might not have a significant effect to sea breeze propagation over Jakarta. Averaged topographical slope of Jakarta is less than 1.9 m km^{-1} in the inland direction (Badan Informasi Geospasial, 2018), thus can be considered almost flat. Along Jakarta Bay's coast, sea-breeze-associated-cloud-line was observed moving in similar speed, at least before reaching city center (Ferdiansyah *et al.*, 2020). On the other hand, surface friction induced by urban roughness elements, such as buildings, structures, and trees, may have more effect on V_{SBF}. Using building-resolving computational fluid dynamics (CFD) simulation with plan area density (λ_p) 0.25, Jiang *et al.* (2017) showed that increasing average buildings height by 40 m could reduce V_{SBF} by 16%. The average building height in Jakarta is between 5 m and 20 m, and the averaged λ_p is 0.2 (Darmanto *et al.*, 2017), thus we expect the reduction of V_{SBF}

due to urban roughness will be less than 16%. This reduction, however, may not contribute to seasonal variation of V_{SBF} as the urban roughness element can be assumed constant throughout the year.

Instead of roughness, surface air temperature variation due to urban existence may have more influence on the sea breeze. This variation may cause stronger land breeze, induce urban heat island (UHI) circulation, or slowing down the sea breeze propagation. These effects will be discussed in the following sub-section.

3.4.4.1 Early morning urban heating effect to land breeze

As shown in Figure 3.5, in the early morning between 00 and 06 LT, there is always a positive temperature gradient between coastal area and inland areas that drive the land breeze in similar manner with the sea breeze. Cold air is heavier than warm air, hence the air flows from inland areas to the coastal areas up to the sea. In the presence of urbanized areas, the land breeze flow might be modified. To assess this, we should isolate the effect of urban existence and compare it to (imaginary) situations where the urban areas do not exist, regardless of seasonal variation. In the night time and early morning, the urban areas tend to be warmer than rural areas because its unique heterogeneities of morphologies and surface material can increase its thermal inertia and prolong the heat release even after the sunset (Grimmond and Oke, 1999b; Oke *et al.*, 2017). Furthermore, urban areas still emit heat in the nighttime via energy conversion which is regarded as anthropogenic heat (AHE). Based on the anthropogenic heat (AHE) estimation by Varquez *et al.* (2021), the nighttime excess heat released in Jakarta could reach between 10 and 20 Watt m^{-2}. With that being said, there is a high probability that the existence of Jakarta city will strengthen the land breeze that is coming from the southern inland area.

In the case of Jakarta, the city of Jakarta can be considered as (mostly) in the coastal areas and the rural area of Bogor is considered as inland areas. As illustrated in Figure 3.14, without the presence or effect of urban areas, the horizontal temperature profile in the early morning will perhaps follow the blue line, assuming it follows the mean temperature values according to ERA5 reanalysis dataset (Figure 3.5). The temperature difference between coastal and inland areas in this case could be between 4 to 6 ℃. Based on observation dataset, however, the temperature difference between coastal area (KKP) and city center area (LLH) is only 0.2 to 0.8 ℃ (Figure 3.9a). Hence, the existence of Jakarta city will alter the horizontal profile into the shape shown by the red line where there is a slight increase in the temperature over the city (see Figure 3.14). This modification

will make the temperature gradient between coastal area and inland area slightly higher. This effect will increase the strength of the land breeze, which eventually weakens the sea breeze propagation.

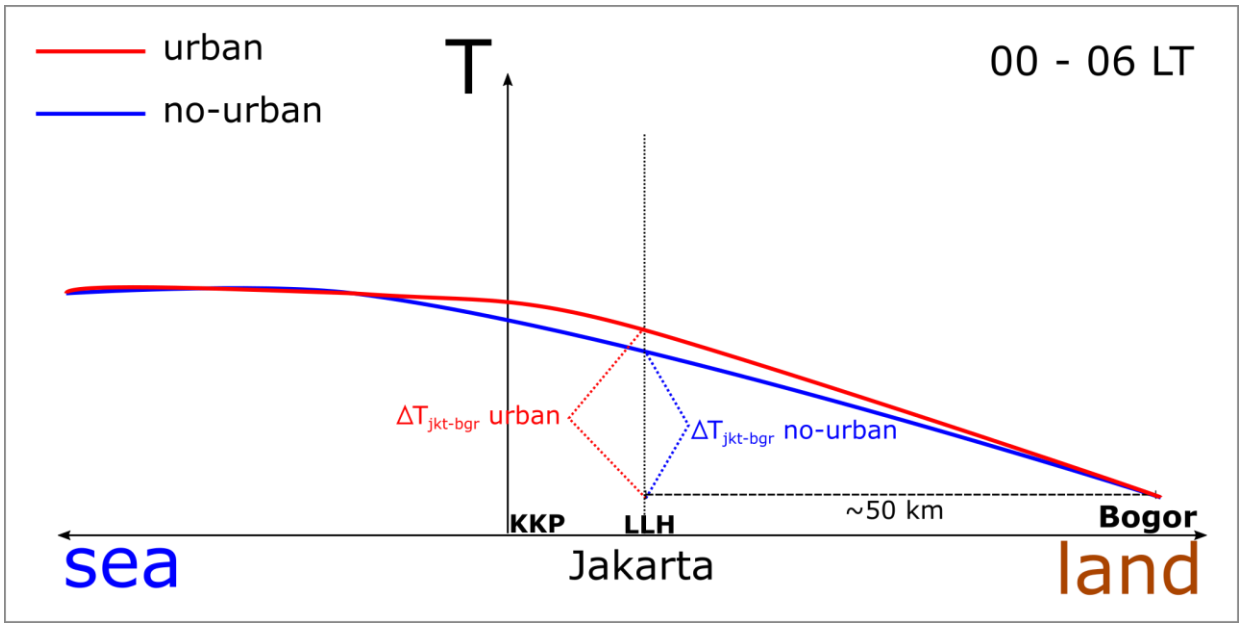

Figure 3.14 Hypothetical and idealized illustration of horizontal temperature distribution during early morning time along sea, coastal and inland areas around Jakarta, with (red) and without (blue) the urban area of Jakarta. The observation sites at KKP and LLH are indicated, and the inland area of Bogor (~50 km south) is considered as a rural area.

The effect of this strengthening is more dominant in the dry season than the rainy season. In the dry season, most of the energy stored by the urban fabrics and the AHE will be released as sensible heat flux which increases the air temperature. However, during the rainy season, these energies will be mostly depleted via latent heat release due to wet surfaces, hence the contribution for heating the air might be negligible (Oke *et al.*, 2017). The heating effect of urban areas to the land breeze is not the same as the heating effect of clouds downwelling as explained previously. Urban areas heating is occurring locally inside the urban perimeter, but the clouds downwelling process spreads the heat through all land areas, from inland to coastal areas (Mori *et al.*, 2018). Thus, urban areas heating only increases air temperature over the urban areas, making the gradient with inland areas higher and strengthening the land breeze. On the other hand, clouds downwelling lift all the horizontal temperature profile, making the gradient with inland areas lower and weakening the land breeze.

3.4.4.2 Morning urban heat island (UHI) circulation and sea breeze onset

The urban existence or urbanization is not only influential to the air condition in the nighttime or early morning. In the morning after the sunrise, the urban areas usually heat up faster because of lower albedo and higher absorptivity/emissivity, especially inside the urban core area (Oke *et al.*, 2017). This will create an imbalance temperature distribution between the city center and the city boundaries. This imbalance can produce the morning time UHI circulation. UHI circulation is commonly found in urban areas that exceed 10 km in width (Yoshikado, 1994). Since the width of Jakarta city is more than 10 km, there is a possibility that UHI circulation occurs over the city.

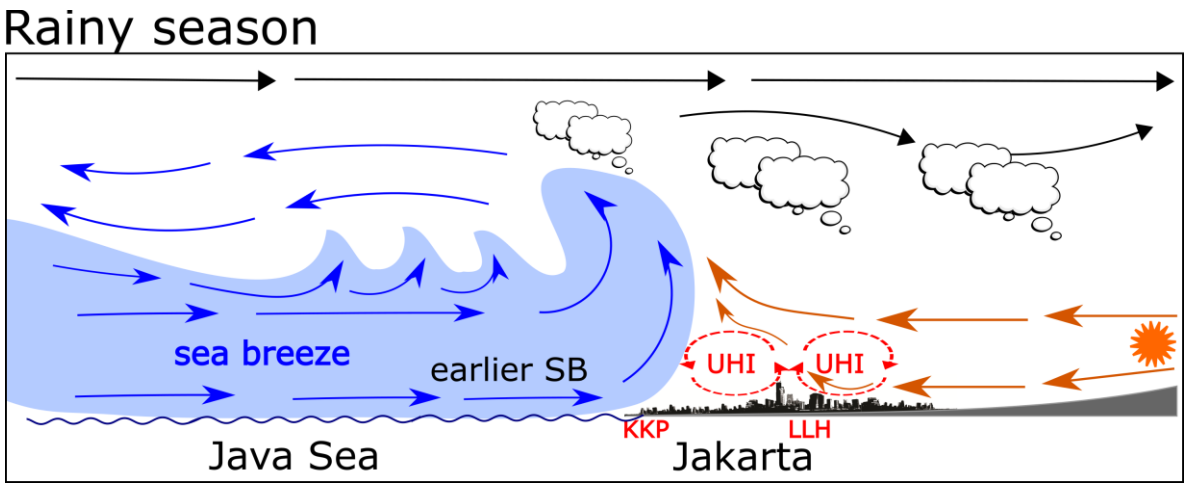

Figure 3.15 Schematic illustration of morning UHI circulation during rainy season that induce earlier sea breeze onset.

To produce UHI circulation in relatively weak background winds like morning time, only a minimum of 20 W m^{-2} excess of heat flux over urban core area is needed (Wang *et al.*, 2019). Prior to sea breeze intrusion at the coastal area (KKP), which typically occurs around 09.00 LT (Table 3-2), the sensible heat flux difference (ΔQ_H) between urban area and coastal area (LLH - KKP) could reach up to 40 W m^{-2} in the rainy season, but only less than 20 W m^{-2} in the dry season (Figure 3.11c). This observation suggests that a morning UHI circulation may be mostly developed in the rainy season than the dry season. As illustrated in the Figure 3.15, the existence of UHI circulation in the morning can accelerate sea breeze intrusion on coastal side but also accelerate the land breeze on inland side of the city (Yoshikado, 1992; Cenedese and Monti, 2003). The effect will causing an earlier sea breeze onset and faster propagation of sea breeze up until reaching the

city center. Using numerical model simulation, Tokairin *et al.* (2010) found that increasing urbanization in Jakarta is causing a more earlier sea breeze development. This result is consistent with the findings that the sea breeze onset during rainy season is earlier, which may be attributed to the existence of morning UHI circulation.

It is also important to note that the merge between sea breeze front and UHI upward flow over Jakarta's urban core area (e.g., LLH) might slow sea breeze propagation when reach this area. Previous studies showed that sea-breeze-associated-cloud-lines move faster in the west and east sides of Jakarta when it reaching the urban core area (Ferdiansyah *et al.*, 2020). However, once the SBF passing the city center, the propagation speed will increase again as the UHI circulation diminished and the opposing land breeze is already weakened due to more homogeneous air temperature distribution over land (Yoshikado and Kondo, 1989; Yoshikado, 1992; Varquez *et al.*, 2015; Wang *et al.*, 2019). Thus, it could be summarized that the morning UHI circulation will cause an earlier sea breeze onset and faster propagation speed until it reaches the city center, but slows it down temporarily until it passes the city center.

3.4.4.3 Surface heating intensity and sea breeze propagation speed

As the sea-breeze-gravity-current propagating the land area, it will continuously heat by the land surface at an increasing rate (see illustration in Figure 3.16). This process will creating an internal temperature gradient within the interior of the cold-gravity-current. This gradient then will induce internal vorticity, which strengthening surface wind speed inside the gravity current. As the front side of the gravity current is heated at longer time, the temperature difference across the front is reduced, thus effectively slowing the front propagation speed (Robinson *et al.*, 2013). V_{SBF} estimation in equation (2.3) assumes sea breeze gravity current move with nearly constant internal temperature. In reality, the internal temperature of the gravity current is change as it propagates inland. That is why the estimated sea breeze propagation speed ($V_{SBF(est)}$) is tend to be overestimate (Figure 3.11), as the equation does not count for this internal temperature change.

Surface heating rate variation across season may have more effect on seasonal variation of sea breeze propagation in Jakarta. Daytime surface heating rate (represented by Q_H in Figure 3.13a and b) in dry season is higher than rainy season, with peak-to-peak difference up to 40 W m^{-2}. In the rainy season, Q_H release over the urban area is reduced significantly by rigorous Q_L release due to wet surface (Oke *et al.*, 2017). Taking account this surface heating difference, it is expected that in dry season V_{SBF} will be slower than in the rainy season due to more rigorous surface heating.

Observed surface sea breeze wind speed (Figure 3.4a and 3.4b), which shows higher speed in the dry season than rainy season, also indicates the effect of continuous surface heating onto the sea breeze propagation speed as studied by Robinson *et al.*, (2013).

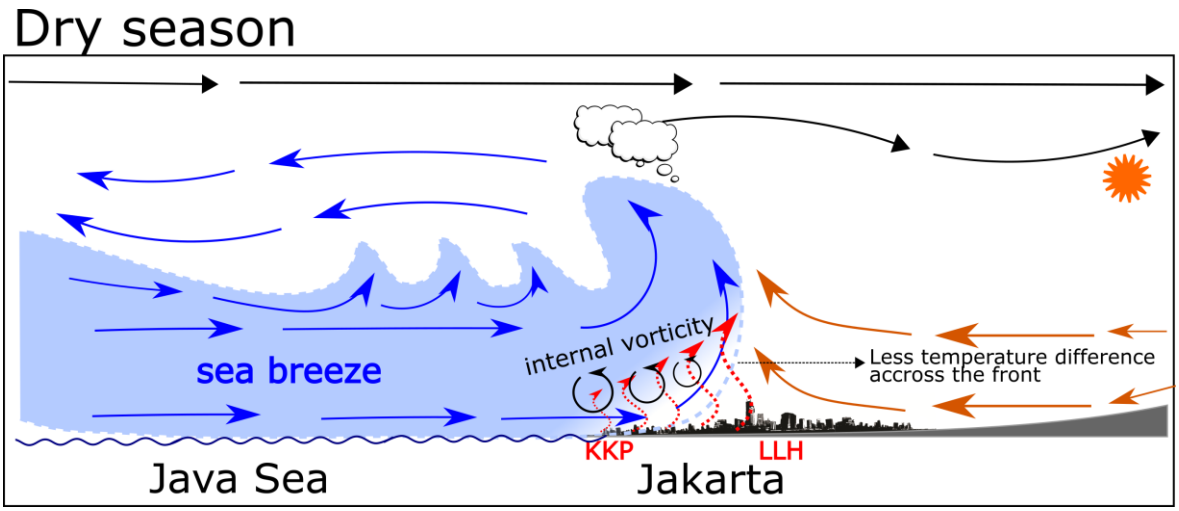

Figure 3.16 Illustration of land surface heating effect to the propagation of sea breeze gravity current during dry season, based on research of Robinson *et al.* (2013).

3.4.4.4 Note on influence of urban area to seasonal sea breeze variation

Although the current observation data in Jakarta shows some evidence on the influence of Jakarta city existence to the sea breeze variation, it is still not adequate to quantitatively assess the effect such large urban area to sea breeze. To fully assess such urban effect, additional observations outside the urban area of Jakarta will be required. This observation is necessary to make the comparison with the existing urban observations. Such comparison could be used to confirm the significant impact of urban area development and urbanization to sea breeze onset and duration. Furthermore, to account for previously discussed surface heating effect, the use of very high-resolution numerical simulations with closely realistic physical setting might also be necessary. While these requirements might not be achieved in the current study, it will be planned for future study. As indicated by many studies (Siswanto *et al.*, 2016, 2022; Wati and Nasution, 2018; Lestari *et al.*, 2022), the rapid changing environment of Jakarta may have been changing many natural aspects of the atmospheric condition. Thus, it is important to quantify such effects on the atmospheric condition of Jakarta to formulate the optimum mitigation policy to deal with it.

3.5 Summary and Conclusion

In this research, seasonal variation in the characteristics of the sea breeze in Jakarta using multi-year near-surface observation data for wind, temperature, humidity, and radiation is analyzed. Observations were conducted from March 2017 to October 2021 at two urban sites in Jakarta, namely KKP and LLH, which are located on the coast of Jakarta Bay and in the urban core, respectively, separated by a distance of approximately 11 km in the cross-shore direction, such that sea breeze propagation between them could be measured. Decomposed wind observations showed a strong relationship between diurnal zonal wind and annual circulation, which was used to differentiate the dry (May–September) and rainy (December–March) seasons in Jakarta, separated by transition periods in April (tr1) and October–November (tr2).

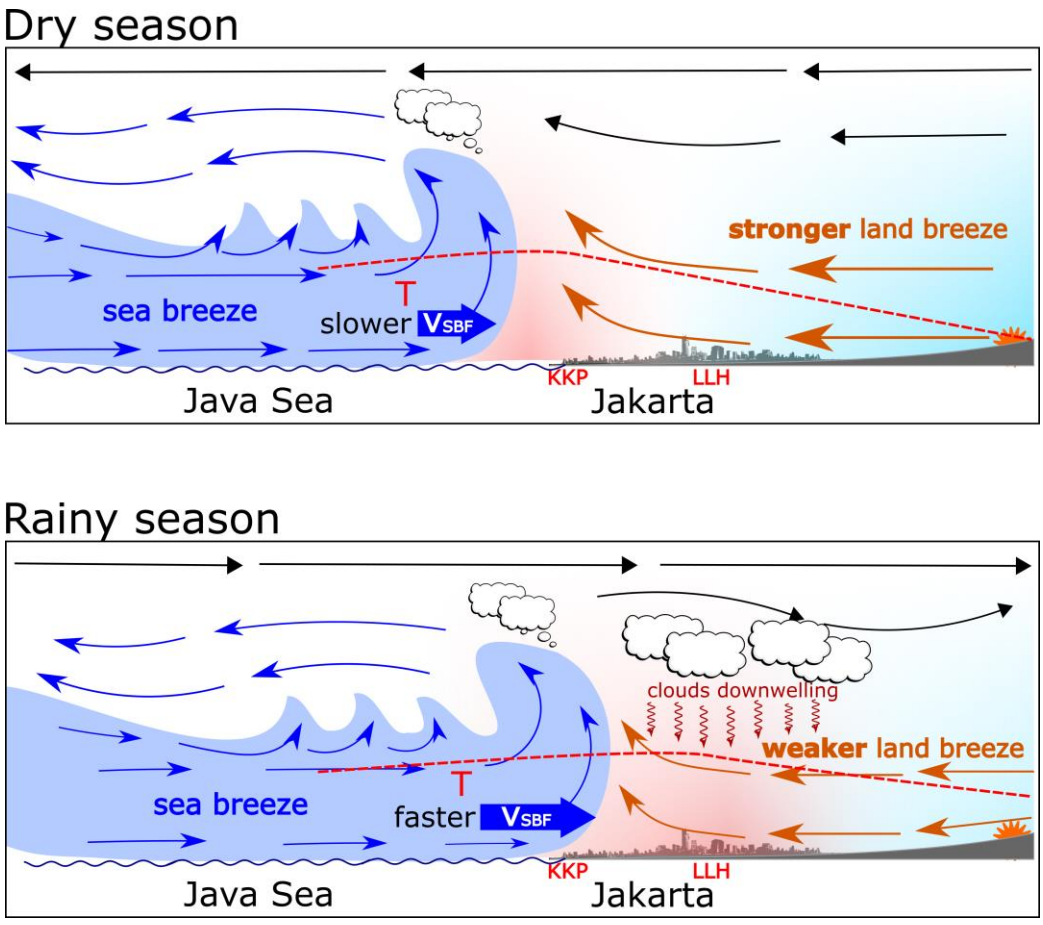

Figure 3.17 Illustration of seasonal variation of sea breeze in Jakarta during the dry (upper) and rainy (lower) season, which is caused by different overland temperature distribution in the morning. Red-dashed line represent horizontal profile of air temperature during morning before sea breeze propagate over land. Shade is used to represent overland temperature gradient between coastal and inland area.

Sea breeze onset, propagation speed, and duration showed strong seasonal variation. In Jakarta, the sea breeze started earlier, propagated faster, and was of shorter duration during the rainy than dry season. As illustrated in Figure 3.17, seasonal variation in sea breeze onset and propagation speed was mainly driven by variation in temperature differences in the morning time prior to sea breeze occurrence. In the dry season, more intense radiative cooling overland will create higher temperature gradient between sea and land which produce stronger land breeze. This will make the sea breeze to start at later time and its propagation become slower due to stronger land breeze. Meanwhile, in the rainy season, the presence of clouds during the night and early morning played an important role in terrestrial heat distribution, making a less gradient between sea and land. This will cause earlier sea breeze onset and faster propagation due to weaker land breeze.

The existence of Jakarta urban area will prolong the sea breeze duration, especially during the dry season. Due to its larger thermal inertia, the urban core stored more energy during the day and released it more slowly overnight, thus prolonging positive temperature differences between urban and coastal areas and promoting longer sea breeze flow. Furthermore, Jakarta urban area may also amplify the land breeze, induce urban heat island (UHI) circulation, or create a more intense daytime heating to the gravity current as its transes the city. These effects will further modify the sea breeze seasonal variation in Jakarta. Stronger land breeze and intense daytime is evident during dry season, while during rainy season morning UHI circulation might developed and induce earlier sea breeze onset. Adding additional observation outside of the Jakarta urban areas is recommended to quantitatively studies the effect of urban areas and urbanization of Jakarta to the atmospheric condition, including sea and land breeze.

Chapter 4 Structure of Boundary Layer during Sea Breeze

As shown in previous chapter, there is a variation in sea breeze propagation due to variation of overland temperature distribution. The results are valid for Jakarta city with assumption that the coastline is relatively straight. However, if we extend our view to include neighboring sub-urban area in the west and east side of Jakarta, the coastal line forms a U-shape with Jakarta city lies in the center of it (see Figure 3.1a). It is known that, coastal line shape will affect the starting point of sea breeze (Miller *et al.*, 2003). For that, this chapter will focus on investigating the coast morphological effect on propagation of sea breeze in Jakarta.

4.1 Introduction

Studying sea breeze structure from points observation will be difficult as it covers only a portion of the circulation. To get more complete information, researcher often combined it with numerical simulations (Gilliam *et al.*, 2004; Childs and Raman, 2005). Studies on coastal morphological effect on sea breeze using numerical simulation has been conducted since a long time, e.g., McPherson (1970). Nowadays, with the more advanced computing capabilities, it is possible to do such simulation in more detail using high-resolution simulation. Recent progress in numerical simulation of sea-breeze was supported by the development of advanced numerical weather prediction models such as Weather Research and Forecasting (WRF) model. An improvement version of WRF with detailed-urban-representation (Varquez *et al.*, 2015; Darmanto *et al.*, 2017) and anthropogenic heat (AHE) distribution dataset was successfully used to simulate sea-breeze in Tokyo.

One constraint in simulating sea-breeze over tropical megacity like Jakarta is lack of high-resolution observation data, either spatial or temporal resolution. This kind of dataset is important for validating the model simulation results, before interpreting it. Such data over tropical urban area usually scarce, thus posing a problem in evaluating the model simulation (Roth *et al.*, 2017). The availability of urban meteorological observation dataset with high-temporal-resolution in Jakarta presents an opportunity to better validate the high-resolution simulation of sea breeze using

a numerical model. A sea-breeze cloud line dataset, derived from Himawari-8 satellite imagery, also recently developed for Jakarta (Ferdiansyah *et al.*, 2020). These datasets were invaluable for the evaluation of sea-breeze simulation in Jakarta.

With all the necessary requirements were satisfied, the research covered in this chapter is aimed to augment the knowledge on sea breeze structure in Jakarta via numerical simulation, back up with validation using the dataset acquired from the Jakarta urban meteorology observation campaign and the satellite-based sea-breeze-cloud-line dataset. The specific objectives of this research are: 1) to simulate typical sea breeze conditions in Jakarta using high-resolution model; 2) to validate the results of the simulation and propose some improvements for future simulations; and 3) to analyze the coastal morphological impact on sea breeze in Jakarta.

4.2 Simulation cases, simulation setup and validation method

Among many sea breeze days (SBD) identified on previous research, 7 SBD was chosen to be simulated. These SBDs had similar characteristics in terms of arrival time at the coastal site (KKP). The purpose is to get ensemble simulation results which represent typical sea breeze in Jakarta. The list of the SBDs with its observed arrival time in KKP and LLH, and its propagation speed will be presented later along with its characteristic derived from numerical simulation results in Table 4-2. The simulation is conducted exclusively during the dry season because all the selected sea breeze days that have similar characteristics were found in dry season. The main purpose of this simulation is to get pictures of how coastline shape will affect the propagation of the sea breeze, and how this will impact the boundary layer structure.

Numerical simulation is conducted using WRF v3.1.1 which has major improvements in its urban surface parameters. The model improvements including new aerodynamic parametrization with a newly constructed urban parameter database (Varquez *et al.*, 2015; Darmanto *et al.*, 2017) and an updated AHE distribution dataset (Varquez *et al.*, 2021) to achieve more realistic representation of urban dynamic in Jakarta. At the time of the writing of this report, these improvements are being ported to the latest version of WRF.

The simulation for each of the SBD is started one day prior the respected SBD (Table 4-3) at 00 UTC (07 Local Time/LT) and ended after 71-hours. The spin-up time of each simulation is 23-hours. Simulation result during this spin-up time is discarded. The validation and analysis are

carried out only for the SBD time frame, from 06 LT to 06 LT the next day. Analysis is conducted based on ensemble result of the simulation and not on individual SBD. This was to ensure that the interpretation is representative of a typical sea breeze day in Jakarta.

4.2.1 Simulation setup

WRF model was configured using two nested domains with 5 km and 1 km resolution, respectively (Figure 4.1). The grid size of the domains in east-west and north-south direction are 131 x 136 for domain 1, and 181 x 251 for domain 2. In vertical direction, 35 η-levels were defined as coordinate. Both domains use the same set parameterization schemes, except for cumulus parameterization on domain 2, which was turned off for explicit convection scheme (Table 4-1). Previous study has shown that this set of WRF parameterization scheme was reliable for atmospheric simulation in Jakarta (Darmanto *et al.*, 2017). Other study also suggests that Kain-Fritsch cumulus scheme for 5-km domain, could produce more realistic cloud distribution for tropical Jakarta (Otsuka *et al.*, 2017).

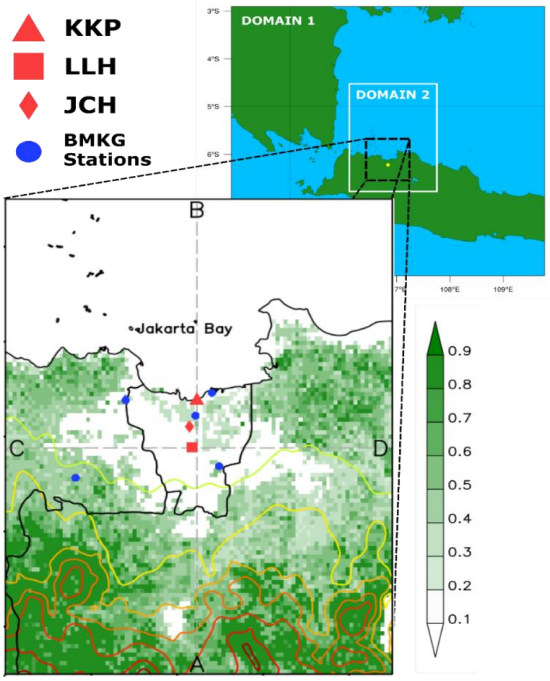

Figure 4.1 WRF simulation domain and focus area. Symbols with red color denote the urban surface observation sites conducted in this research. JCH (Jakarta City Hall) is an additional temporary observation site where radiation measurement was conducted. Symbol with blue color denotes the location of the Meteorological Agency (BMKG) stations. Focus map shows vegetation fraction data (unitless) from WRF and terrain height (contour). A-B line and C-D line indicate the location of the north-south and east-west vertical cross section of the subsequent figures.

Table 4-1 WRF parameterization schemes used for simulation.

Physical Parameter	Parameterization/Sub-model
Shortwave radiation	Goddard scheme
Longwave radiation	Rapid Radiative Transfer Model
Land surface physics	NOAH Land Surface Model
Surface layer physics	MM5 Similarity scheme
Urban surface physics	Single Layer Urban Canopy Model
Boundary layer physics	Mellor-Yamada-Nakanishi-Niino (MYNN) Level 2.5
Cumulus parameterization	Kain-Fritsch scheme **) No Cu param for Domain 2*
Microphysics	New Thompson scheme

Initial and boundary condition for WRF, was obtained from ERA5 reanalysis data from European Center for Medium-range Weather Forecast (ECMWF). Compared to other reanalysis data (e.g., FNL, MERRA and JRA-55), ERA5 has higher spatio-temporal resolution, i.e., 0.3° horizontal, 137 vertical level, and 1-hour temporal. Several studies suggest that ERA5 is better at representing near surface wind and have better accuracy when compared to surface observation(Fan *et al.*, 2020). Initial and boundary values of sea surface temperature (SST) and land surface temperature (LST) also come from ERA5 dataset. SST values of each SBD case vary slightly, but constant throughout each 71-hours of simulation. To produce more realistic surface parameters such as LST, a modified MODIS (Moderate Resolution Imaging Spectroradiometer) land cover dataset is used in the simulations. Population density with nighttime lights adjustment is used to modify the MODIS 21-class land-use supplied by WRF (Varquez *et al.*, 2017).

4.2.2 Validation method

WRF simulation results (hereinafter WRF) were evaluated against previous studies. Model output interval is set to 10 minutes to match the time interval of urban surface observation data (hereinafter OBS). For quantitative evaluation, Pearson correlation (P-corr), root mean square error (RMSE) and bias between WRF and OBS were calculated for wind speed (WS), temperature (T) and relative humidity (RH). WRF variables at 10-m (WS10) and 2-m (T2 and RH2) were chosen for the comparison since it more represents surface layer compared to variables in first model level. The model's first level is around 45 m to 55 m, which is much higher than observation height. Simulation results presented in this paper are all based on composite average of seven

simulations, except for comparison with satellite cloud line. Time series plot were smoothed using 30 minutes window moving average for clarity. However, calculation of statistics and arrival time identification were conducted using 10 minutes interval data without such smoothing.

Model evaluation statistics also calculated using surface observation data from five stations of Badan Meteorologi Klimatologi dan Geofisika (BMKG) or the Indonesian Meteorological Climatological and Geophysical Agency (see the locations at Figure 4.1). Due to limited number of data and longer time intervals, statistics for BMKG stations are calculated for all stations as one dataset. Vertical profile of WS and virtual potential temperature (θ_v) also compared with profile from radiosonde observation at Soekarno-Hatta International Airport (CGK). Satellite cloud line data (Ferdiansyah *et al.*, 2020) is compared with first atmospheric level convergence in similar way as previous research (Varquez *et al.*, 2015). The cloud line data is available in 10 minutes interval, however not all of it contains cloud lines. Thus, the cloud lines comparison is only conducted when the time frame has cloud lines.

4.3 Results and discussion

Sea breeze arrival time and propagation speed from model simulation is presented in Table 4-2. It is presented along with arrival time and propagation speed from urban surface observation data in Jakarta for comparison. It is obvious that the model is producing earlier sea breeze than the observed. This will be discussed in the next section.

Table 4-2 SBF arrival time and penetration speed obtained from observation (OBS) and simulation (WRF).

Sea breeze day (SBD)	OBS			WRF		
	Arrival time		Propagation speed (m s^{-1})	Arrival time		Propagation speed (m s^{-1})
	KKP	LLH		KKP	LLH	
2017-07-17	10:50	12:10	2.31	9:30	12:50	0.93
2017-08-15	10:30	12:10	1.85	9:10	11:40	1.23
2017-09-01	10:40	12:20	1.85	9:10	11:20	1.42
2018-07-25	10:10	12:30	1.32	9:20	11:30	1.42
2018-07-31	10:20	12:40	1.32	9:40	12:10	1.23
2018-08-05	10:30	13:00	1.23	9:40	12:20	1.16
2018-09-04	10:40	12:50	1.42	10:10	12:40	1.23
Average	***10:31***	***12:31***	***1.62***	***9:31***	***12:04***	***1.23***

4.3.1 Model validation

Model evaluation statistics of WRF simulation against surface level observation are presented in Table 4-3. The RMSE and bias shows that the model could well simulate all parameters with similar magnitude to observed values. These results were consistent or might be better than the previous sea-breeze simulation in Tokyo (Varquez *et al.*, 2015). Between daytime and nighttime, daytime statistics show better results. This indicates that WRF with detailed urban representation could perform sea-breeze simulation in tropical Jakarta very well. Consistent results shown between high-temporal-resolution observation at KKP and LLH, with lower-resolution BMKG stations further validating the WRF simulations. While correlation of T shows very good correlation during daytime, correlation of WS and RH show slightly lower values. This lower correlation could be associated with earlier development of sea-breeze in the simulation as seen from SBF arrival time difference between WRF and OBS (Table 4-2). On average, simulated SBF arrival in KKP is an hour earlier than OBS and the arrival time in LLH is 30 minutes earlier.

Table 4-3 Statistical evaluation of WS, T, RH at KKP, LLH and BMKG stations for all-time, daytime, and nighttime.

Site		WS			T			RH		
		P-corr	RMSE	Bias	P-corr	RMSE	Bias	P-corr	RMSE	Bias
KKP	All-time	0.72	1.03	-0.38	0.93	1.34	-1.03	0.76	7.72	-0.53
	Daytime	0.59	1.24	-0.50	0.89	0.77	-0.50	0.75	7.67	-3.76
	Nighttime	0.40	0.77	-0.27	0.80	1.73	-1.54	0.65	7.77	2.59
LLH	All-time	0.68	0.87	0.06	0.93	1.31	-0.62	0.87	7.98	-0.84
	Daytime	0.65	1.04	0.11	0.89	0.99	0.10	0.82	8.83	-6.29
	Nighttime	0.41	0.67	0.00	0.83	1.56	-1.31	0.73	7.05	4.53
BMKG stations	All-time	0.61	1.28	0.02	0.91	1.35	-0.43	0.75	10.99	-6.44
	Daytime	0.57	1.36	0.07	0.88	1.14	0.04	0.74	11.81	-9.52
	Nighttime	0.36	1.16	-0.04	0.74	1.58	-1.06	0.46	10.10	0.02

Indication of earlier simulated sea-breeze is obvious from composite averaged time series of WS, wind direction (WD), and RH (Figure 4.2a, b and d). Model early sea-breeze development might be caused by overestimation of downward shortwave radiation (S_d) and underestimation of latent heat flux (Q_L) in WRF simulation (Figure 4.2g and i). Since the model could produce cloud properly, overestimation of S_d might be attributed to inconsideration of water vapor absorption in

ultraviolet (UV) region and photo-synthetically active region (PAR) in the Goddard shortwave schemes of WRF (Chou and Suarez, 1999). This inconsideration might not be suitable for Jakarta since water vapor availability is quite high. Another possible cause of this overestimation is the absence of aerosol scattering process inside the model. Aerosol scattering could reduce shortwave radiation, especially in Jakarta where bad air quality is a major problem during dry season. Usage of different shortwave schemes or incorporation of aerosol scattering process into the model might improve the result.

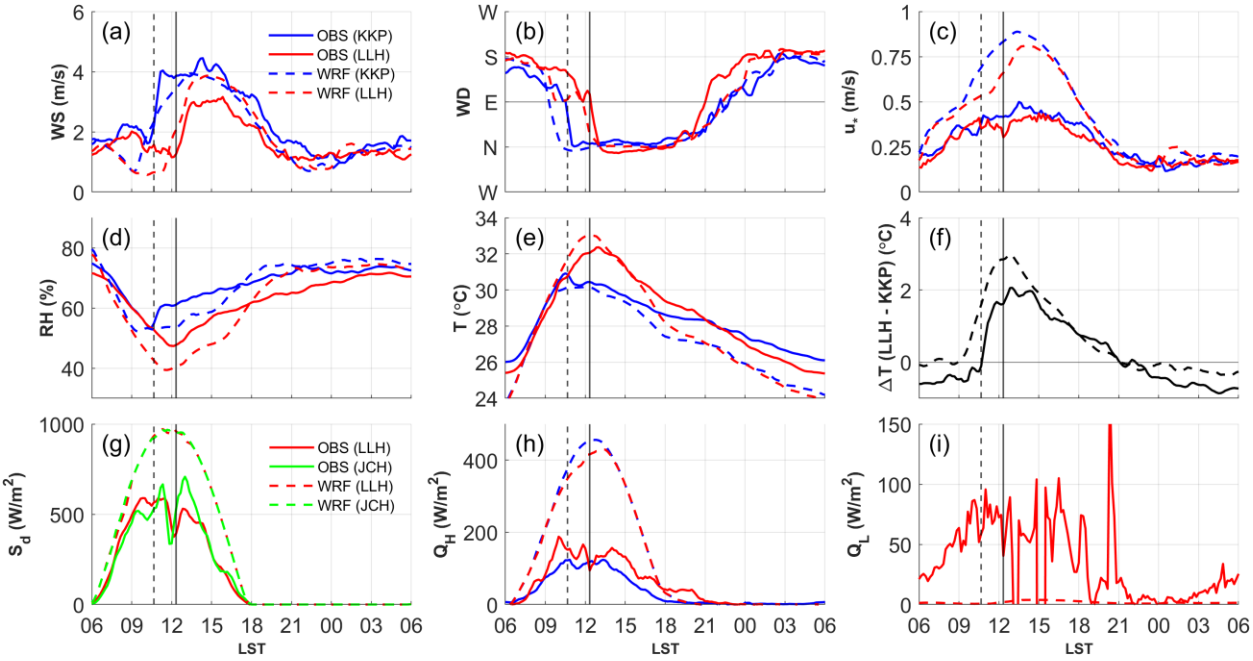

Figure 4.2 Time series comparison between OBS data (solid lines) and WRF simulation (dashed lines) for (a) wind speed, (b) wind direction, (c) friction velocity, (d) relative humidity, (e) temperature, (f) ΔT between LLH and KKP site, (g) downward shortwave radiation, (h) sensible heat flux, and (i) latent heat flux. Vertical lines denote the average arrival time of SBF in KKP (dashed) and LLH (solid) from observation data.

Underestimation of Q_L over land will likely produce imbalance higher Q_H (Figure 4.2h) to account for small Q_L. In the morning, this imbalance will produce faster temperature contrast between inland area and coastal area (Figure 4.2f), thus triggering an earlier sea-breeze. Under-representation of vegetation fraction (Figure 4.1) may contribute to this problem. Improvement on vegetation fraction data may improve model simulated Q_L. This problem also discussed in previous

research (Tokairin *et al.*, 2010). They also found that sea-breeze develops earlier due to significant temperature increase around LLH area by heat advection from expanded urban area in the south.

Although sea-breezes in simulation developed earlier, however its penetration speed are slower compared to OBS. Slow penetration speed in WRF simulation could be attributed to higher drag over city which obvious from u_* magnitude, especially during sea-breeze hours (Figure 4.2c). Since u_* is parameterized with high dependence on roughness length (z_0), this overestimation could be attributed to z_0. Compared to another megacity, Jakarta has much lower z_0 (Darmanto *et al.*, 2017). Even so, the estimation used in this simulation might still be too high as the number of tall buildings and skyscrapers were relatively low. Adjustment to roughness length in WRF is required to improve the simulation result.

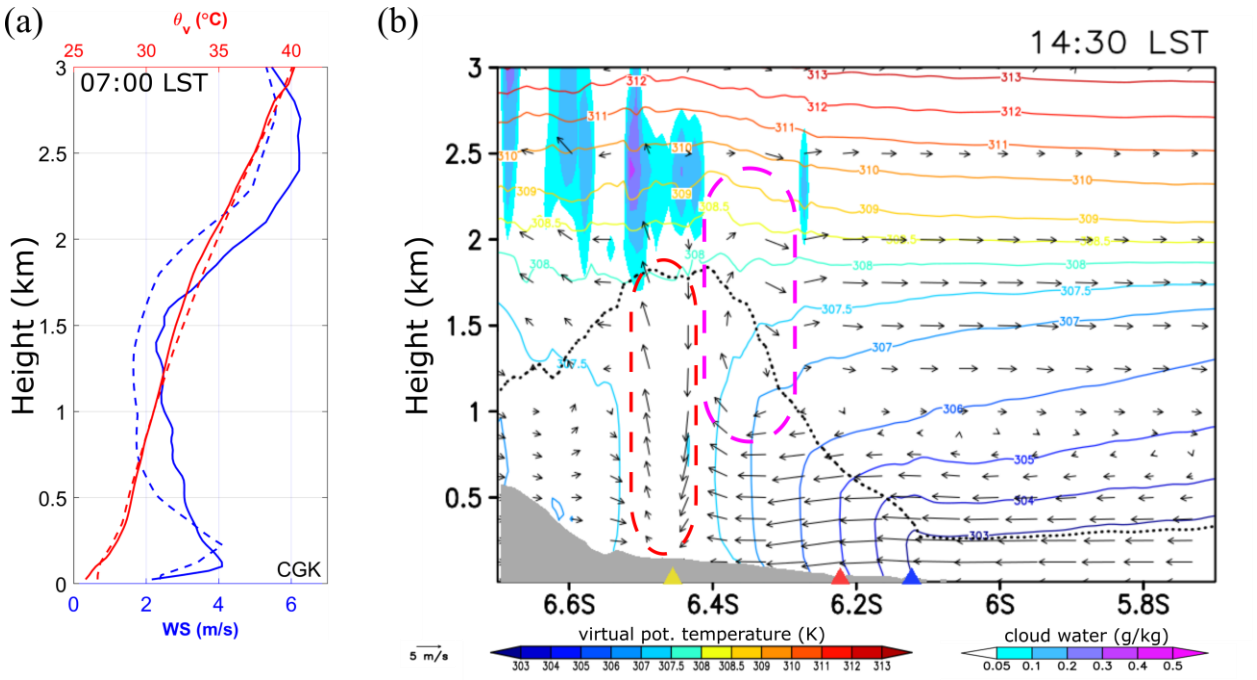

Figure 4.3 (a) Vertical profile comparison of WS and θ_v between radiosonde observation (solid) and WRF simulation (dashed) at CGK for 07 LST (00 UTC); and (b) vertical cross section of θ_v (contour lines), v-w wind (arrows) and cloud water (shaded) from composite averaged WRF simulation in north-south direction (A-B line in Figure 4.1). For wind vector w component is multiplied by 5. Blue-triangle denotes KKP site, red-triangle denotes LLH site, and yellow-triangles mark the southern boundary of Jakarta city. A red dashed ellipse indicates the SBF, and magenta dashed ellipse indicates location of SBH.

Nevertheless, overall verification shows good agreement with observation. Prior to the sea-breeze event, simulated WS and θ_v profile shows good agreement with radiosonde observation at

CGK (Figure 4.3a). The correlation, RMSE and bias of WS are 0.68, 1.38 and -0.58, respectively. Although WS is slightly underestimated, especially above 500 m, θ_v profile shows a remarkable match with correlation of 0.93, RMSE 0.52 and bias 0.08, respectively. Thus, the model is deemed valid for simulating sea breeze in Jakarta.

4.3.2 Simulated sea breeze structure

The WRF simulation properly produces the sea breeze circulation feature as shown in Figure 4.3b. The sea breeze front (SBF), sea breeze head (SBH), the convective cloud above the SBH, and the gravity current associated internal boundary layer (TIBL) were also produced realistically. SBF could be identified from low-level convergence and strong vertical velocities, often accompanied by cloud on top of it (shade of cloud water), as indicated by red-dashed region in Figure 4.3b (Miller *et al.*, 2003). SBH is in a raised area behind SBF where the sea-breeze offshore flow joins the ambient upper flow (magenta-dashed region).

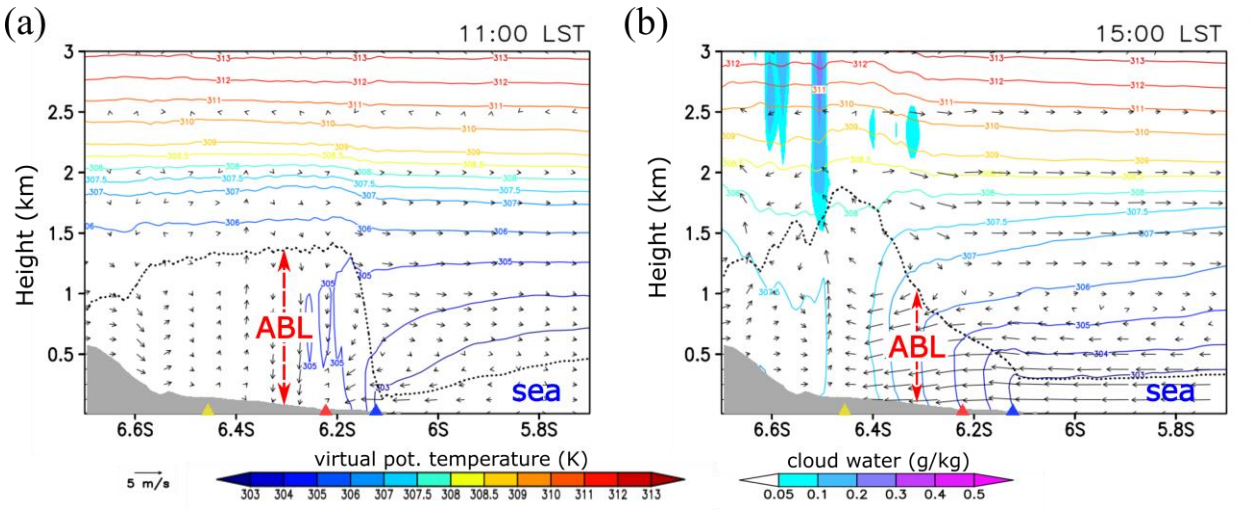

Figure 4.4 Same as Figure 4.3b but for 11:00 LST (a) and 15:00 LST (b).

The impact of sea breeze penetration to the atmospheric boundary layer (ABL) height can be seen from Figure 4.4. The WRF simulation uses the MYNN scheme for the boundary layer parameterization. In this scheme, the height of boundary layer is estimated as the height at which the turbulent kinetic energy (TKE) falls below a critical value which is 1.0×10^{-6} m^2 s^{-2}. Simulation results show that around 11:00 LST, inland ABL height could reach 1.4 km prior to SBF passage (Figure 4.4a). Comparison to observation by other researcher using boundary layer radar (Hadi *et*

al., 2000) shows that the simulated boundary layer heights are similar to those observation. When the sea-breeze penetrates the same area by 15:00 LST, the developed boundary layer over land will be eroded by the instability created by strong shear in SBH region (Figure 4.4b). This unstable region under SBH then trapped by more stable marine air above it and create thermal induced boundary layer (TIBL), which is lower than the previous inland boundary layer (Hadi *et al.*, 2000; Miller *et al.*, 2003). Only around 3/4 of the original ABL height is retained after the passage of SBF, indicating the approximate height of the sea breeze gravity current (SBG) around this value.

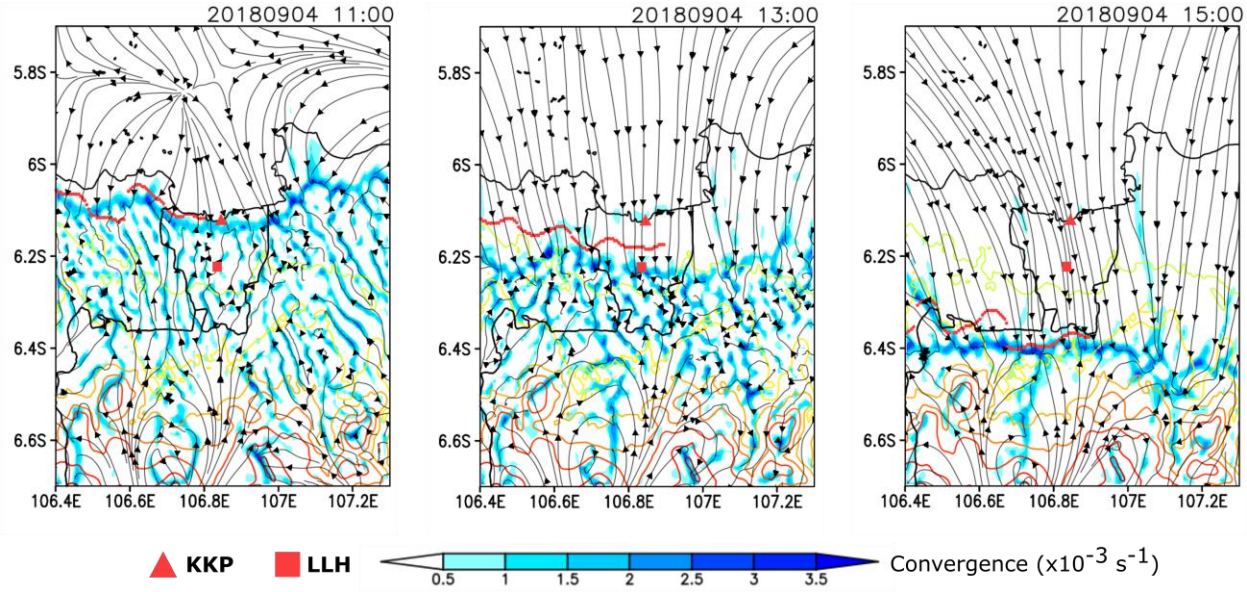

Figure 4.5 First atmospheric level convergence (shaded) and wind streamline from WRF simulation, overlayed with satellite derived cloud line (red line) for SBD case of 4 September 2018 at 11:00, 13:00 and 15:00 LST. Colored contours indicate terrain height.

In a horizontal point of view, it is difficult to see the propagation speed of sea breeze. Since SBF is characterized by strong convergence, we could use the value of convergence to identify the SBF (Varquez *et al.*, 2015). convergence is defined as:

$$Convergence = -\left(\frac{\partial u}{\partial x} + \frac{\partial v}{\partial y}\right) \quad (4.1)$$

where u and v are the vector component of horizontal wind. Figure 4.5 shows that simulated convergence line moves in different starting point spanwise. Around 11:00 LST, over the area outside Jakarta, sea breeze convergence line starts further north, following the coastline. Around 13:00 LST, convergence line outside Jakarta could catch up with convergence line over Jakarta.

By the time the convergence line pass Jakarta, around 15:00, the line could be assumed nearly straight in the west-east direction. This result indicate that SBF propagation speed is slower over the city compare to over less-urban area outside of Jakarta (Ferdiansyah *et al.*, 2020).

Comparison with satellite derived cloud line shows that six out of seven SBD simulations (see Table 4.2) were showing a good match between SBF associated convergence line and the satellite cloud line. Most matched lines are found in simulation for 2018-07-31, 2018-08-05 and 2018-09-04. Only simulation for 2017-08-15 shows no match for entire day. In this day, simulated sea-breeze convergence moves faster, while satellite cloud line still above coastline. By the time simulated convergence passes Jakarta's urban area, the cloud line arrives at the city center, but stagnant over the area. The cloud line then moves to coast, indicating cloud development by urban convective activities.

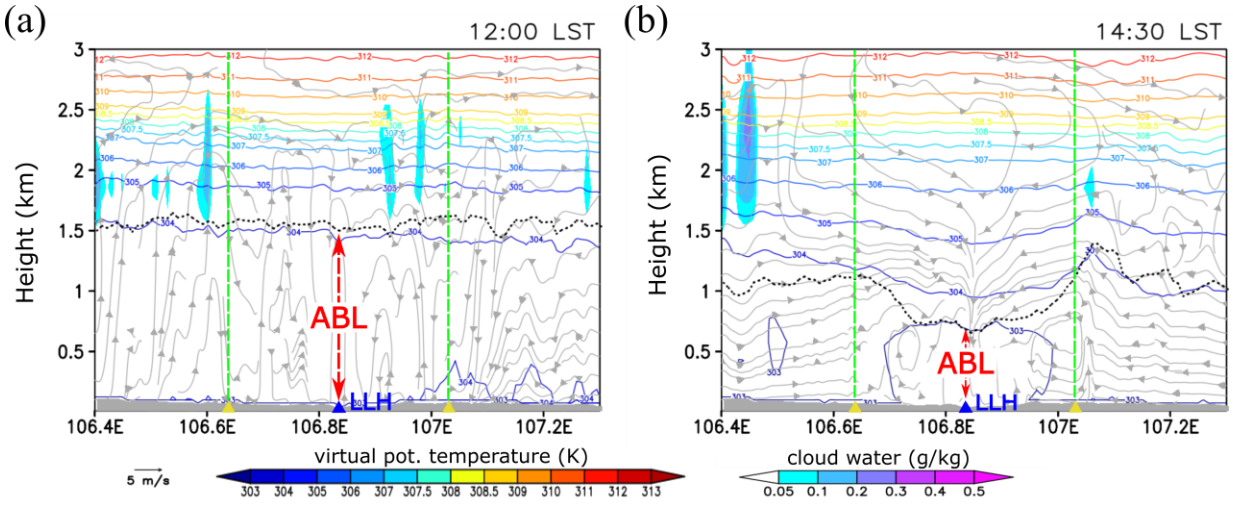

Figure 4.6 Vertical cross section of θ_v (contour lines), u-w wind (streamline) and cloud water (shaded) from composite averaged WRF simulation in east-west direction (C-D line in Figure 4.1). Blue triangle denotes the location of LLH site. Green dashed lines indicate the location of Jakarta Bay edges which coincide with west and east administrative boundary of Jakarta city.

Match between SBF convergence and cloud line were not found for every time frame. As seen in the example in Figure 4.3, matched lines are usually found before noon, during early stage of sea-breeze. The matched lines were also found when SBF has passed the urban areas. Most of the un-matched lines were found when SBF was around urban areas, especially near the city center. These un-matched lines usually comes from stagnant clouds behind SBF which caused by opposing flow in the upper part of sea-breeze (Ferdiansyah *et al.*, 2020) or clouds that developed by convective activities over the city area. Another cause of un-matched lines that was found are

clouds that already exist prior to the sea-breeze. These clouds mostly do not have an association with sea breeze.

When compared along a west-east line, the SBF from Jakarta Bay arrived earlier than the SBF from the west and east of the bay. This causes the ABL height in the west-east line to vary significantly, whereas over Jakarta is lower than over the sub-urban area in the west and east of it. This was clearly shown in Figure 4.6. At noon time, the height of the ABL is still quite uniform in the east-west direction (Figure 4.6a). The ABL height is around 1.5 km from the ground. After the sea breeze over Jakarta passes LLH site at around 14:30 LST, the ABL height over Jakarta is reduced to around 800 m (Figure 4.6b). However, the ABL height over east and west side of Jakarta were still much higher, around 1 km from the ground. This condition seems to create a lateral secondary circulation with an upward region parallel to the Jakarta Bay edges (green line on Figure 4.6) and downward region over Jakarta city center (LLH). After half an hour (not shown), as the sea breeze from the side of Jakarta Bay area catches up and the internal boundary layer over Jakarta developed, the ABL height in the east-west direction becomes uniform again.

4.3.3 Impact of sea breeze front passage

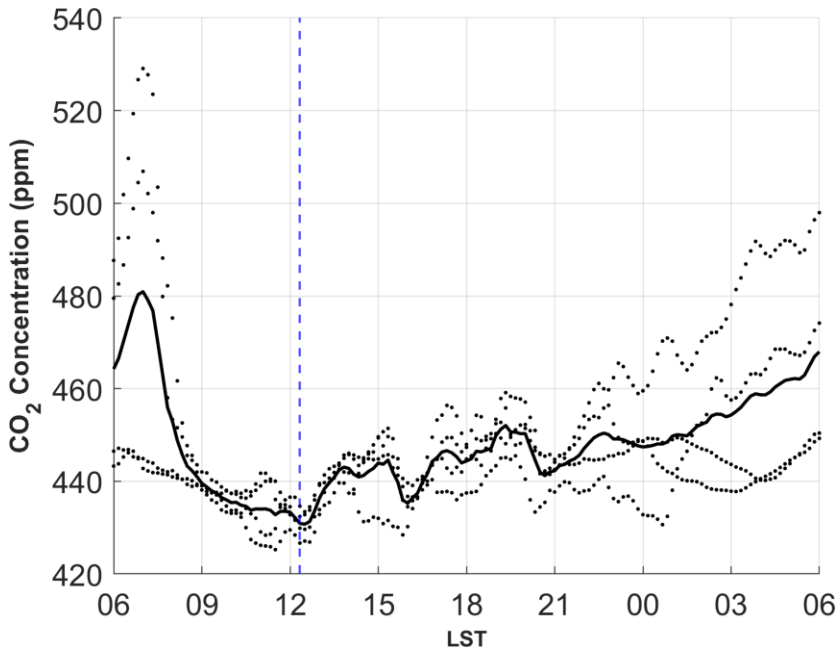

Figure 4.7 Time series of CO_2 concentration in LLH measured during 2018 SBD cases (dotted). No CO_2 measurement during 2017 cases. The composite average is shown in solid-black line. dashed-blue line shows average arrival time of SBF at LLH.

To proof that the increase in CO_2 concentration is caused by reduction in due to SBF passage, we can integrate them over the boundary layer height, before and after the SBF passage. As illustrated in Figure 4.8, the hatched area under the profile should be invariant if the change in concentration is only caused by ABL height reduction, as formulated by:

$$\int_{z=0}^{H_{BL}} C_{CO_2}(z)\,dz \quad _{<before\ SB>} = \int_{z=0}^{H_{BL}} C_{CO_2}(z)\,dz \quad _{<after\ SB>} \qquad (4.2).$$

Here the H_{BL} is assumed to change because of the sea breeze passage and the vertical profile of CO_2 concentration as function of z is known.

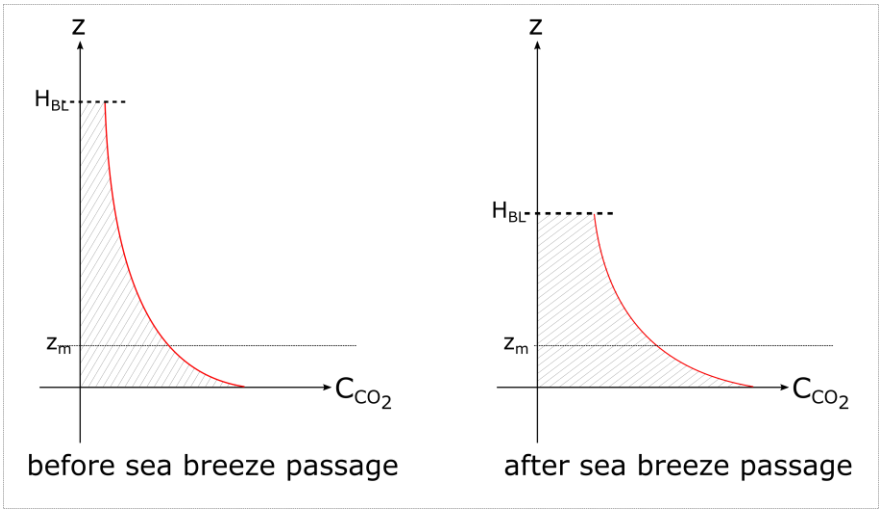

Figure 4.8 Illustration of change in CO_2 concentration (C_{CO_2}) profile due to sea breeze passage which reduce the ABL height (H_{BL}). A line marked with z_m indicates the measurement height.

However, since measurement is conducted only at one level (z_m in Figure 4.8), hence the full vertical profile of C_{CO_2} is not known, it is impossible to calculate the integral in equation (4.2). It would require at least two measurements to calculate the integral. Another approach is to assume a constant concentration throughout the ABL and divide it by the boundary layer height. Although this assumption is not correct, i.e., C_{CO_2} is decreasing with height (Garratt and Pearman, 1973), it could distinguish between impact of ABL change and change in source of CO_2. As shown in Figure 4.9a, the change in does not always correspond to change in ABL height, especially seen after 12 LST. Even so, the result of division between the concentration and ABL height (R_{CO_2}) clearly indicates the change associated with ABL change (Figure 4.9b). In the morning when boundary

layer expands due to daytime heating, the C_{CO_2} is rapidly decreasing, although in slower rate during 9 to 12 LST. The sudden increase after 12 LST is matched with the sea breeze passage over the observation site. Between 13 to 21 LST, there are many ups and downs in C_{CO_2}, but in Figure 4.9b there is no such variation, indicating that this variation might not be associated with boundary layer change. After 21 LST, the C_{CO_2} is increased again following the rapid decline of H_{BL}, which clearly depicted in Figure 4.9b.

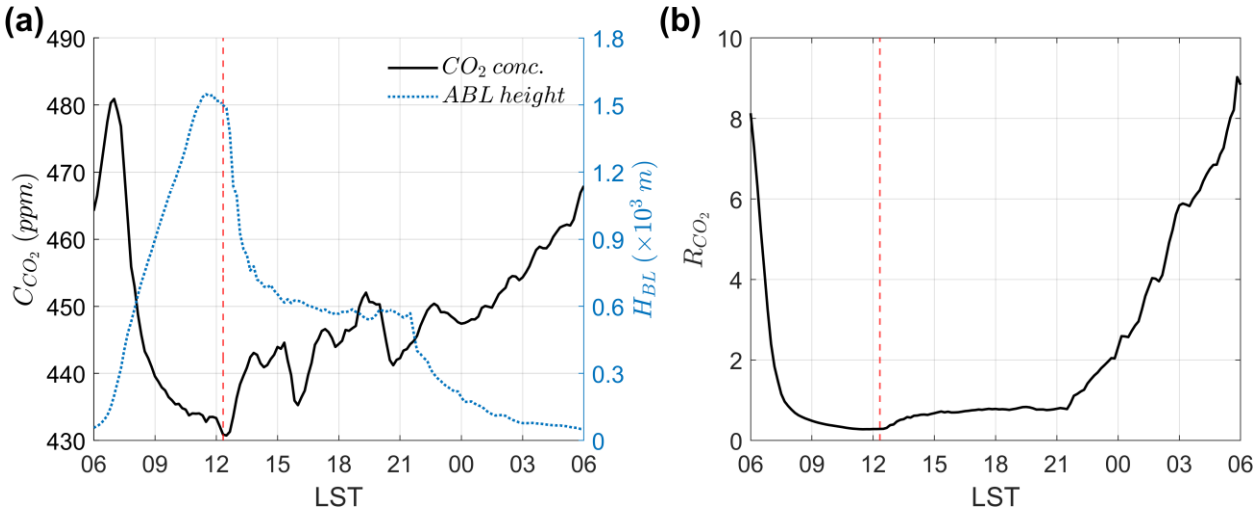

Figure 4.9 Composite average of CO_2 concentration in black-solid-line, overlaid with boundary layer height in blue-dotted-line (a), and the division result (R_{CO_2}) between CO_2 concentration and boundary layer height (b). Vertical red-dashed-line indicate the timing of SBF passage on the site.

These findings show that sea breeze passage might momentarily change the concentration of CO_2. This might also apply to other gases and pollutants. Thus, sea breeze can be considered as having an important role in governing the pollutants and other gases. It would be beneficial to assess the dynamic of such a trace gas like CO_2 to fully understand the impact of sea breeze on air quality in Jakarta.

4.4 Concluding Remark

The structure of atmospheric boundary layer in Jakarta during sea breeze passage is analyzed using numerical simulation of 7 typical sea breeze days. The simulation is conducted using WRF with detailed urban representation. The WRF simulation is validated using high-

temporal-resolution urban surface observation data, radiosonde data at CGK, and satellite derived cloud line dataset. Although WRF produce earlier sea-breezes, the evaluation statistic shows consistently small error and bias, either in high-temporal-resolution data or in lower-temporal-resolution data from BMKG. The WRF model was able to simulate sea-breeze features and boundary layer characteristic of the targeted area.

A lower boundary layer over the city after sea-breeze passage is well simulated and indicates the existence of TIBL. The shape of the coastal line around Jakarta Bay influences the starting point of sea breeze landfall and affects the condition of the boundary layer above Jakarta. Different timing of arrival between SBF over Jakarta and SBF over east and west sub-urban area causing non-uniform ABL height in the east-west direction, where the ABL over Jakarta is lower than the sub-urban area. This variation might affect pollutant concentration in Jakarta as it was observed to CO_2. Further research on trace gas dynamics is recommended. Several improvements for the numerical simulation were also suggested as reference for future simulation.

Chapter 5 Diurnal Variation of CO_2 flux and concentration in Jakarta

Sea breeze propagation in Jakarta could momentarily increase CO_2 concentration by reducing the boundary layer height. It was also amplified by the effect of lateral circulation induced by uneven lateral ABL height due to coastal shape effect of Jakarta. However, the influence of sea breeze in Jakarta to the vertical exchange of CO_2 is unknown. In fact, the diurnal variation of CO_2 flux in Jakarta has never been reported before. In this chapter, CO_2 flux and concentration in Jakarta is analyzed using observation data from CO_2/H_2O gas analyzer at LLH site. The influence of sea breeze on CO_2 flux and concentration is also investigated.

5.1 Introduction

Among many human settlements, cities and other urban areas are the major consumers of energy. Despite only covering less than 4% of earth's land area (Liu *et al.*, 2014), urban area consumed more than 75% of total world energy (Grubler *et al.*, 2012). With higher energy consumption, cities and urban areas will contribute to CO_2 emission significantly, thus understanding the CO_2 variations in the areas becomes important. Such knowledge will provide policymakers with an effective emissions mitigation strategy, as well as important information for communities and stakeholders towards addressing environmental problems related to carbon emissions (Duren and Miller, 2012). In addition to that, CO_2 is also an excellent passive tracer which could become proxy for certain pollutants, hence also useful in solving pollution problem (Arrillaga *et al.*, 2018; Lin *et al.*, 2018). To serves these purposes, urban CO_2 observations and scientific data analysis will be necessary. Duren and Miller (2012) also notes that, megacities (metropolitan urban area with more than 10 million population) tend to emit higher CO_2 emissions, thus deserve special attention in CO_2 observation and analysis.

Many CO_2 observation studies using the eddy covarianve (EC) method have been conducted in various cities around the world (e.g., Nemitz *et al.*, 2002; Grimmond *et al.*, 2004; Moriwaki and Kanda, 2004; Velasco *et al.*, 2005, 2009; Pawlak *et al.*, 2011; Liu *et al.*, 2012, 2021;

Christen, 2014; Hirano *et al.*, 2015; Ao *et al.*, 2016; Schmutz *et al.*, 2016; Ueyama and Ando, 2016; Roth *et al.*, 2017; Cheng *et al.*, 2018; Park *et al.*, 2022). Comprehensive comparison and summary of CO_2 flux measurement from various cities and other urban areas have shown that result of these urban CO_2 flux studies vary significantly across location (Velasco and Roth, 2010; Grimmond and Christen, 2012). More importantly, these reports also show that most urban CO_2 flux studies were conducted in mid-latitude cities, with only two cities (Mexico City and Singapore) were representing the tropical areas (Velasco *et al.*, 2005, 2009, 2013; Roth *et al.*, 2017). Since almost 40% of global population is living in the tropical cities (State of The Tropics, 2020; Marcotullio *et al.*, 2021), in terms of urban CO_2 exchange studies, tropical cities were really under-represented. As noted by Roth *et al.*, (2017), under-representation of tropical cities will bias the empirical model towards condition found in mid-latitudes and may lead to ineffective climate change mitigation policies for the tropical cities. This is one of the reasons that motivate us to carry out CO_2 observation research in the tropical megacity of Jakarta.

Jakarta is a rapidly-growing tropical megacity, which are home to more than 10 million people (BPS Provinsi DKI Jakarta, 2023). Most of transportation system in Jakarta is still using fossil fuel as energy sources, hence contributing to more than 80% of city's CO_2 emissions (Dinas Lingkungan Hidup DKI Jakarta, 2017). Transportation system also contributing to more than 90% of carbon monoxide (CO), the toxic form of carbon oxide which produced by incomplete combustion (Lestari *et al.*, 2022). With the population of Jakarta projected to increase significantly in the next few years, hence increasing the CO_2 emission, it is necessary to investigate the CO_2 exchange and accumulation in Jakarta as a current and future reference.

The objective of this research is to analyze the micrometeorological variation of CO_2 flux and concentration in the urban area of Jakarta using dataset from the long-term EC measurement. Emphasize is given to diurnal variation and long-term trend of CO_2 flux and concentrations. Since the measurement was still on-going during the Corona Virus Disease of 2019 (COVID-19) pandemic, analysis on the impact of social restrictions during pandemic to CO_2 variation is also carried out. This research is expected to contribute to global urban CO_2 dataset as one representative of tropical cities and become foundation for subsequent CO_2-related research in Jakarta. It is also wished to become scientific base for carbon-related policy making in Jakarta, or more general in Indonesia.

5.2 Methodology

This research is focused on LLH site which is located in the urban core area of Jakarta. Jakarta itself is situated on the northern coast of western Java Island (Figure 5.1a). The administrative area of Jakarta City is approximately 651.5 km^2 as bounded by black dashed line on Figure 5.1a. The northern part of the city is the coastal area of Jakarta Bay which spans around 30 km in west-east directions. Over land, Jakarta is surrounded by sub-urban areas, namely Bogor, Depok, Tangerang, and Bekasi, which create the metropolitan area called Jabodetabek. Details of the measurement site, instruments, data processing, flux calculation, quality check, flux footprint, and site's diurnal atmospheric condition will be explained in the next section.

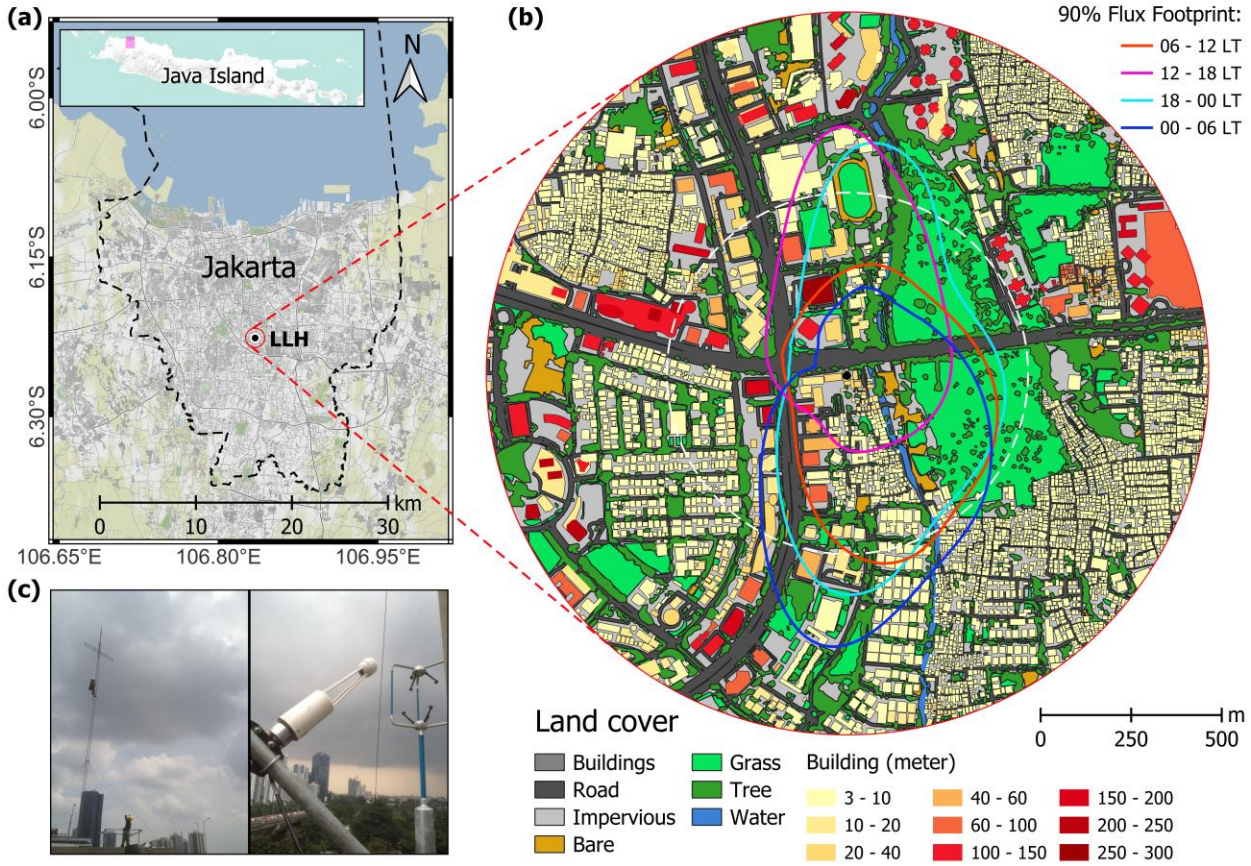

Figure 5.1 Map of Jakarta with mark on the observation site of LLH (a); detailed land cover over 1-km radius around LLH site (b); and photograph of the tower and instruments at the observation site (c). Black dashed line on (a) denotes the administrative boundary of Jakarta City. Blue, orange, magenta and cyan line on (b) shows the 90% climatological flux footprint estimated using Kljun *et al.* (2015) method. White dashed circle in (b) marks the 0.5-km radius from observation site. Each land cover category in (b) is represented by one color patch, except for the buildings, which are color coded using yellow-to-red gradation based on the building height.

5.2.1 Instrumentation, additional datasets, observation site, and flux source area

CO_2 observation is conducted on top of a building that belongs to Laboratorium Lingkungan Hidup (LLH), Dinas Lingkungan Hidup Provinsi DKI Jakarta (The Environmental Protection Agency of Jakarta City). The LLH building heights is around 22 m from the ground. The main instruments, which consist of an ultrasonic anemometer and a gas analyzer, were mounted on a tower at the top of the building (see Figure 5.1c). The main instruments were placed at a 7.3-m height from the roof top, making the total measurement height (z_m) at 29.7 m from the ground. Other additional instruments, such as the temperature-humidity gauge and automatic weather station (AWS), were placed at 1.5 m above the roof top, hence their measurement height is 23.5 m above the ground. The parameters acquired from the main instruments are the 3-D wind components (u, v, w), sonic temperature (T_s), molar density of CO_2 (ρ_v), and molar density of H_2O (ρ_v). The additional instruments of temperature-humidity logger an AWS provide the ambient temperature (T_a), ambient relative humidity (RH_a), and rainfall rate (R_r). Detailed specifications of each instrument used in this study are given on Table A.1 on Appendix A.

Apart from the main observation data, additional datasets were also acquired to support this research. Land cover and buildings dataset were acquired from Open Street Map (OSM) database (OpenStreetMap contributor, 2023), except for the trees and grass land cover, which were manually delineated from aerial photograph. The building height dataset is also updated using the newest information from various sources. Traffic density data is downloaded from TomTom traffic index (TomTom International BV, 2022). The boundary layer height (H_{BL}) estimation is acquired from ERA5 reanalysis dataset (Hersbach *et al.*, 2020), which is extracted at the nearest grid point to the observation site. The ERA5 dataset has spatial resolution of 31 km and temporal resolution of 1-hour. All these datasets are open datasets which could be downloaded via the internet.

The land cover and building height around 1-km radius from the site is presented on Figure 5.1b. It can be seen from this figure that there are many high-rise buildings (buildings with more than 5 floors) along the main roads in the north, west and south of the observation site. Some of these buildings were higher than 100 m high, hence can be considered as skyscrapers. The areas behind these buildings, on the opposite side of the main road, are filled with residential houses that are usually around 1 to 3 stories high. Residential houses also dominate the areas in the southern to northeastern sectors of the site. Several green areas in the eastern side of the observation site were cemeteries and were mostly covered by grass. The landcover fraction of each sector around

the site is shown in Figure 5.2a. There is a significant variation in landcover fraction around the site. The eastern sectors were dominated by greenery, while the western sectors were filled with buildings, roads, and impervious surfaces like parking lots, concrete and pavement.

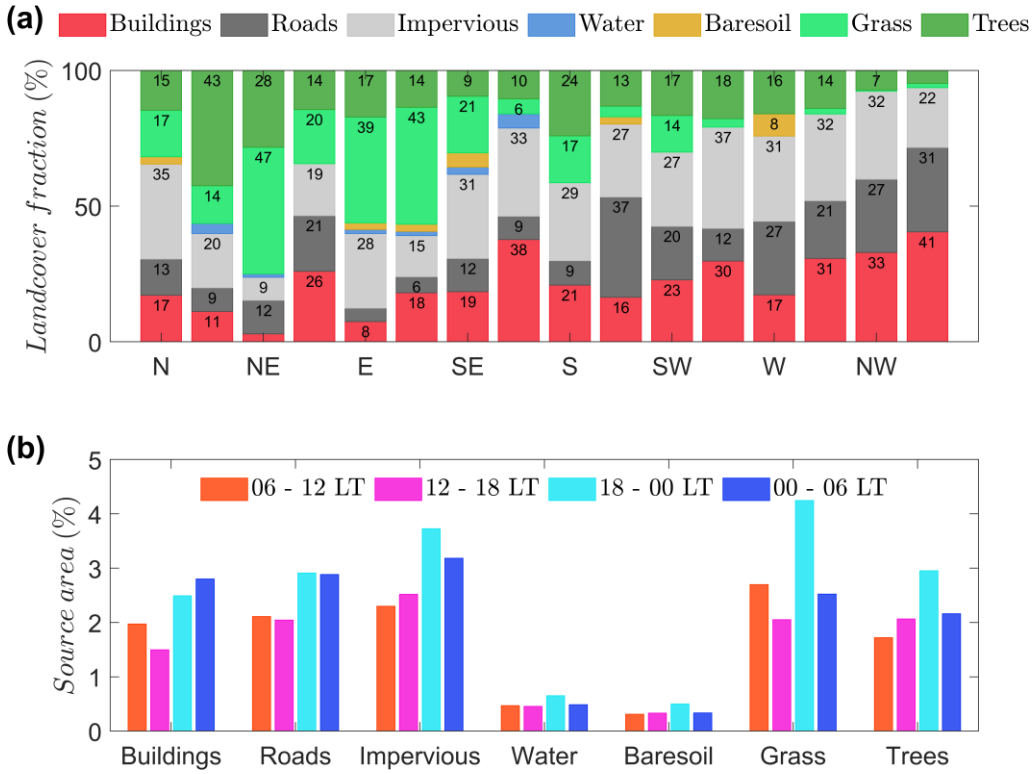

Figure 5.2 Directional based landcover fraction in 1 km radius around observation site (a), and percentage of each landcover category in the flux footprint/source area that is depicted in Figure 5.1b (b).

The climatological flux source area is estimated using flux footprint prediction method by Kljun *et al.* (2015) and is overlaid on Figure 5.1b. The source area is estimated for four timeframes of the day, morning (06 – 12 LT), afternoon (12 – 18 LT), evening (18 – 00 LT), and early-morning (00 – 06 LT). The flux during early-morning and morning mostly comes from the south of the site, while during the afternoon is dominated from the northern area of the site. During evening, the flux source area is balanced between the northern and southern side of the site. The percentage contribution of each land cover category to the source area for each timeframe is presented in Figure 5.2b. For each timeframe there is a difference dominant category. In the morning and evening the source area is dominated by grass and impervious, while for afternoon and early morning the source area is dominated by impervious and roads.

5.2.2 Data processing, flux calculations, and quality assurance

CO_2 flux (F_{CO_2}) is estimated using the eddy covariance (EC) method which is already explained in Chapter 2 section 2.3. The flux averaging window is 1-hour with detrend method using block average. Prior to the flux calculation several standard and suggested pre-processing procedures were applied to the observation dataset (Lee *et al.*, 2005; Velasco *et al.*, 2005; Aubinet *et al.*, 2012; Burba, 2013; Fratini and Mauder, 2014). The procedures including un-physical data screening, spike removal, coordinate rotation, statistical test, density fluctuation compensation (WPL terms), data detrending, and spectral correction. These pre-processing procedures, flux calculations, as well as several post-processing analysis were conducted using EddyPro software (Burba, 2013; Fratini and Mauder, 2014). Several important procedures in EddyPro software, including the selected method and its references were presented in Table 5-1.

Table 5-1 Several procedures and selected methods in EddyPro software that were used in data processing and CO_2 flux calculation.

	Procedure	Selected method	References
Raw data processing	Coordinate rotation	Double rotation	(McMillen, 1988))
	Detrend method (Averaging window)	Block average (1-hour)	Moncrieff *et al.* (2005)
	Time lag detection	Covariance maximization	Fan *et al.* (1990)
	Density fluctuation compensation	WPL terms	Webb *et al.* (1980)
	Quality check	0-1-2 system	Mauder and Foken (2006)
Statistical analysis	Statistical test for raw data screening	Spike count/removal	Mauder *et al.* (2013)
		Amplitude resolution	Vickers and Mahrt (1997)
		Drop-outs	
		Absolute limits	
		Skewness and kurtosis	
	Random uncertainty estimation	Finkelstein and Sims method	Finkelstein and Sims (2001)
Spectral analysis and corrections	Tapering window	Hamming	Stull (1988)
	Low frequency range spectral correction	Analytic correction of high-pass filtering effects	Moncrieff *et al.* (2005)
	High frequency range spectral correction	Analytic correction of low-pass filtering effect	Moncrieff *et al.* (1997)

Apart from CO_2 flux, the momentum flux τ, sensible heat flux (Q_H), and latent heat flux (Q_L) were also calculated. Q_H and Q_L were corrected according to equations (2.20) – (2.22) in Chapter 2. Several important surface layer parameters such as Obukhov length (L), stability parameter (ζ) and friction velocity (u_*) are calculated using the same formula as in equation 3.4 and (3.5) in Chapter 3. Average concentration of CO_2 (C_{CO_2}) also calculated to be analyzed with F_{CO_2}. Variables from additional instruments were averaged with the same 1-hour window and used for assessing general diurnal atmospheric condition of the study area.

5.2.3 Flux data acquisition and quality assurance

The measurement was carried out from April 2019 until September 2021. Due to several technical issues and COVID-19 restriction, several months of data were lost, mainly during the year 2020. From the total span of the observation period, around 74.8% of 1-hour averaged flux were acquired. To ensure the quality of the flux measurement several screening procedures were conducted to the acquired flux dataset. First, the flux dataset is screened based on the quality check or flagging results (Mauder and Foken, 2006). Only flux with 0 (best) and 1 (moderate) flag is retained. Since the CO_2 flux is sensitive to latent and sensible heat flux, when these two fluxes are screened out, the CO_2 flux is also removed. To ensure that the flux is estimated under turbulence conditions, flux data when the wind speed is very low (i.e., < 0.1 m s^{-1}) is discarded. As the gas analyzer is sensitive to rain, flux data during rain with intensity of more than 1 mm $hour^{-1}$ is also discarded. All these screening procedures reduced the dataset significantly, leaving only 59% of the original flux dataset.

Due to the high roughness of the areas surrounding the site, fetch direction was also evaluated. For this purpose, the urban aerodynamic parameters surrounding the observation site is estimated using morphometric method of Kanda *et al.*, (2013). Urban aerodynamic parameters of each 5 sector in 500-m radius circling the site is estimated using the QGIS Urban Multi-scale Environmental Predictor (UMEP) plugin (Lindberg *et al.*, 2018). The estimated urban aerodynamic parameters were shown in Figure 5.3a-b along with distribution of mean streamwise wind speed ($\overline{U}$), which is acquired after coordinate rotation, and plot of drag coefficient (C_D), which can be estimated using:

$$C_D = \left(\frac{u_*}{\overline{U}}\right)^2 \quad (5.1).$$

Figure 5.3a-b clearly shows the existence of very rough elements from the south-southwest (SSW) direction until north-northwest (NNW) direction. However, boxplot of $\overline{U}$ and and C_D do not indicate strong attenuation on flow that comes from west-northwest direction to north-northwest direction. Thus, only data with the mean streamwise wind comes from south-southwest (SSW) to west (W) direction were discarded (grey shade on Figure 5.3). Another strong reason to remove the flux data with flow come from the west is the fact that the mounting arm of the instruments is directed toward this direction. Thus, the flow coming from the west might be strongly modified by the measurement tower itself. This directional based screening procedure reduces 6.4% of the flux dataset, leaving only 52.6% of qualified flux datasets.

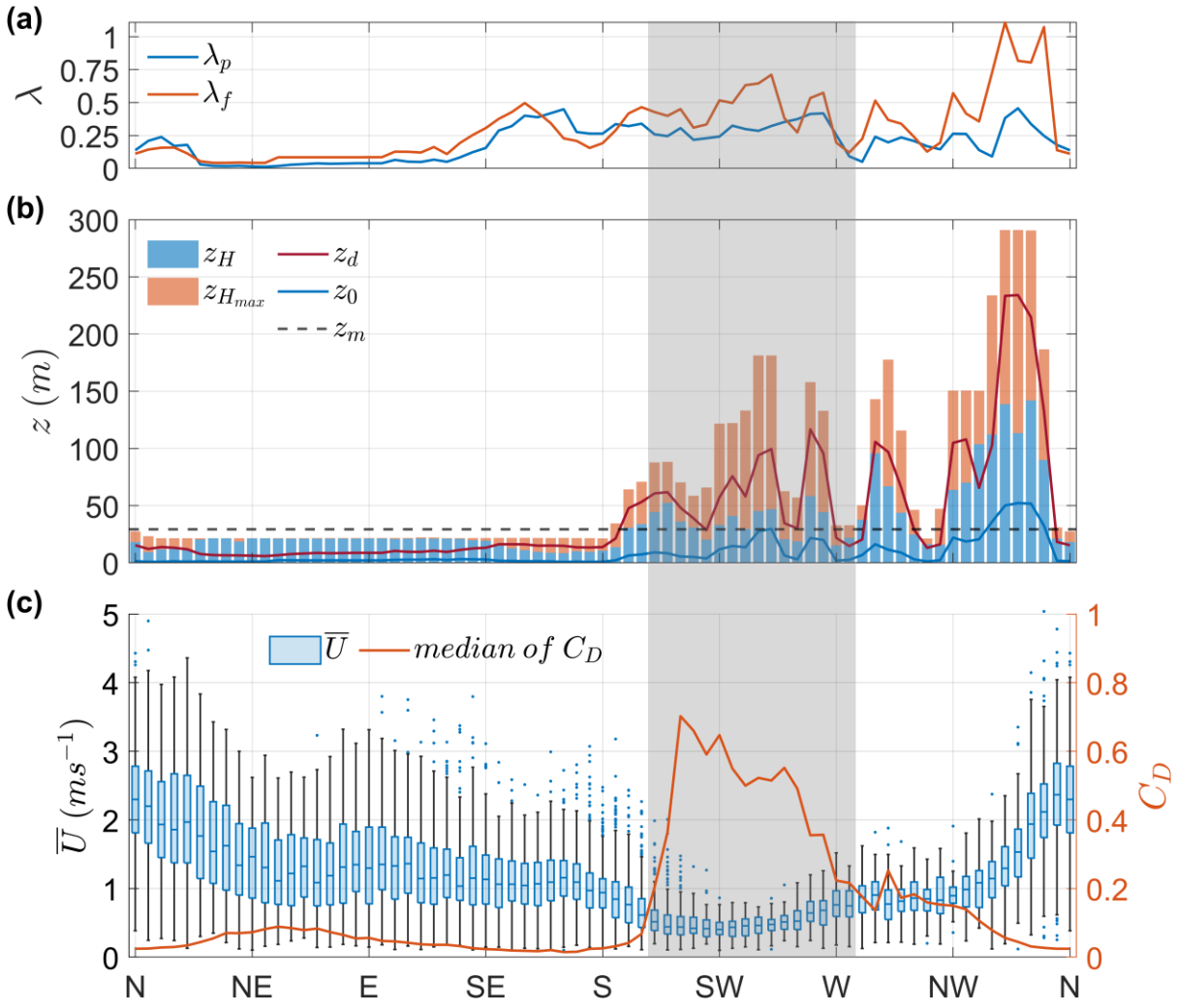

Figure 5.3 Urban aerodynamic parameters around 500-m radius from observation site (a and b), and boxplot of mean streamwise wind speed ($\overline{U}$), overlaid with drag coefficients (C_D) calculated from observation data (c). Grey shaded area indicates the sectors of wind direction where flux dataset is removed.

Due to the frequency range limitation of the instruments, an EC system will attenuate the true turbulent signal at very high and very low frequencies (Massman, 2005; Burba, 2013). Hence, it is necessary to inspect the spectral density (spectra) and co-spectral density (co-spectra) of the signal. The binned normalized spectra of w and ρ_c, and normalized co-spectra of $w\rho_c$ were calculated with Hamming window taper. Comparison of the spectra and co-spectra of those variables under neutral condition, as shown on Figure 5.4a, shows similarities to the well-known model of Kaimal *et al.* (1972). Both spectra show the -2/3 slope, and the co-spectra shows the -4/3 slope in the inertial sub-range, confirming the validation of the measurements (Roth and Oke, 1993; Massman, 2005). The ogives of each spectra and co-spectra (Figure 5.4b) also shows asymptotic shape towards the maximum and minimum frequency, indicating adequacy of the averaging window length of 1-hour. These results confirm that the CO_2 flux measurement in Jakarta is valid and acceptable for further analysis.

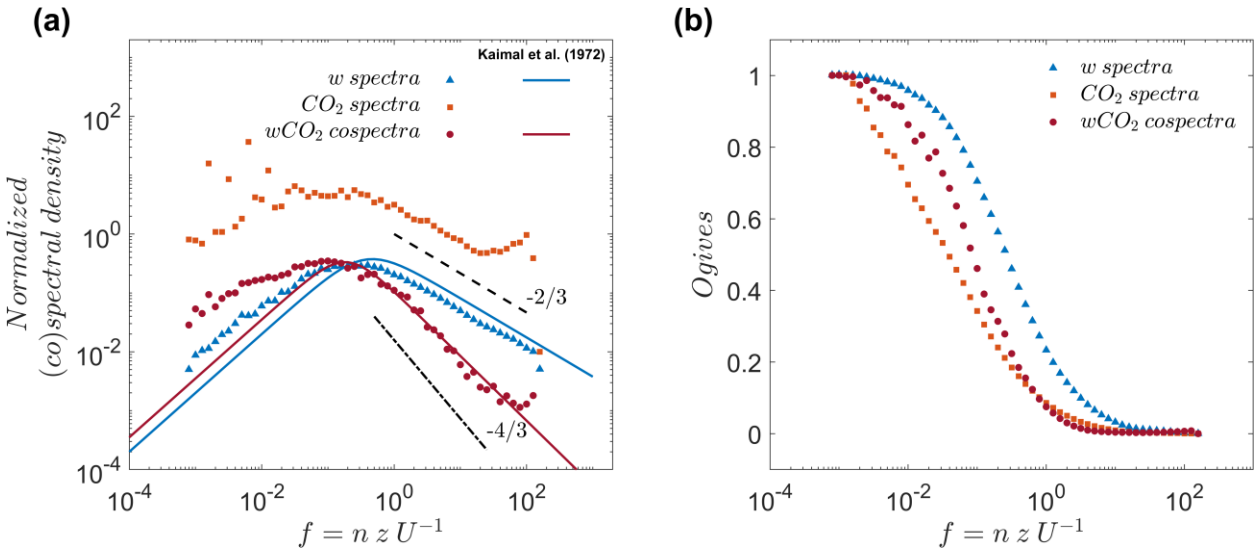

Figure 5.4 Normalized spectra/co-spectra of w, ρ_c and $w\rho_c$ during neutral conditions (a), and their respective ogives (b).

5.2.4 General diurnal atmospheric and traffic condition

To support the discussion of CO_2 flux in Jakarta, average characteristics of weather and climate in Jakarta were checked from average ambient measurement. The traffic condition also evaluated using traffic percentage data from TomTom traffic index.

Based on K*ö*ppen-Geiger classification (see Kottek *et al.*, 2006; Peel *et al.*, 2007), Jakarta's climate can be considered as tropical rainforest (Af) or tropical monsoon (Am) with monthly-mean temperature higher than 18 ℃ and precipitation on driest month above 30 mm. The average diurnal temperature observed at LLH is between 26 to 32 ℃, while the relative humidity is between 58 to 88% (Figure 5.5a, b). The diurnal wind observed at LLH site (Figure 5.5c) is dominated by meridional wind with an average range between -2 to 1 m s^{-1}, clearly indicating sea and or land breeze signal. The average zonal wind only ranges between 0 to 0.5 m s^{-1}, clearly indicating highly attenuated flow by the roughness element shown in Figure 5.3.

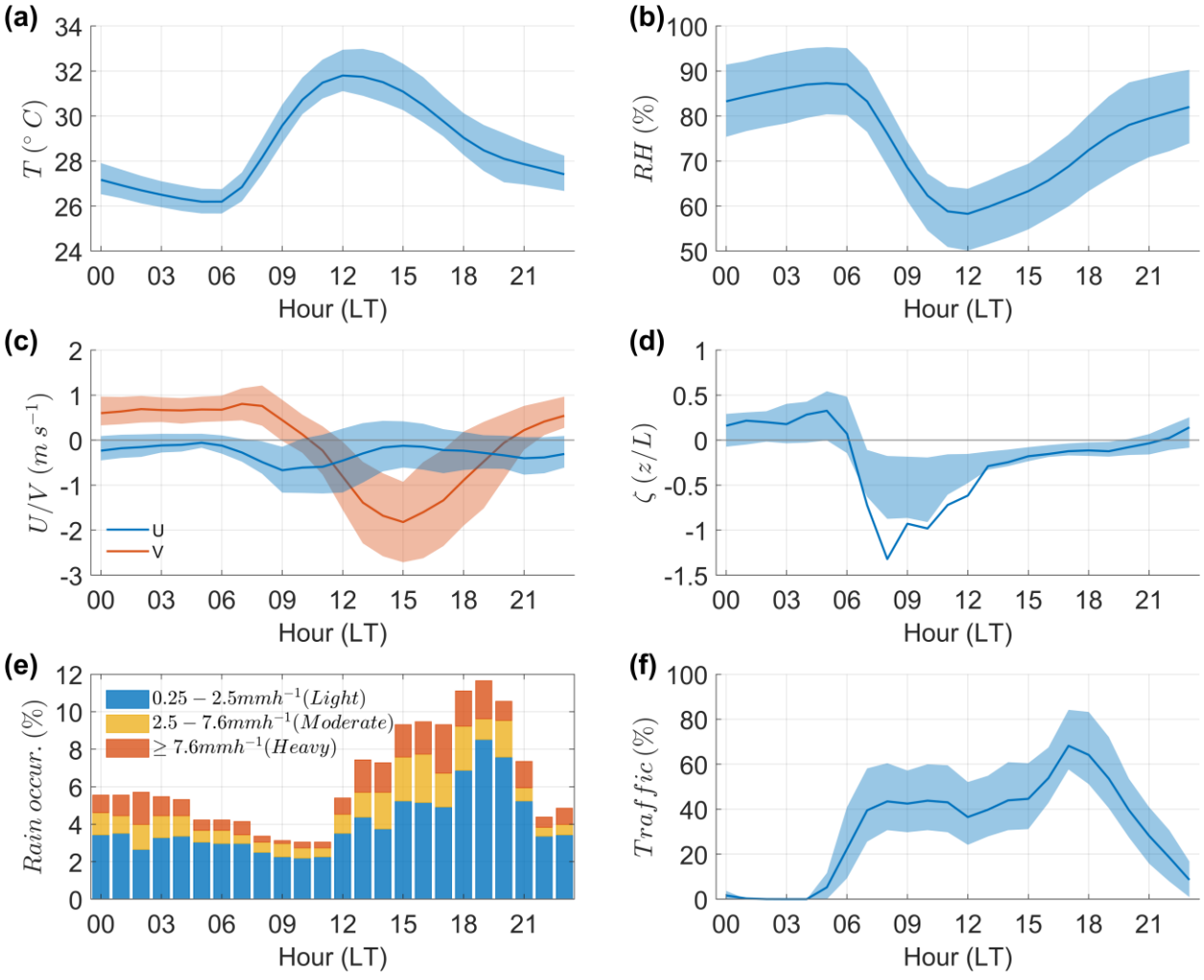

Figure 5.5 Average diurnal condition of temperature (a), relative humidity (b), zonal and meridional wind components (c), stability parameter (d), percentage of rain occurrence (e), and percentage of traffic in Jakarta(f). Blue or red shade in (a)-(d) and (f) shows the interquartile range (IQR) of each parameter. Plot (a)-(e) are based on data observed at LLH, while traffic percentage at (e) is based on data from TomTom traffic website (TomTom International BV, 2022).

Diurnal stability parameters (ζ) shows mostly weakly stable condition during nighttime, and a mostly unstable condition during daytime (Figure 5.5d). Unstable air relatively developed rapidly in the morning, immediately after sunrise. However, transition into stable condition in the nighttime is quite slow, long after sunset, an indication of the existence of anthropogenic heat in typical urban areas. On the other hand, rainfall data record at LLH (Figure 5.5e) shows that rain mostly occurs in the afternoon and evening, clearly a typical tropical-monsoonal rainfall pattern (Renggono *et al.*, 2001; Yamanaka, 2016). While mostly dominated by light rain, between 15:00 to 18:00 LT, the frequency of moderate and heavy rainfall is also high, almost the same as light rain. The lowest frequency of rain is found in the morning, around 08:00 to 11:00 LT.

Typical daily traffic conditions in Jakarta, as shown in Figure 5.5f, peak around 16:00 to 18:00 LT, during end of working hour. In the morning there is a steep increase in traffic percentage, starting at 04:00 until around 08:00, which can be associated with morning rush hour. The typical traffic condition in Jakarta drops to minimum value only after 23:00 LT and last until the start of the morning rush hour.

5.3 Results and discussion

Monthly-diurnal pattern of CO_2 flux and concentration is presented on Figure 5.6a and b. Both flux and concentration clearly indicate a diurnal pattern, however on seasonal scale the flux pattern is less clear. Even so, it is obvious that the flux rate is much higher in 2019 compared to the subsequent year. The concentration, however, does not show such a similar pattern. Instead, it seems to increase toward 2022. Lighter shade around dry season of May to September 2019 and 2020 become darker in the following year, suggesting an inter-annual increase in CO_2 concentration. The diurnal pattern of F_{CO_2} show peak during daytime, while C_{CO_2} peaked during early morning, just around sunrise.

Table 5-2 All-time average of CO_2 flux (F_{CO_2}) and concentration (C_{CO_2}) observed in Jakarta

	F_{CO_2} (mg m^{-2} s^{-1})	C_{CO_2} (ppm)
Daytime (07 - 18 LT)	1.51 ± 1.22	414.83 ± 18.22
Nighttime (19 - 06 LT)	0.57 ± 0.94	426.72 ± 23.24
All-day (24 hour)	1.09 ± 1.20	420.19 ± 21.47

The average daily CO_2 emission and concentration observed in Jakarta is tabulated on Table 5-2. Comparison between daytime and nighttime is also presented. On average, the urban atmosphere in Jakarta received 1.09 mg m-2 s-1, while the all-time averaged concentration is 420.19 ppm. When comparing between daytime and nighttime, it is obvious that turbulent exchange of CO_2 into the atmosphere is mostly active during daytime. However, deposition of CO_2 into the ground is more rigorous in the nighttime than daytime, causing a higher average value of concentration.

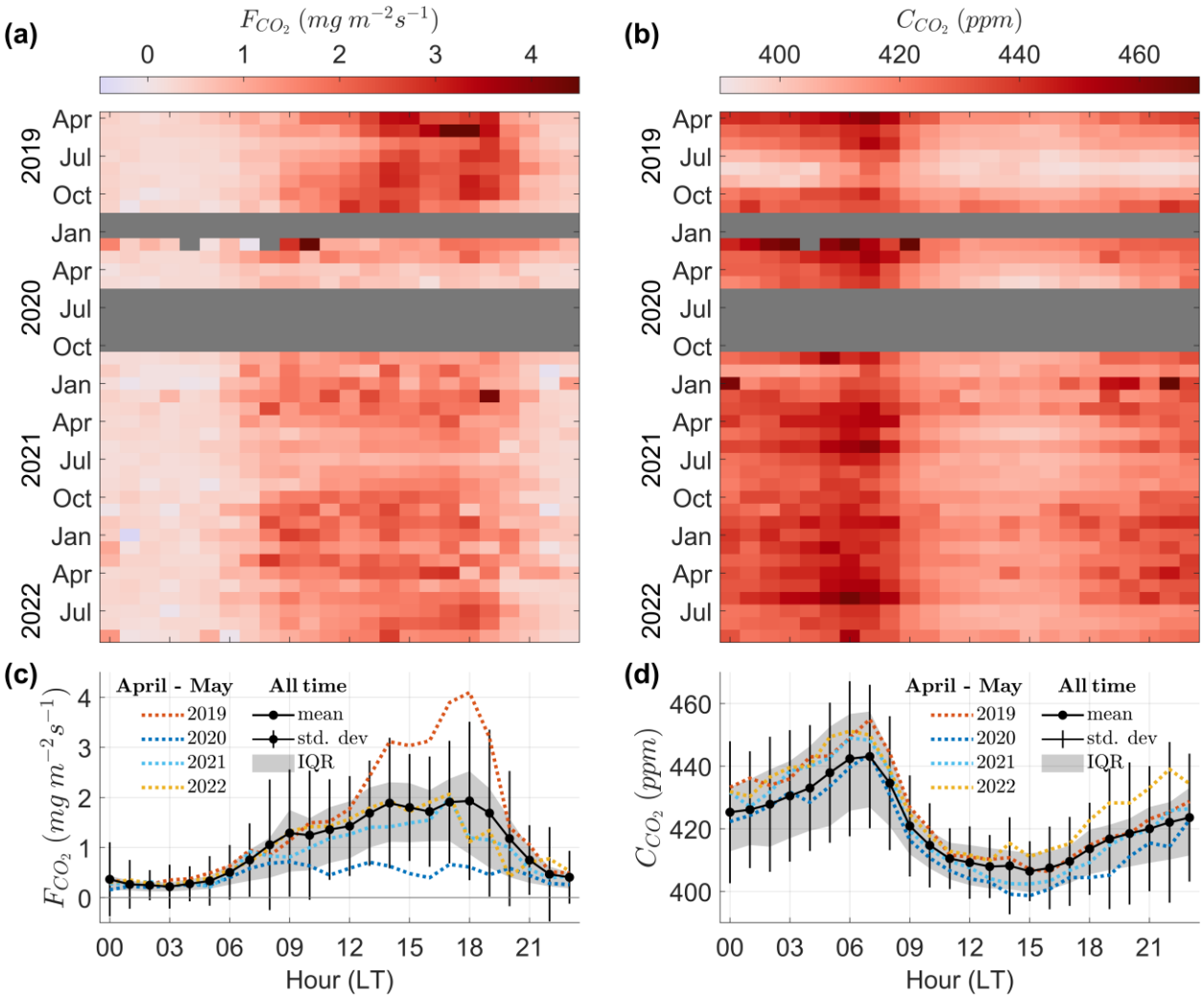

Figure 5.6 Monthly-diurnal average of CO_2 flux (a) and CO_2 concentration (b); and their corresponding all-time diurnal average (solid line with black circle), standard deviation (errorbar), and interquartile range/IQR (grey shade) (c and d). On c and d, the yearly based diurnal average during April to May also plotted as an inter-annual comparison.

The all-time diurnal pattern of CO_2 flux (Figure 5.6c) shows a maximum average value around 2 mg m^{-2} s^{-1}, almost double than the average values observed in other cities like Singapore (Roth *et al.*, 2017), Tokyo (Moriwaki and Kanda, 2004; Hirano *et al.*, 2015; Sugawara *et al.*, 2021), Sakai (Ueyama and Ando, 2016; Ueyama and Takano, 2022), and Mexico City (Velasco *et al.*, 2009). The pattern also shows a distinguishing shape with only one peak in the late afternoon. Even though the traffic percentage shows steep increase in the morning hour (Figure 5.5f), there is no sharp increase in the morning F_{CO_2} pattern. Instead, a close dual peak is observed at 14:00 and 18:00 LT. The peak at 18:00 LT can be associated with the afternoon traffic peak, but the 14:00 peak might be caused by a different factor.

On the other hand, the diurnal CO_2 concentration pattern is similar to the patterns found in many other cities such as Singapore and Tokyo. The peak C_{CO_2} is observed in the morning at 07:00 LT and the minimum value is observed at 15:00 LT. The magnitude of C_{CO_2} also comparable to F_{CO_2} observed in Tokyo during winter time (Moriwaki and Kanda, 2004), but still higher than Singapore (Roth *et al.*, 2017). It is important to note that, increase rate of CO_2 concentration in each city is different and most of the studies were conducted several years earlier, thus a significant difference in concentration is expected.

5.3.1 Weekly rhythm of CO_2 flux and concentration

The weekly diurnal rhythm of CO_2 flux shows similar resemblence to traffic pattern, except for Monday (Figure 5.7a). It is obvious that the weekdays pattern were much similar to the general pattern shown in Figure 5.6c. The highest CO_2 emission is observed on Friday, a day which is associated with highly jammed traffic outflow where many of Jakarta citizens opt to go outside the city. On Monday, the traffic flow is reversed, hence the morning traffic peak is obvious. However, the CO_2 emission is not corresponds to this traffic increase. Instead, a gradual increase in the flux is observed. No explanation could be found for this, as on any other days-od-the-week, the CO_2 flux corresponds to traffic patterns quite well.

During weekend, the traffic condition is much relaxed, hence the CO_2 flux shows much lower values. There is also shift in the peak, whereas during weekdays the peak of CO_2 flux usualy occur around 18:00 LT, but during the weekend the peak shift earlier to around 14:00 or 15:00 LT. This shift is more obvious from the comparison between composite of all weekdays and all weekend presented on Figure 5.8a. Double afternoon peaks that was shown on general diurnal

pattern of CO_2 flux (Figure 5.6c) was caused by shift of weekend peak to an earlier hour. If the weekdays is holiday, the CO2 flux shows significant reduction. This probably caused by the tendency of Jakarta citizen to stay at home during these days, hence reducing the number of traffic.

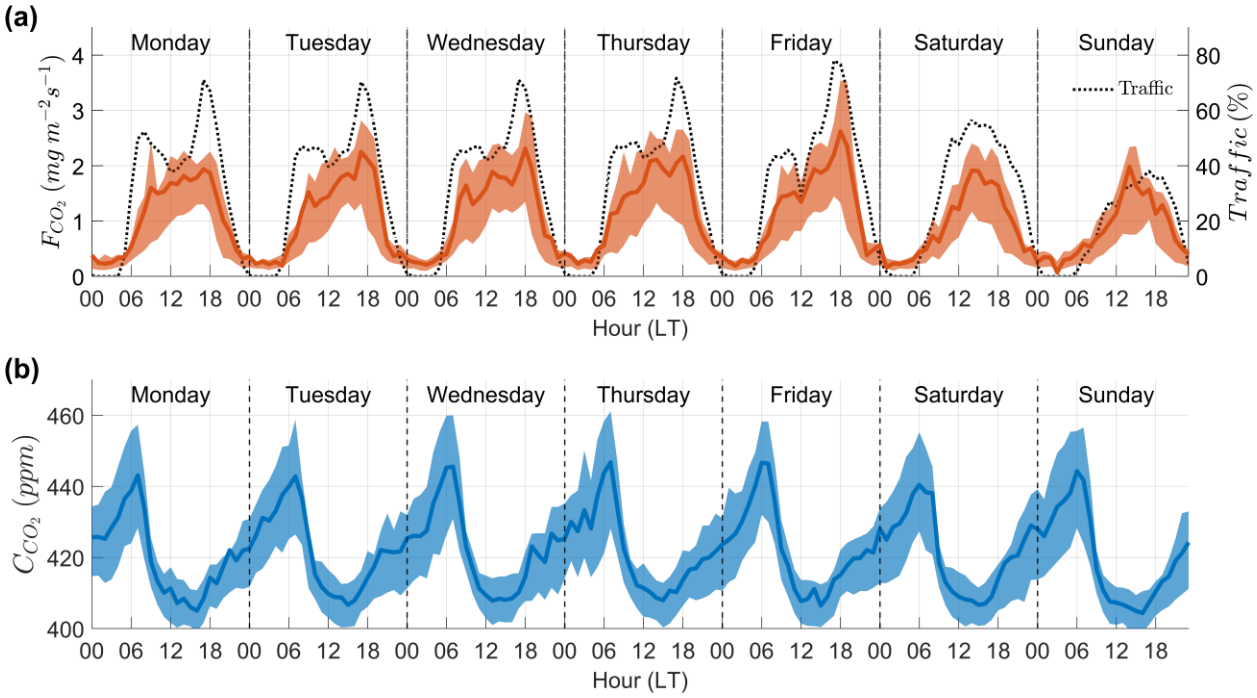

Figure 5.7 Day-of-the-week-averaged diurnal pattern of CO_2 flux (a) and concentration (b). Red (blue) shade denotes the interquartile range of CO_2 flux (concentration). Dashed line in (a) shows the average traffic percentage in Jakarta.

On the other hand, weekly pattern of CO_2 concentration does not seem to change so much between weekdays and weekend, even between days (Figure 5.7b). The weekly C_{CO_2} pattern almost identical with its general diurnal pattern with peak around 07:00 LT and lowest values around 14:00 to 15:00 LT. It can be seen from Figure 5.8b, that the diurnal concentration pattern between weekdays and weekends is similar to the genaral diurnal pattern of CO_2 concentration. Even so, when the flux is reduced significantly, as the case of holidays during the weekdays, the concentration also reduced. This confirm that CO_2 concentration might not only regulated by CO_2 emission, but also by many different mechanism. In the study of pollutants and air quality, the source-sink relationship, as well as the transfer or dispersion mechanism should be addressed carefuly (Stull, 2020).

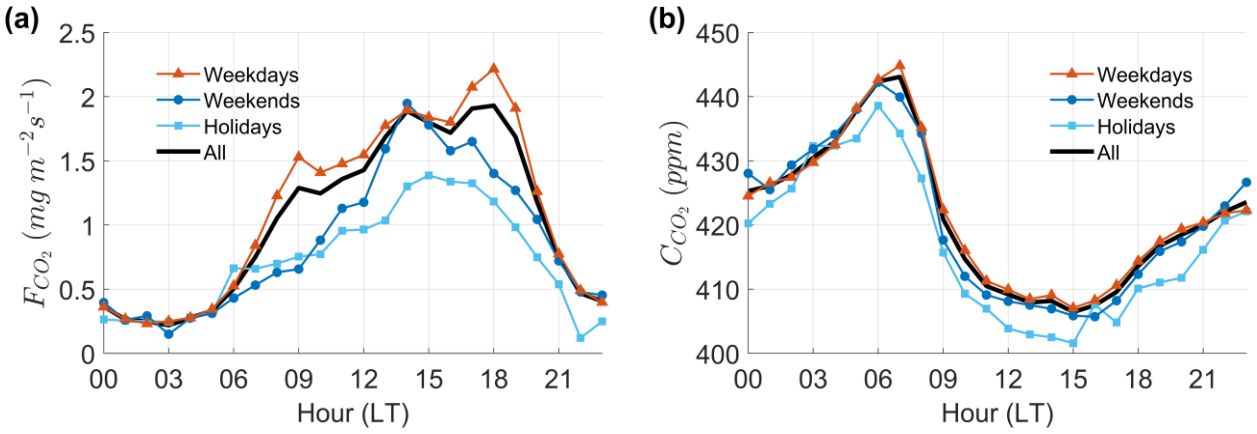

Figure 5.8 Diurnal pattern comparison between weekdays (red-triangle), weekends (blue-circle), and non-weekend holidays (cyan-square) for CO_2 flux (a) and CO_2 concentration (b). Black solid line shows the all-time averaged diurnal pattern, same as in Figure 5.6c and d.

5.3.2 CO_2 flux and diurnal circulation of sea and land breeze

During weekdays, traffic pattern always show morning peak between 07:00 and 08:00 LT, however the CO_2 flux does not show that morning peak, just as shown on Figure 5.6c. One explanation for this is that turbulence is not yet developed due to stable surface condition (Aubinet *et al.*, 2012; Foken *et al.*, 2012). This will causing the CO_2 stay below the sensor, hence reducing the flux. However, stability parameter shown in Figure 5.5d has shown that after 06:00 LT turbulence condition has already developed, hence this reasoning cannot be proven.

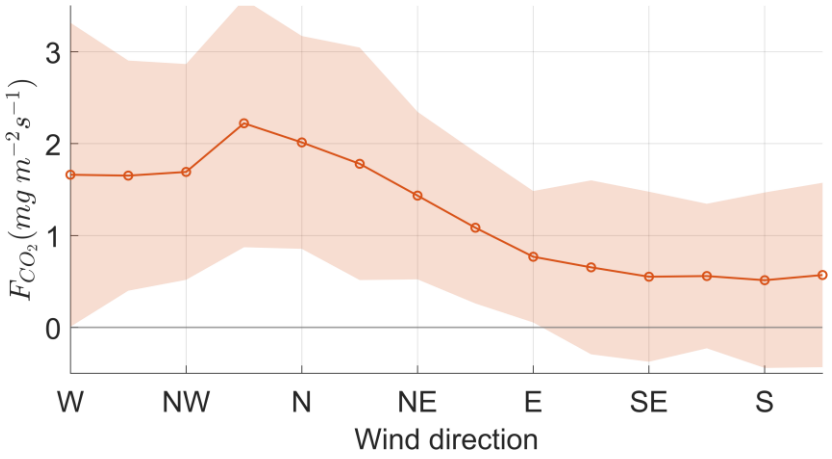

Figure 5.9 Plot of F_{CO_2} versus horizontal wind direction with mean values shown with red line with circle and red shade shows the interquartile range of F_{CO_2} with wind comes from respective direction.

Investigating the relationship between F_{CO_2} and wind direction it was obvious that wind from west (W) to north east (NE) is associated with higher F_{CO_2} than wind from east (E) to south west (SW) (Figure 5.9). The discrepancy in F_{CO_2} between these sectors could reach over 1 mg m-2 s-1, which is very significant. Many researcher have been showing the strong dependence of CO_2 flux to the source area (Velasco *et al.*, 2009; Roth *et al.*, 2017). Change in flow direction will causing the shift of source area percieved by the sensor. In case the source area contains many potential CO_2 emitter, such as main road or fossil fuel power plant, the magnitude of flux coming from such areas will increase significantly. Existence of major roads in the northern area of the site may contribute to the higher CO_2 flux when the flow comes from this direction (see Figure 5.1).

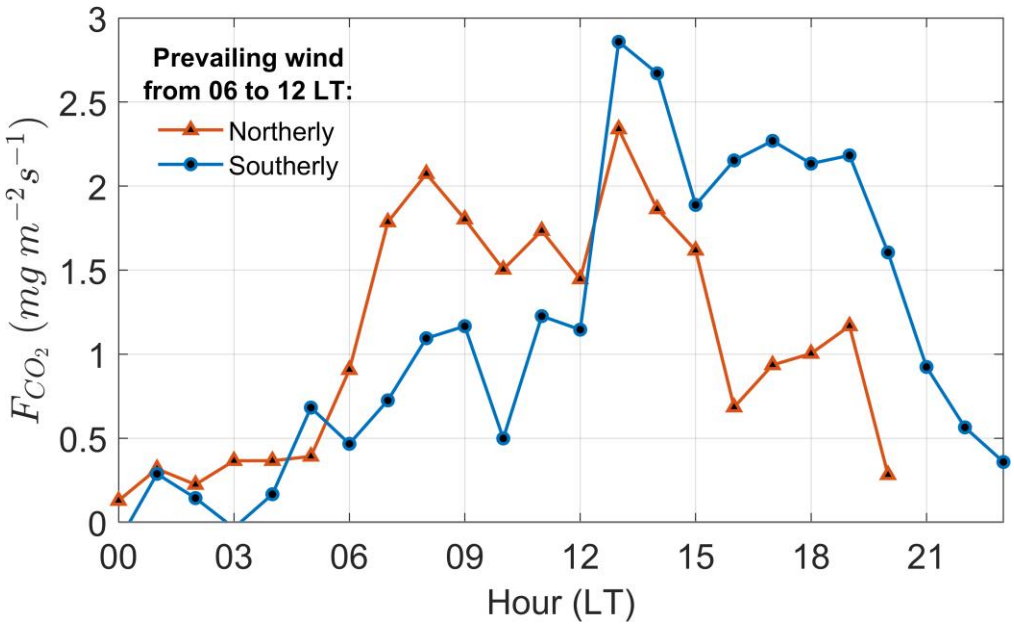

Figure 5.10 Composite diurnal average of CO_2 flux when morning (06:00 – 12:00 LT) wind dominated by northerly wind (red) and southerly wind (blue).

However, footprint analysis in Figure 5.1b shows that dominant source area from the northern side of the site is mostly occurring in the afternoon or evening, which explains why the peaks of CO_2 flux occur around this timeframe. To investigate the no-peak case in the morning, flux data when dominant wind in the morning (06:00 – 12:00) comes from northern sectors (northerly) were isolated. The composite average of this flux dataset is then compared with flux dataset when morning wind flow is dominated by southerly wind. The result is presented in Figure

5.10. The figure clearly shows that when dominant wind in the morning is northerly, the morning peak in CO_2 flux is observed, while in normal cases of southerly wind the peak is diminished. As shown in the previous chapter, the north-south wind (meridional) in Jakarta is driven by sea and land breeze. Thus, this result shows that the sea and land breeze might control the CO_2 flux condition via change in the source area. When the sea breeze reaches earlier in the LLH site, there is a possibility that the morning peak in flux will be observed. This might be the case that often occurs in rainy season as during this season the sea breeze starts earlier and propagates faster. On dry season, land breeze usually still predominant in LLH area and sea breeze usually arrive late in the afternoon, hence the flux pattern will not be showing a peak in the morning.

5.3.3 CO_2 concentrations and the atmospheric boundary layer

In the previous section, it was shown that CO_2 concentrations might be regulated by other mechanisms as it did not correspond well to any changes in the flux or the source (traffic). Since concentration is similar to storage term, then the most possible parameter that regulate it is the length scale of boundary layer or boundary layer height (Stull, 1988; Arya, 2001). Figure 5.11 shows the scatter plot of daily mean ABL height and daily mean CO_2 concentration. It was clearly shown that there is an almost linear relationship between the two variables. With a slope of -0.07, the CO_2 concentration has a strong relationship with the inverse of boundary layer height.

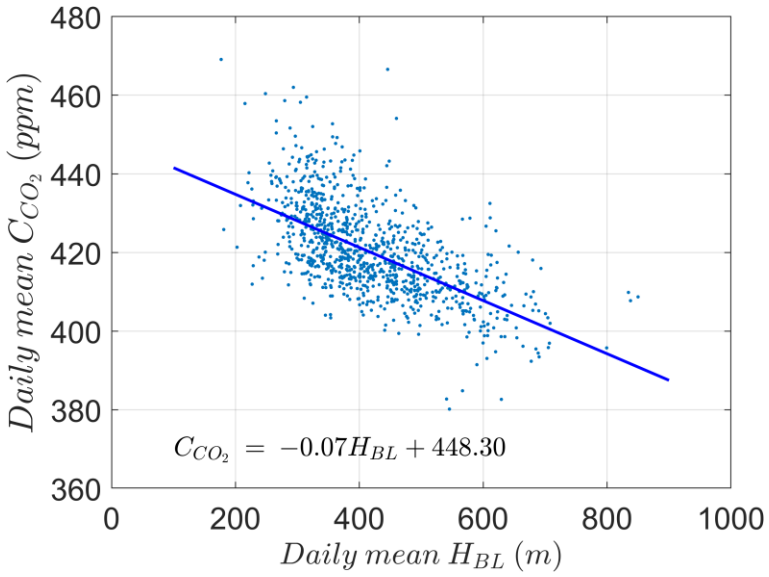

Figure 5.11 Scatter plot between daily mean atmospheric boundary layer height (H_{BL}) with daily mean CO_2 concentration observed at LLH.

In Figure 5.12, the inverse diurnal average of ABL height (H_{BL}^{-1}) from ERA5 reanalysis is compared against diurnal average of CO_2 concentration observed at LLH. It shows a remarkable similarity in the pattern with correlation around 0.84. By applying a time lag of 1-hour to the H_{BL}^{-1} data, it was found that both data match with correlation of 0.97. This result can be interpreted as the lag time between change of boundary layer height to respond of CO_2 concentration is around 1-hour. This result clearly shows the importance of ABL height to the accumulation of CO_2 and maybe other gases and pollutants. Thus, it is beneficial to study ABL height variability in order to study the behavior of GHGs and pollutant concentration in Jakarta.

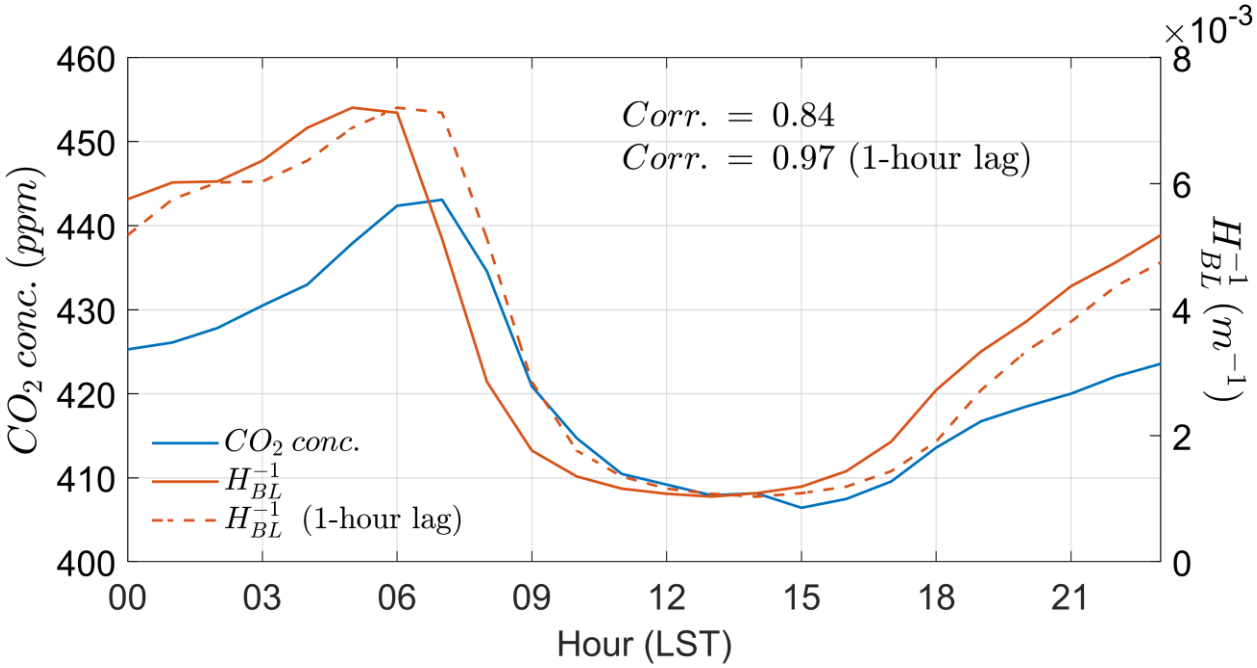

Figure 5.12 Diurnal average of CO_2 concentration (blue solid line) compared to diurnal average of inverse boundary layer height (H_{BL}^{-1}) (red solid line). The dashed red line is the H_{BL}^{-1} with a lag of 1-hour.

5.3.4 Impact of social restriction during COVID-19 pandemic

The CO_2 observation data in LLH contains data during the period of COVID-19 pandemic. Despite severe consequences caused by the pandemic, this presents an opportunity to assess drastic measures in reducing CO_2 emission. During the pandemic, the Indonesian Government through the Governor of Jakarta imposed an intermittent large scale social restriction in Jakarta. There are two major types of social restrictions that were imposed in Jakarta. First is the strict social restriction where mobility is suppressed at the minimum level, and second is the relaxed social

restriction where human mobility is allowed to a certain extent (Anugerah *et al.*, 2021). The strict social restrictions were mostly imposed during the early year of pandemic, while the relaxed one is implemented mostly in the last year. By collecting the records of these restrictions from various sources and using it to cluster the CO_2 flux and concentration, the average diurnal condition of each level of restriction is calculated. The result is presented in Figure 5.13.

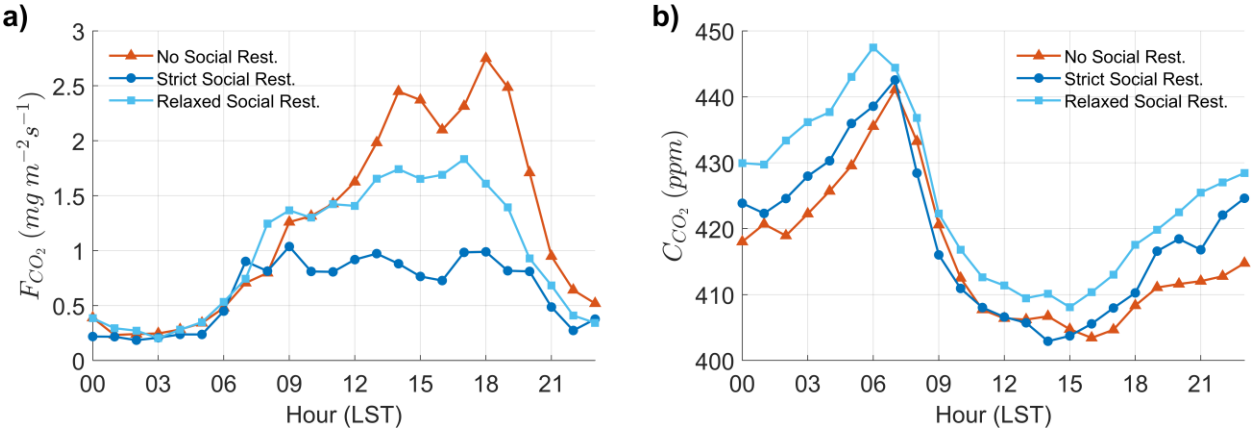

Figure 5.13 Average diurnal pattern of CO_2 flux (a) and concentration (b) composited during days when no large scale social restriction (red), strict social restriction (dark blue), and relaxed social restriction (blue) is applied in relation with COVID-19 pandemic.

Figure 5.13a clearly shows the reduction of CO_2 flux observed during the restriction, either in strict or relaxed restriction. The strict social restriction results in reduction of more than 50% during daytime compared to days without the restriction. This reduction value is much larger than flux reduction reported in other city (Sugawara *et al.*, 2021; Velasco, 2021; Venturi *et al.*, 2021; Ueyama and Takano, 2022). In the relaxed restriction period, the reduction in daytime CO_2 flux was only less than a half of the strict restriction. Nighttime flux does not seem to show significant difference as during this time either the citizen's activities reduced, or the air become fully stable and inhibit vertical flux exchange. This result clearly shows that such a drastic measure in limiting mobility, hence transportation, will significantly contribute to reduction of CO_2 emission.

In contrast, CO_2 concentration seems to be not affected by the restriction at all. The highest average concentration is found during relaxed social restrictions as opposed to no social restrictions. This finding confirms that the main governing factor of CO_2 concentration in a city is not only its emission rate (source), but also many other processes and conditions, such as the

transfer rate, the spatial length scale to mixing it, and most importantly, its storage process rate (sink). These processes are illustrated in Figure 5.14.

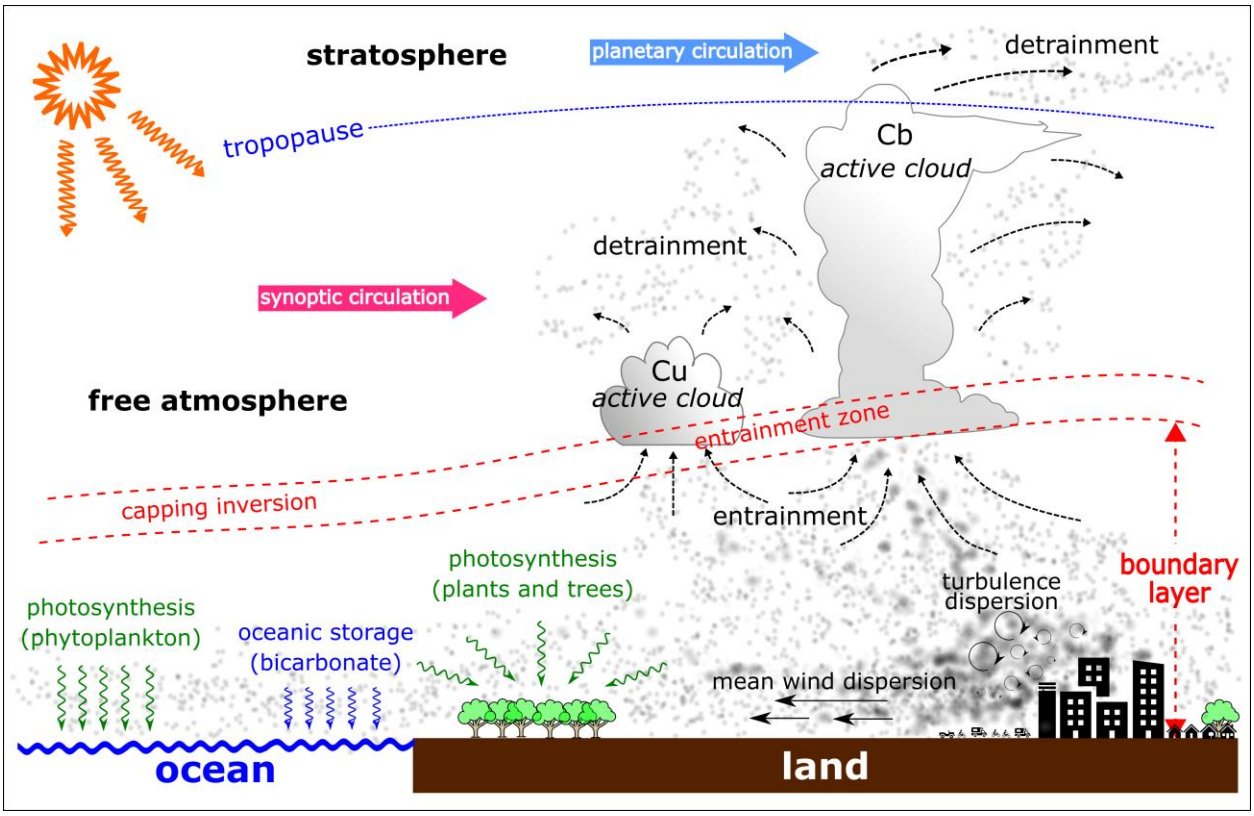

Figure 5.14 Illustration of various CO_2 transfer and sink processes that are important in reducing the CO_2 concentration.

In a short period, reduction of in a place is govern by its dispersion rate, either horizontally by the mean (prevailing) wind or vertically by turbulence transfer (Figure 5.14). Prevailing wind flow will carry CO_2 out of the city and reduce its concentration. In Jakarta, the prevailing wind is dominated by the sea and land breeze. During daytime the sea breeze might sweep out the CO_2 to southern areas of Jakarta, such as Depok and Bogor, but in the nighttime the land breeze might carry it again to Jakarta while being "packed" by the compressed boundary layer. As explained in Chapter 2, the sea breeze front might also lift the CO_2 from the surface and carry it to the sea via the sea breeze return flow. However, there is also possibility that these CO_2 will be carried again to the shore in the next cycle of the sea breeze (Talbot *et al.*, 2007; Arrillaga *et al.*, 2018). On the other hand, vertical turbulence transfer is limited by the height of ABL. On top of ABL, there is a capping inversion which acts like a lid and prevent material transfer from the ABL out into the

free atmosphere above it (Stull, 1988, 2020). In the presence of active clouds, such as convective cumulus (Cu) clouds, the CO_2 from ABL could be entrained into the clouds and then detrained out in the free atmosphere, effectively passing the capping inversion. In the free atmosphere, this CO_2 then spreads by synoptic flows, such as trade winds and monsoon, to a much larger area. On cases of very strong active clouds like cumulonimbus (Cb), CO_2 from the ground may reach the stratosphere. Cb clouds can knock the tropopause, creating a distinguished table shape with bulges on its top. Once detrained into the stratosphere, the CO_2 could be picked up by planetary circulation, such as the Brewer-Dobson circulation (Butchart, 2014; Diallo *et al.*, 2021), and then distributed in much wider scales. This entrainment-detrainment process by active clouds is the mechanism that might be responsible for the regional or global dispersion of CO_2 and other atmospheric constituents.

While the transfer process may reduce CO_2 concentration at some place, it is not removed it from the atmosphere. The transfer process only distributes the CO_2 in bigger space, in other words, diluting the CO_2. Processes that effectively remove the CO_2 from atmosphere are photosynthesis by plants, trees and phytoplankton in the ocean, and chemical interactions with ocean to produce calcium bicarbonate (CaCO3) (Figure 5.14). These processes are known as the CO_2 biogeochemical sinks (Moore III and Braswell, 1994; Archer *et al.*, 2009). With the limited amount of vegetation in the city and two of these biogeochemical processes occurring in the ocean, an effective transfer of CO_2 into the ocean might play important roles in determining the rate of CO_2 reduction from a city.

The finding that social restriction during COVID-19 pandemic does not reduce the CO_2 significantly confirms that the time required to reduce the CO_2 concentration might be much longer than the restriction period. Even with very effective transfer and sink processes, it still requires a long time to reduce the amount of excess CO_2. It is estimated that it would require 27 to 49 years to reduce the excess CO_2 after we stop emitting anthropogenic CO_2 completely (Moore III and Braswell, 1994). Without terrestrial vegetation, this number could increase to 92 years. Thus, unsignificant reduction in CO_2 concentration even after 2 years of emissions reduction during pandemic is to be expected, as the lifetime of CO_2 is much longer than that. This result also confirms the necessity to do continuous reduction of CO_2 emission in Jakarta for long periods, much longer than the lifetime of CO_2 in the atmosphere, in order to effectively reduce its concentration.

5.3.5 Annual variability of CO_2

As the diurnal circulation of sea and land breeze were affected by seasonal change, it is expected that micro-scale CO_2 flux and concentration is also affected by seasonal change. In the previous section has been shown that CO_2 flux increases when sea breeze dominates the wind field. However, distribution plot of F_{CO_2} does not seem to exhibit such seasonal patterns (Figure 5.15a). A slight variation was only found for October, where it seems higher and has a wider range, similar to distribution of March. Compared to observation in Singapore (Roth *et al.*, 2017), the closest comparator for tropical city, the observed flux has a seasonal variation which induced by change in source areas by the prevailing wind. Since both cities were governed by the same Asian-Australian Monsoon, these discrepancies need to be investigated further. There is no valid explanation for the time being, but further analysis will be required.

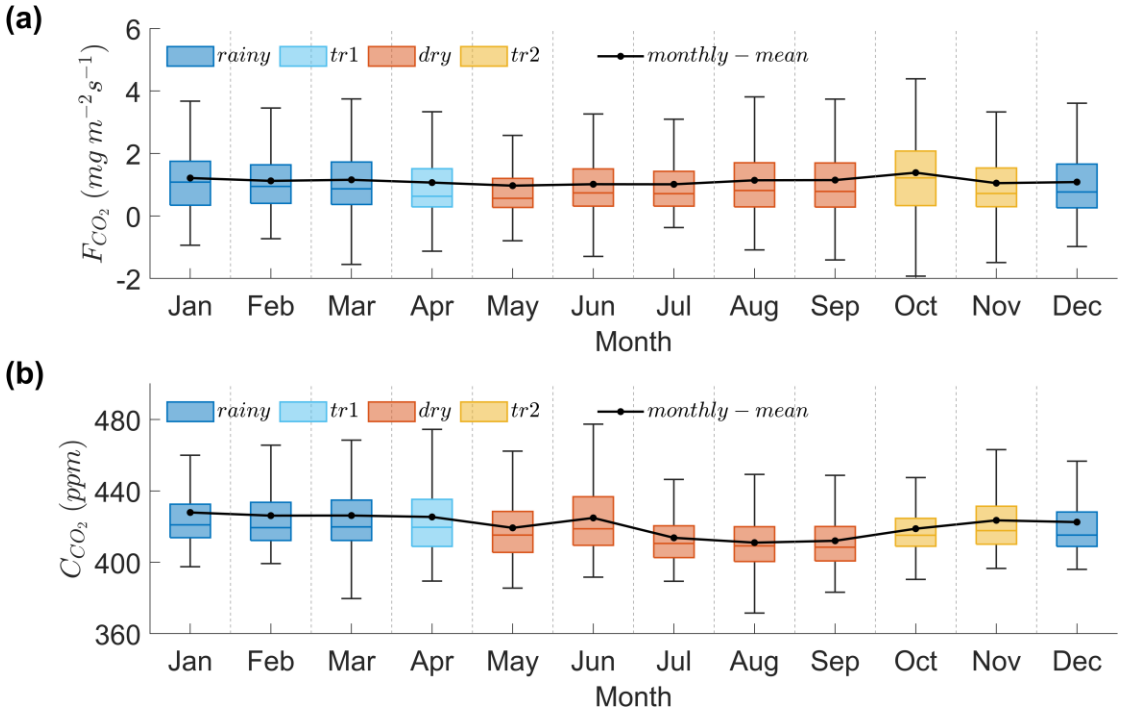

Figure 5.15 Monthly distribution of CO_2 flux (a) and CO_2 concentration (b) in the form of boxplot. The box plot is color coded for different periods of season as defined in Chapter 3 of this document.

As opposed to the CO_2 flux, the concentration shows an annual variation (Figure 5.15b). However, this variation does not seem to match the seasonal change. It could be traced that this variation might be driven by variation of ABL height. For that reason, a dataset of boundary layer

height will be required. The boundary layer dataset from ERA5 might not adequate since its resolution (~30 km) is still too coarse for urban micro-scale studies. These conditions open an opportunity to do further research related to annual variation of CO_2 flux and concentration in Jakarta. As will be addressed in the next chapter, this research topic will become one of the research projects to be conducted as the continuation of this study.

5.3.6 Long-term trend of CO_2 flux and concentration in Jakarta

Even though CO_2 flux in Jakarta did not show significant seasonal variation, in the longer term, it shows a decreasing trend (Figure 5.16a). This decreasing trend might be caused by the large-scale social restriction that was imposed during the COVID-19 pandemic. Even though decreasing, however, it is expected that it only for a temporary period. As shown in yearly comparison of April-May composite on Figure 5.6c, the diurnal CO_2 flux rate in 2022 slowly increases to return to condition in 2019. If the observation continued, perhaps such a bounce back process will be evident.

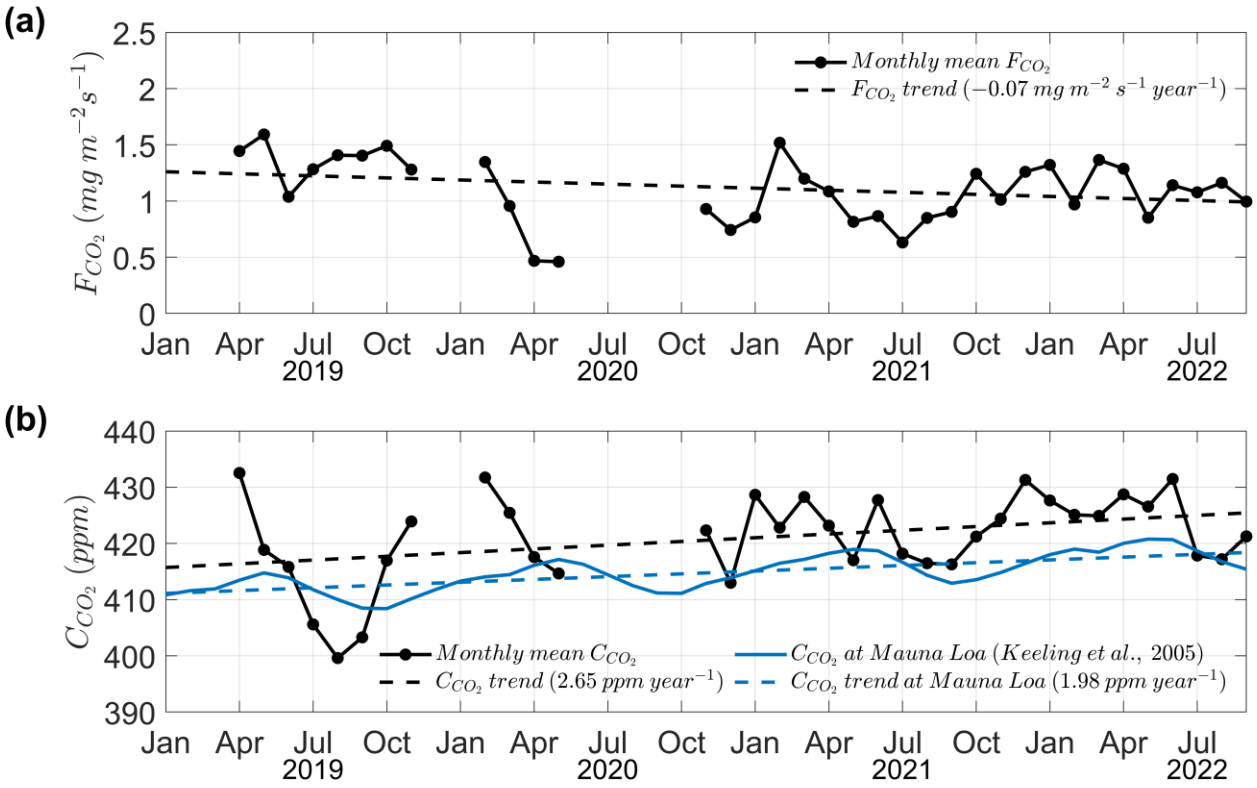

Figure 5.16 The long-term monthly average of CO_2 flux (a) and concentrations (b) that were acquired during observation campaign in Jakarta. Solid and dashed blue lines on (b) shows long-term monthly average of global CO_2 background concentration observed at Mauna Loa, Hawaii (Keeling *et al.*, 2001).

While the flux decreases, the CO_2 concentration still steadily increases. As shown in Figure 5.16b, the CO_2 concentration in Jakarta increases by 2.65 ppm $year^{-1}$. This slope is slightly larger than the increasing slope of global background CO_2 observation at Mauna Loa, Hawaii. The trend of CO_2 in Jakarta is larger by 0.67 ppm $year^{-1}$. This result confirms that cities, especially megacities like Jakarta, are net source of CO_2 (Velasco and Roth, 2010; Grimmond and Christen, 2012; Oke *et al.*, 2017). With the number of Jakarta's population is expected to grow rapidly (UN DESA, 2018; BPS Provinsi DKI Jakarta, 2023), its CO_2 concentration is also expected to increase (Hofmann *et al.*, 2009). Thus, several strategic policies are required to reduce the CO_2 concentration in Jakarta. These policies are important, not only to mitigate the effects of global climate change, but also to improve the local air quality of Jakarta.

5.4 Summary and conclusion

Daily average CO_2 flux in Jakarta is 1.09 mg m^{-1} s^{-1} and daily average CO_2 concentration is 419.12 ppm. The diurnal pattern of CO_2 flux shows one peak in the afternoon, which differs from daily traffic condition which shows peaks in the morning and afternoon. Sea and land breeze advection strongly influence the diurnal pattern of CO_2 flux in Jakarta. Diurnal pattern of CO_2 concentration shows inclination during nighttime with peak after sunrise. Daily averaged CO_2 concentration has strong inverse-correlation with daily averaged boundary layer height with lag time of 1-hour. Thus, the height of atmospheric boundary layer is one of the major influential factors to the near surface CO_2 concentration in Jakarta.

On a weekly basis, a higher CO_2 peak is observed on Friday afternoon which is caused by traffic surge out from Jakarta. However, this short-term increase of CO_2 flux does not affect CO_2 concentration which shows similar pattern as any other days. A significant decrease in CO_2 flux is observed in 2020 due to traffic restriction imposed during early COVID-19 pandemic, although it is evident that the flux slowly increases in the next two years. While CO_2 flux varying significantly because of the pandemic, CO_2 concentration shows less significant changes and almost return to previous condition (2019) in 2022. Since the lifetime of CO_2 in the atmosphere is more than 19 years, reduction of CO_2 emission during COVID-19 pandemic does not result in significant reduction of CO_2 concentration in Jakarta.

On longer time scales, CO_2 flux does not exhibit annual variation or significant increasing trend. Instead, the long-term flux trend shows a decreasing trend. On the contrary, CO_2 concentration shows an annual variation which might be induced by annual variation of boundary layer height. In a long-term near surface CO_2 concentration shows a steady increasing trend that is in line with the global background CO_2 trend, although the trend of Jakarta is slightly higher. The CO_2 concentration trend in Jakarta is 0.6 ppm year-1 higher than global trend suggesting that Jakarta can be considered as net source of CO_2.

Chapter 6 Concluding Remarks

The ability of a city to cope with urbanization effects and global changing climate will heavily depend on the understanding of physics and dynamic atmospheric processes in that city. Such knowledge will be invaluable for the formulation of mitigation strategies and policies. In recent years, the megacity of Jakarta has seen a more frequent severe impact of changing atmospheric as the consequences of rapid urbanization and climate change. It was hypothesized that these events might be related to modification of the diurnal circulation (sea/land breeze) and variation in turbulence transport of energy and other scalars inside Jakarta. Interaction between various scale atmospheric phenomena inside the lowest layer of atmosphere is the main driver of weather and climate patterns. While there are many studies dedicated to macro-scale phenomena, there are only limited studies on meso- to micro-scale urban atmospheric dynamics in Jakarta.

This study aims to extend the knowledge on mesoscale circulation of sea breeze in Jakarta and touch the micro-scale atmospheric condition in Jakarta. This study might be the first attempt to study the micrometeorological urban CO_2 flux exchange in Jakarta. It is hoped that this study will contribute to atmospheric sciences in Indonesia, especially for meso- and micro-scale meteorology. The observation results conducted in this study is also hoped to become measurement baseline for micro-scale atmospheric variation in Jakarta and serve as invaluable reference for future urban micrometeorological studies in Jakarta or generally in Indonesia.

6.1 Research findings

Although only covered a limited interaction between meso- and micro-scale phenomena in urban atmospheric environments of Jakarta, there are several findings that were revealed from this study. Several of the major findings are listed in the following.

1) There is a seasonality in the diurnal circulation of sea breeze in Jakarta, where the sea breeze started earlier, propagated faster, but last in shorter periods during the rainy season than the dry season.
2) The overland temperature distribution induced by early-morning cloudiness plays an important role in the seasonality of sea breeze in Jakarta.
3) The urban surface heating rate and possible urban heat island (UHI) circulation may also contribute seasonal differences of sea breeze in Jakarta.
4) Coastal morphology of Jakarta and surrounding areas might induce lateral variation in boundary layer height during sea breeze propagation that could trigger momentary deposition of CO_2 or other pollutants.
5) The CO_2 emission rate and concentration in Jakarta is comparable to several other cities in the world, however the peak diurnal CO_2 emission shows a higher value of almost twice compared to several cities.
6) The diurnal CO_2 flux in Jakarta has an inline pattern with traffic condition as the main source of emissions, but also highly regulated by the sea and land breezes as it controls the source area of the flux.
7) Daily CO_2 concentrations in Jakarta have a strong correlation with atmospheric boundary layer height as it is the indicator of the spatial extent of CO_2 turbulent mixing.
8) The large-scale social restriction during COVID-19 pandemic is shown to significantly reduce CO_2 emission in Jakarta, however it is not contributing much to the reduction of near surface CO_2 concentration. It is proof that a drastic reduction of CO_2 emission will not give immediate results in solving CO_2 related problems due to the lifetime of CO_2 that spans more than 19 years.
9) Long-term trend of CO_2 emission in Jakarta during observation period show a slight decrease, however the trend of CO_2 concentration is still steadily increasing with a larger rate than the global background CO_2 trend. These results confirm the role of the city of Jakarta as a net source of global CO_2 emissions.

6.2 Future research direction

The research conducted in this study might not serve the whole main objective that was stated in the introduction chapter. More research is needed to gain a complete understanding of atmospheric physics and dynamics in Jakarta. There are many aspects that could still be explored using the current existing surface observation data and the subsequent dataset since the observation campaign is still in continuation. Several research that could be conducted with this dataset are listed below.

1) Study on turbulence statistics in tropical urban areas, either under sea breeze condition and or in conjunction with seasonal change. In recent years, there have been increasing cases of intense-localized severe rainfall events in Jakarta (Trilaksono *et al.*, 2011; Siswanto *et al.*, 2022). While several researchers linked these events to cross-equatorial northerly surge (Yulihastin *et al.*, 2020, 2022), these kinds of event did not occur all the time during the surge periods. Perhaps, it is possible to isolate several cases of these severe rainfall and investigate its trigger mechanisms via the turbulence statistics.
2) Reports on surface energy balance. The current dataset includes data from net radiometer, pyranometer and pyrgeometer. This dataset has not been explored much. Combined with observed sensible and latent heat flux observed at LLH, it is possible to explore and report on surface energy balance in Jakarta (e.g., Christen and Vogt, 2004; Roth *et al.*, 2017; Shi *et al.*, 2019). It is also possible to use these datasets to verify the urban energy balance model or the radiation model (Kanda *et al.*, 2005, 2013; Kawai *et al.*, 2009). Furthermore, based on sea breeze simulation results using WRF, it is found that overestimation of shortwave radiation and underestimation of latent heat flux affect model performance (Junnaedhi *et al.*, 2021). Investigating this matter might be beneficial for the improvement of weather prediction in Jakarta.
3) Research on boundary layer climatology in Jakarta. It was shown that atmospheric boundary layer (ABL) height has a high correlation with CO_2 concentration, and possibly other gases and pollutants. However, little is known about seasonal or annual variability og ABL height in Jakarta. With more frequent events of severe air quality in Jakarta (Kusuma *et al.*, 2019; Lestari *et al.*, 2022), especially during dry season, it is crucial to explore the ABL variability in Jakarta. The surface layer parameters derived from surface observations at LLH and KKP might be used in such kind of research in

combination with other available datasets such as radiosonde and radar data. With the role of sea breeze to ABL height revealed, investigation on ABL height variability could also extended to daily basis.

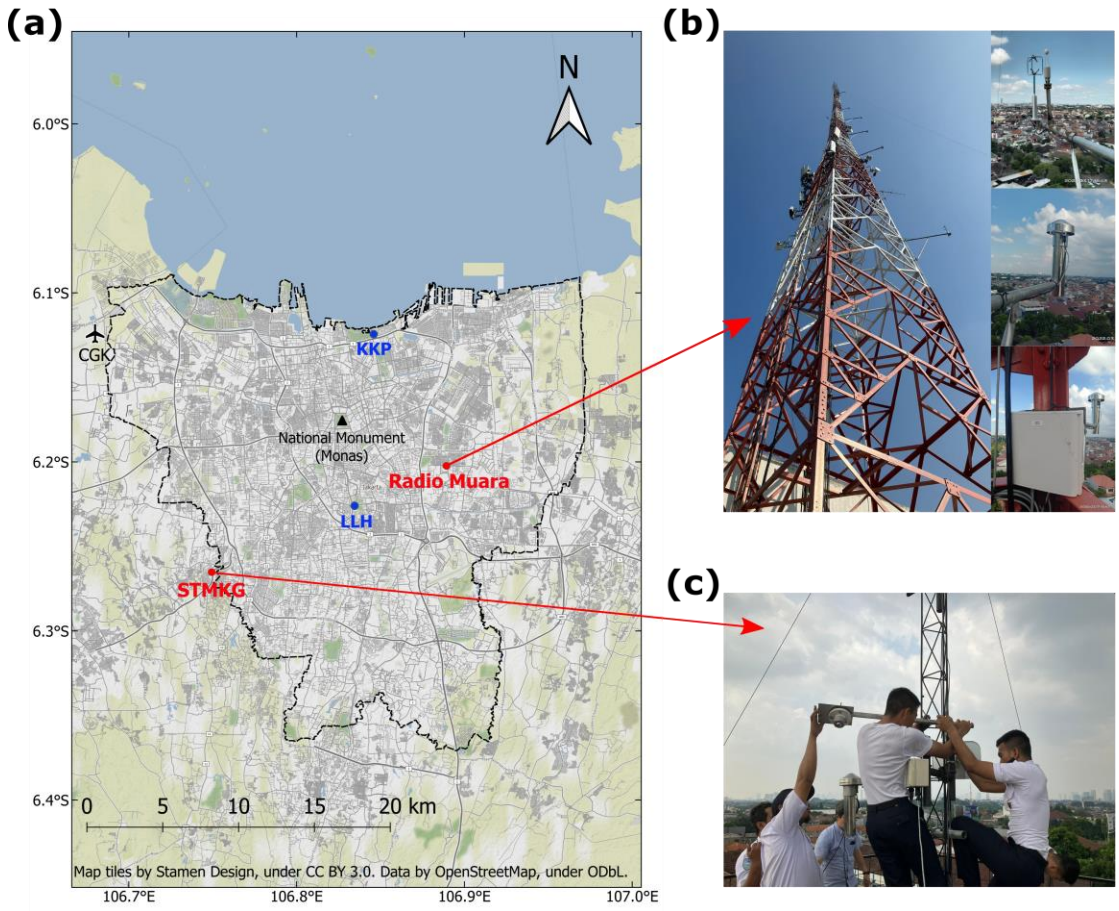

Figure 6.1 Map of Jakarta showings the location of the new multi-level observation tower at Radio Muara and Indonesian Academy of Meteorology/STMKG (a); photographs of the observation tower at Radio Muara and installed instruments (b); and photograph of instruments installation by students of STMKG (c). Photographs courtesy of Dr. Atsushi Inagaki, Dr. M. Rais Abdillah, and Mr. Aldi Nursepta.

While there are several topics that could be explored using the existing dataset, a new observation tower has been set up in the eastern area of Jakarta (see Figure 6.1a and b). This new observation tower presents opportunities to explore more on urban microclimate condition of Jakarta. The previous CO_2 measurement of LLH has given some knowledge on CO_2 emissions in Jakarta, however it is still a representative of micro-scale or neighborhood area. The new tower, however, allows us to measure at a higher level, up to 60 m above ground, in an area that is

dominated by lower residential areas. Thus, this new measurement might represent local-scale or district area of Jakarta. With multi-level instruments installed in the tower, it is also possible to explore on the urban roughness parameters via anemometric methods or validating the morphometric method which used previously (Grimmond *et al.*, 1998; Kanda *et al.*, 2007, 2013; Darmanto *et al.*, 2017; Kent *et al.*, 2017).

Finally, there are so many opportunities in future direction of study on the urban meso- to micro-meteorological condition in Jakarta. Thus, this last part might not be the end, but another beginning in urban atmospheric study of Jakarta.

6.3 Summary

Understanding the whole spectrum of meteorological phenomena of vulnerable areas, such as urban areas, is important to formulating strategies in adapting and mitigating the impacts of radical change that happen in such areas. This study is aimed to understand various-scale variations of atmospheric conditions in Jakarta based on mostly, but not limited to, atmospheric measurement data that has been acquired through the intensive, multi-year observation campaign.

Several new findings are identified from this study. However, the existing dataset still provides a large room to be explored. In addition to that, a new observation campaign is initiated. The objectives are not only to expand the spatial extent of the research in urban meteorology in Jakarta, but also to expand the collaborator and induce awareness of important stakeholders, such as the meteorological agency, to give attention to urban meso- and micro-scale atmospheric research. This study is hoped to become a base for subsequent urban atmospheric studies in Jakarta, as well as a contribution that represent tropical megacities to the global urban climate studies.

Appendix A: Instruments Specification

Detailed specification of the instruments used in this research is presented in Table A.1 below. Not all instruments were available on each site. Only ultrasonic anemometer and temperature humidity gauge were available for both sites (KKP and LLH). Gas analyzer, net radiometer, and automatic weather station (AWS) were installed only on LLH site. Additional AWS is installed at Cibinong (CBN), but only for temperature measurement. Almost all instruments were logged using the same analog datalogger, except for the net radiometer and AWS. The net radiometer also logged using analog data logger, but the using different data logger since its output voltage is too low for the main logger. The AWS is logged using digital datalogger embedded with the AWS.

Table A.1 Detailed specification of the instruments

Instrument (Brand and type)	Parameters acquired (unit)	Resolution	Accuracy/ Uncertainty	Measurement range	Meas. frequency (interval)	Logger type
Ultrasonic anemometer (Gill - Windmaster)	wind component u/v/w (m s^{-1})	0.001 m s^{-1}	<1.5% RMS *(i)*	0 to 50 m s^{-1}	10 Hz (0.1 sec)	Analog (-5 to +5 V)
	sonic temperature T_s (℃)	0.01 ℃	±2 ℃ *(i)*	-40 to +70 ℃		
	(i) accuracy @ 12 m s^{-1} and -20 ℃ and +30 ℃					
CO_2 and H2O gas analyzer (Licor - LI-7500)	CO_2 molar density ρ_c (mmol m^{-3})	0.0001 mmol m^{-3}	0.0043 mmol m^{-3} *(ii)*	0 to 117 mmol m^{-3}	10 Hz (0.1 sec)	Analog (0 to 5V)
	H_2O molar density ρ_v (mmol m^{-3})	0.001 mmol m^{-3}	0.18 mmol m^{-3} *(ii)*	0 to 2340 mmol m^{-3}		
	(ii) RMS noise @ 10 Hz, 370 ppm					

Temperature humidity gauge (Vaisala - HMP 155)	ambient temperature T_a (℃)	0.0035 ℃ *(iii)*	±0.055 + 0.0057 × T ℃ *(iv)*	-20 to +40 ℃	10 Hz (0.1 sec)	Analog (0 to 5V)
	ambient relative humidity RH_a (%)	0.0025 % *(iii)*	±1.0 + 0.008 × RH % *(v)*	0 to 100%		
	(iii) based on analog to digital converter (ADC) resolution *(iv) from +20 ℃ to +60 ℃* *(v) from -20 ℃ to +40 ℃*					
Net radiometer (Kipp and Zonen - CNR4)	shortwave radiation (down and up) S_d & S_u (W m^{-2})	< 0.06 W m^{-2}	< 5 % (for daily total)	0 to +2000 W m^{-2}	0.016 Hz (1 min)	Analog (0 to 40 mV)
	longwave radiation (down and up) L_d & L_u (W m^{-2})	< 0.12 W m^{-2}	< 10 % (for daily total)	-250 to +250 W m^{-2}		(-5 to +5 mV)
Automatic weather station (Meter - Atmos 41)	rain rate R_r (mm hr^{-1})	0.017 mm hr^{-1}	±5 % of measurement *(vi)*	0 to 400 mm hr^{-1}	0.083 Hz (5 min)	Digital (SD12)
	ambient temperature T_a (℃)	0.1 ℃	±0.42 ℃	–50 to 60 ℃		
	(vi) from 0 to 50 mm hr^{-1}					

References

Ahrens CD. 2001. *Essentials of meteorology: an invitation to the atmosphere*. Brooks/Cole/Thomson Learning: Australia, Pacific Grove, CA.

Anthes RA. 1978. The Height of the Planetary Boundary Layer and the Production of Circulation in a Sea Breeze Model. *Journal of the Atmospheric Sciences*. American Meteorological Society, 35(7): 1231–1239. https://doi.org/10.1175/1520-0469(1978)035<1231:THOTPB>2.0.CO;2.

Anugerah AR, Muttaqin PS, Purnama DA. 2021. Effect of large-scale social restriction (PSBB) during COVID-19 on outdoor air quality: Evidence from five cities in DKI Jakarta Province, Indonesia. *Environmental Research*, 197: 111164. https://doi.org/10.1016/j.envres.2021.111164.

Ao X, Grimmond CSB, Chang Y, Liu D, Tang Y, Hu P, Wang Y, Zou J, Tan J. 2016. Heat, water and carbon exchanges in the tall megacity of Shanghai: challenges and results. *International Journal of Climatology*, 36(14): 4608–4624. https://doi.org/10.1002/joc.4657.

Araki R, Yamanaka MD, Murata F, Hashiguchi H, Oku Y, Sribimawati T, Kudsy M, Renggono F. 2006. Seasonal and Interannual Variations of Diurnal Cycles of Wind and Cloud Activity Observed at Serpong, West Jawa, Indonesia. *Journal of the Meteorological Society of Japan. Ser. II*, 84A: 171–194. https://doi.org/10.2151/jmsj.84A.171.

Archer D, Eby M, Brovkin V, Ridgwell A, Cao L, Mikolajewicz U, Caldeira K, Matsumoto K, Munhoven G, Montenegro A, Tokos K. 2009. Atmospheric Lifetime of Fossil Fuel Carbon Dioxide. *Annual Review of Earth and Planetary Sciences*, 37(1): 117–134. https://doi.org/10.1146/annurev.earth.031208.100206.

Argüeso D, Di Luca A, Evans JP. 2016. Precipitation over urban areas in the western Maritime Continent using a convection-permitting model. *Climate Dynamics*, 47(3): 1143–1159. https://doi.org/10.1007/s00382-015-2893-6.

Arrillaga JA, de Arellano JV-G, Bosveld F, Baltink HK, Yagüe C, Sastre M, Román-Cascón C. 2018. Impacts of afternoon and evening sea-breeze fronts on local turbulence, and on CO2 and radon-222 transport. *Quarterly Journal of the Royal Meteorological Society*, 144(713): 990–1011. https://doi.org/10.1002/qj.3252.

Arya PS. 2001. *Introduction to Micrometeorology*. Academic Press.

Aubinet M, Vesala T, Papale D (eds). 2012. *Eddy covariance: a practical guide to measurement and data analysis*. Springer: Dordrecht ; New York.

Azorin-Molina C, Chen D, Tijm S, Baldi M. 2011. A multi-year study of sea breezes in a Mediterranean coastal site: Alicante (Spain). *International Journal of Climatology*, 31(3): 468–486. https://doi.org/10.1002/joc.2064.

Badan Informasi Geospasial. 2018. *DEMNAS*. *Digital Elevation Model (DEM) Nasional*. https://tanahair.indonesia.go.id/demnas/#/ (Accessed February 8, 2023).

Baldocchi DD. 2020. How eddy covariance flux measurements have contributed to our understanding of Global Change Biology. *Global Change Biology*, 26(1): 242–260. https://doi.org/10.1111/gcb.14807.

Barlow JF. 2014. Progress in observing and modelling the urban boundary layer. *Urban Climate*, 10: 216–240. https://doi.org/10.1016/j.uclim.2014.03.011.

Belgaman HA, Ichiyanagi K, Suwarman R, Tanoue M, Aldrian E, Utami AID, Kusumaningtyas SDA. 2017. Characteristics of seasonal precipitation isotope variability in Indonesia. *Hydrological Research Letters*, 11(2): 92–98. https://doi.org/10.3178/hrl.11.92.

Bell S. 2001. *A Beginner's Guide to Uncertainty of Measurement*. National Physical Laboratory.

Birch CE, Roberts MJ, Garcia-Carreras L, Ackerley D, Reeder MJ, Lock AP, Schiemann R. 2015. Sea-Breeze Dynamics and Convection Initiation: The Influence of Convective Parameterization in Weather and Climate Model Biases. *Journal of Climate*. American Meteorological Society, 28(20): 8093–8108. https://doi.org/10.1175/JCLI-D-14-00850.1.

BPS Provinsi DKI Jakarta. 2023. *Kependudukan*. *Badan Pusat Statistik Provinsi DKI Jakarta*. https://jakarta.bps.go.id/subject/12/kependudukan.html#subjekViewTab3.html (Accessed June 1, 2023).

Burba G. 2013. *Eddy covariance method for scientific, industrial, agricultural, and regulatory applications: a field book on measuring ecosystem gas exchange and areal emission rates*. .

Butchart N. 2014. The Brewer-Dobson circulation. *Reviews of Geophysics*, 52(2): 157–184. https://doi.org/10.1002/2013RG000448.

Canadell JG, Le Quéré C, Raupach MR, Field CB, Buitenhuis ET, Ciais P, Conway TJ, Gillett NP, Houghton RA, Marland G. 2007. Contributions to accelerating atmospheric CO2 growth from economic activity, carbon intensity, and efficiency of natural sinks. *Proceedings of the National Academy of Sciences*. Proceedings of the National Academy of Sciences, 104(47): 18866–18870. https://doi.org/10.1073/pnas.0702737104.

Cantero E, Sanz J, Borbón F, Paredes D, García A. 2022. On the measurement of stability parameter over complex mountainous terrain. *Wind Energy Science*. Copernicus GmbH, 7(1): 221–235. https://doi.org/10.5194/wes-7-221-2022.

Cenedese A, Monti P. 2003. Interaction between an Inland Urban Heat Island and a Sea-Breeze Flow: A Laboratory Study. *Journal of Applied Meteorology and Climatology*. American Meteorological Society, 42(11): 1569–1583. https://doi.org/10.1175/1520-0450(2003)042<1569:IBAIUH>2.0.CO;2.

Chang C-P, Harr PA, Chen H-J. 2005a. Synoptic Disturbances over the Equatorial South China Sea and Western Maritime Continent during Boreal Winter. *Monthly Weather Review*. American Meteorological Society, 133(3): 489–503. https://doi.org/10.1175/MWR-2868.1.

Chang C-P, Wang Z, McBride J, Liu C-H. 2005b. Annual Cycle of Southeast Asia—Maritime Continent Rainfall and the Asymmetric Monsoon Transition. *Journal of Climate*. American Meteorological Society, 18(2): 287–301. https://doi.org/10.1175/JCLI-3257.1.

Cheng XL, Liu XM, Liu YJ, Hu F. 2018. Characteristics of CO2 Concentration and Flux in the Beijing Urban Area. *Journal of Geophysical Research: Atmospheres*, 123(3): 1785–1801. https://doi.org/10.1002/2017JD027409.

Chiba O. 1993. The turbulent characteristics in the lowest part of the sea breeze front in the atmospheric

surface layer. *Boundary-Layer Meteorology*, 65(1): 181–195. https://doi.org/10.1007/BF00708823.

Childs PP, Raman S. 2005. Observations and Numerical Simulations of Urban Heat Island and Sea Breeze Circulations over New York City. *pure and applied geophysics*, 162(10): 1955–1980. https://doi.org/10.1007/s00024-005-2700-0.

Chou M-D, Suarez MJ. 1999. Technical Report Series on Global Modeling and Data Assimilation. , 15: 51.

Chow WTL, Roth M. 2006. Temporal dynamics of the urban heat island of Singapore. *International Journal of Climatology*, 26(15): 2243–2260. https://doi.org/10.1002/joc.1364.

Christen A. 2014. Atmospheric measurement techniques to quantify greenhouse gas emissions from cities. *Urban Climate*, 10: 241–260. https://doi.org/10.1016/j.uclim.2014.04.006.

Christen A, Vogt R. 2004. Energy and radiation balance of a central European city. *International Journal of Climatology*, 24(11): 1395–1421. https://doi.org/10.1002/joc.1074.

Clayson CA, Brown J, NOAA CDR Program. 2016. WHOI Climate Data Record (CDR) of Sea Surface Temperature (SST) - Version 2. Wood Hole Oceanographic Institute. https://www.ncei.noaa.gov/access/metadata/landing-page/bin/iso?id=gov.noaa.ncdc:C00972 (Accessed May 5, 2022).

Crawford KC, Hudson HR. 1973. The Diurnal Wind Variation in the Lowest 1500 ft in Central Oklahoma. June 1966–May 1967. *Journal of Applied Meteorology and Climatology*. American Meteorological Society, 12(1): 127–132. https://doi.org/10.1175/1520-0450(1973)012<0127:TDWVIT>2.0.CO;2.

Darmanto NS, Varquez ACG, Kanda M. 2017. Urban roughness parameters estimation from globally available datasets for mesoscale modeling in megacities. *Urban Climate*, 21: 243–261. https://doi.org/10.1016/j.uclim.2017.07.001.

Darmanto NS, Varquez ACG, Kawano N, Kanda M. 2019. Future urban climate projection in a tropical megacity based on global climate change and local urbanization scenarios. *Urban Climate*, 29: 100482. https://doi.org/10.1016/j.uclim.2019.100482.

Diallo M, Ern M, Ploeger F. 2021. The advective Brewer–Dobson circulation in the ERA5 reanalysis: climatology, variability, and trends. *Atmospheric Chemistry and Physics*. Copernicus GmbH, 21(10): 7515–7544. https://doi.org/10.5194/acp-21-7515-2021.

Dijk A, Moene AF, de Bruin H. 2004. The principles of surface flux physics: Theory, practice and description of the ECPACK library. *The Principles of Surface Flux Physics: Theory, Practice and Description of the ECPACK Library*.

Dinas Lingkungan Hidup DKI Jakarta. 2017. *Dokumen Informasi Kinerja Pengelolaan Lingkungan Hidup Daerah Provinsi DKI Jakarta Tahun 2016*. . https://ppid.jakarta.go.id/detail/165/892 (Accessed June 1, 2023).

Duren RM, Miller CE. 2012. Measuring the carbon emissions of megacities. *Nature Climate Change*. Nature Publishing Group, 2(8): 560–562. https://doi.org/10.1038/nclimate1629.

Fajber R, Monahan AH, Merryfield WJ. 2014. At What Time of Day Do Daily Extreme Near-Surface Wind Speeds Occur? *Journal of Climate*. American Meteorological Society, 27(11): 4226–4244. https://doi.org/10.1175/JCLI-D-13-00286.1.

Fan S-M, Wofsy SC, Bakwin PS, Jacob DJ, Fitzjarrald DR. 1990. Atmosphere-biosphere exchange of CO2 and O3

in the central Amazon Forest. *Journal of Geophysical Research: Atmospheres*, 95(D10): 16851–16864. https://doi.org/10.1029/JD095iD10p16851.

Fan W, Liu Y, Chappell A, Dong L, Xu R, Ekström M, Fu T-M, Zeng Z. 2020. Evaluation of global reanalysis land surface wind speed trends to support wind energy development using in-situ observations. *Journal of Applied Meteorology and Climatology*, 1(aop). https://doi.org/10.1175/JAMC-D-20-0037.1.

Feigenwinter C, Vogt R, Christen A. 2012. Eddy Covariance Measurements Over Urban Areas. In: Aubinet M, Vesala T and Papale D (eds) *Eddy Covariance: A Practical Guide to Measurement and Data Analysis*. Springer Netherlands: Dordrecht, 377–397.

Feng X, Haines K, de Boisséson E. 2018. Coupling of surface air and sea surface temperatures in the CERA-20C reanalysis. *Quarterly Journal of the Royal Meteorological Society*, 144(710): 195–207. https://doi.org/10.1002/qj.3194.

Ferdiansyah MR, Inagaki A, Kanda M. 2020. Detection of sea-breeze inland penetration in the coastal-urban region using geostationary satellite images. *Urban Climate*, 31: 100586. https://doi.org/10.1016/j.uclim.2020.100586.

Ferijal T, Batelaan O, Shanafield M, Alfahmi F. 2022. Determination of rainy season onset and cessation based on a flexible driest period. *Theoretical and Applied Climatology*. https://doi.org/10.1007/s00704-021-03917-1.

Finkele K, Hacker JM, Kraus H, Byron-Scott RAD. 1995. A complete sea-breeze circulation cell derived from aircraft observations. *Boundary-Layer Meteorology*, 73(3): 299–317. https://doi.org/10.1007/BF00711261.

Finkelstein PL, Sims PF. 2001. Sampling error in eddy correlation flux measurements. *Journal of Geophysical Research: Atmospheres*, 106(D4): 3503–3509. https://doi.org/10.1029/2000JD900731.

Foken T, Aubinet M, Leuning R. 2012. The Eddy Covariance Method. In: Aubinet M, Vesala T and Papale D (eds) *Eddy Covariance: A Practical Guide to Measurement and Data Analysis*. Springer Netherlands: Dordrecht, 1–19.

Fratini G, Mauder M. 2014. Towards a consistent eddy-covariance processing: an intercomparison of EddyPro and TK3. *Atmospheric Measurement Techniques*. Copernicus GmbH, 7(7): 2273–2281. https://doi.org/10.5194/amt-7-2273-2014.

Freitas ED, Rozoff CM, Cotton WR, Dias PLS. 2007. Interactions of an urban heat island and sea-breeze circulations during winter over the metropolitan area of São Paulo, Brazil. *Boundary-Layer Meteorology*, 122(1): 43–65. https://doi.org/10.1007/s10546-006-9091-3.

Friedlingstein P, Jones MW, O'Sullivan M, Andrew RM, Hauck J, Peters GP, Peters W, Pongratz J, Sitch S, Le Quéré C, Bakker DCE, Canadell JG, Ciais P, Jackson RB, Anthoni P, Barbero L, Bastos A, Bastrikov V, Becker M, Bopp L, Buitenhuis E, Chandra N, Chevallier F, Chini LP, Currie KI, Feely RA, Gehlen M, Gilfillan D, Gkritzalis T, Goll DS, Gruber N, Gutekunst S, Harris I, Haverd V, Houghton RA, Hurtt G, Ilyina T, Jain AK, Joetzjer E, Kaplan JO, Kato E, Klein Goldewijk K, Korsbakken JI, Landschützer P, Lauvset SK, Lefèvre N, Lenton A, Lienert S, Lombardozzi D, Marland G, McGuire PC, Melton JR, Metzl N, Munro DR, Nabel JEMS, Nakaoka S-I, Neill C, Omar AM, Ono T, Peregon A, Pierrot D, Poulter B, Rehder G, Resplandy L, Robertson E, Rödenbeck C, Séférian R, Schwinger J, Smith N, Tans PP, Tian H, Tilbrook B, Tubiello FN, van der Werf GR, Wiltshire AJ, Zaehle S. 2019. Global Carbon Budget 2019. *Earth System Science Data*. Copernicus GmbH, 11(4): 1783–1838. https://doi.org/10.5194/essd-11-1783-2019.

Garratt JR. 1994. Review: the atmospheric boundary layer. *Earth-Science Reviews*, 37(1): 89–134.

https://doi.org/10.1016/0012-8252(94)90026-4.

Garratt JR, Pearman GI. 1973. CO2 concentration in the atmospheric boundary-layer over South-East Australia. *Atmospheric Environment (1967)*, 7(12): 1257–1266. https://doi.org/10.1016/0004-6981(73)90135-2.

Gilliam RC, Raman S, Niyogi DDS. 2004. Observational and Numerical Study on the Influence of Large-Scale Flow Direction and Coastline Shape on Sea-Breeze Evolution. *Boundary-Layer Meteorology*, 111(2): 275–300. https://doi.org/10.1023/B:BOUN.0000016494.99539.5a.

Grau A, Jiménez MA, Cuxart J. 2021. Statistical characterization of the sea-breeze physical mechanisms through in-situ and satellite observations. *International Journal of Climatology*, 41(1): 17–30. https://doi.org/10.1002/joc.6606.

Grimm NB, Faeth SH, Golubiewski NE, Redman CL, Wu J, Bai X, Briggs JM. 2008. Global Change and the Ecology of Cities. *Science*. American Association for the Advancement of Science, 319(5864): 756–760. https://doi.org/10.1126/science.1150195.

Grimmond C, Christen A. 2012. Flux measurements in urban ecosystems. *FluxLetter - Newsletter of Fluxnet*, 5: 1–8.

Grimmond CSB, King TS, Roth M, Oke TR. 1998. Aerodynamic Roughness of Urban Areas Derived from Wind Observations. *Boundary-Layer Meteorology*, 89(1): 1–24. https://doi.org/10.1023/A:1001525622213.

Grimmond CSB, Oke TR. 1999a. Aerodynamic Properties of Urban Areas Derived from Analysis of Surface Form. *Journal of Applied Meteorology and Climatology*. American Meteorological Society, 38(9): 1262–1292. https://doi.org/10.1175/1520-0450(1999)038<1262:APOUAD>2.0.CO;2.

Grimmond CSB, Oke TR. 1999b. Heat Storage in Urban Areas: Local-Scale Observations and Evaluation of a Simple Model. *Journal of Applied Meteorology and Climatology*. American Meteorological Society, 38(7): 922–940. https://doi.org/10.1175/1520-0450(1999)038<0922:HSIUAL>2.0.CO;2.

Grimmond CSB, Salmond JA, Oke TR, Offerle B, Lemonsu A. 2004. Flux and turbulence measurements at a densely built-up site in Marseille: Heat, mass (water and carbon dioxide), and momentum. *Journal of Geophysical Research: Atmospheres*, 109(D24): D24101. https://doi.org/10.1029/2004JD004936.

Grubler A, Bai X, Buettner T, Dhakal S, Fisk DJ, Ichinose T, Keirstead JE, Sammer G, Satterthwaite D, Schulz NB, Shah N, Steinberger J, Weisz H, Ahamer G, Baynes T, Curtis D, Doherty M, Eyre N, Fujino J, Hanaki K, Kainuma M, Kaneko S, Lenzen M, Meyers J, Nakanishi H, Novikova V, Rajan KS, Seo S, Shrestha RM, Shukla PR, Sverdlik A, Sathaye J. 2012. Urban Energy Systems. In: Global Energy Assessment Writing Team (ed) *Global Energy Assessment: Toward a Sustainable Future*. Cambridge University Press: Cambridge, 1307–1400.

Guo J, Miao Y, Zhang Y, Liu H, Li Z, Zhang W, He J, Lou M, Yan Y, Bian L, Zhai P. 2016. The climatology of planetary boundary layer height in China derived from radiosonde and reanalysis data. *Atmospheric Chemistry and Physics*. Copernicus GmbH, 16(20): 13309–13319. https://doi.org/10.5194/acp-16-13309-2016.

Gurjar BR, Lelieveld J. 2005. New Directions: Megacities and global change. *Atmospheric Environment*, 39(2): 391–393. https://doi.org/10.1016/j.atmosenv.2004.11.002.

Hadi TW, Horinouchi T, Tsuda T, Hashiguchi H, Fukao S. 2002. Sea-Breeze Circulation over Jakarta, Indonesia: A Climatology Based on Boundary Layer Radar Observations. *Monthly Weather Review*, 130(9): 2153–2166. https://doi.org/10.1175/1520-0493(2002)130<2153:SBCOJI>2.0.CO;2.

Hadi TW, Tsuda T, Hashiguchi H, Fukao S. 2000. Tropical Sea-breeze Circulation and Related Atmospheric Phenomena Observed with *L*-band Boundary Layer Radar in Indonesia. *Journal of the Meteorological Society of Japan. Ser. II*, 78(2): 123–140. https://doi.org/10.2151/jmsj1965.78.2_123.

Hamada J-I, Yamanaka MD, Matsumoto J, Fukao S, Winarso PA, Sribimawati T. 2002. Spatial and Temporal Variations of the Rainy Season over Indonesia and their Link to ENSO. *Journal of the Meteorological Society of Japan. Ser. II*, 80(2): 285–310. https://doi.org/10.2151/jmsj.80.285.

Hansen JE, Sato M, Lacis A, Ruedy R, Tegen I, Matthews E. 1998. Climate forcings in the Industrial era. *Proceedings of the National Academy of Sciences*. Proceedings of the National Academy of Sciences, 95(22): 12753–12758. https://doi.org/10.1073/pnas.95.22.12753.

He B-J, Ding L, Prasad D. 2020. Relationships among local-scale urban morphology, urban ventilation, urban heat island and outdoor thermal comfort under sea breeze influence. *Sustainable Cities and Society*, 60: 102289. https://doi.org/10.1016/j.scs.2020.102289.

Hersbach H, Bell B, Berrisford P, Hirahara S, Horányi A, Muñoz-Sabater J, Nicolas J, Peubey C, Radu R, Schepers D, Simmons A, Soci C, Abdalla S, Abellan X, Balsamo G, Bechtold P, Biavati G, Bidlot J, Bonavita M, Chiara GD, Dahlgren P, Dee D, Diamantakis M, Dragani R, Flemming J, Forbes R, Fuentes M, Geer A, Haimberger L, Healy S, Hogan RJ, Hólm E, Janisková M, Keeley S, Laloyaux P, Lopez P, Lupu C, Radnoti G, Rosnay P de, Rozum I, Vamborg F, Villaume S, Thépaut J-N. 2020. The ERA5 global reanalysis. *Quarterly Journal of the Royal Meteorological Society*, 146(730): 1999–2049. https://doi.org/10.1002/qj.3803.

Hirano T, Sugawara H, Murayama S, Kondo H. 2015. Diurnal Variation of CO_2 Flux in an Urban Area of Tokyo. *Sola*, 11: 100–103. https://doi.org/10.2151/sola.2015-024.

Hofmann DJ, Butler JH, Tans PP. 2009. A new look at atmospheric carbon dioxide. *Atmospheric Environment*, 43(12): 2084–2086. https://doi.org/10.1016/j.atmosenv.2008.12.028.

Holton JR. 2004. *An Introduction to Dynamic Meteorology*. Elsevier.

Hong J-W, Lee S-D, Lee K, Hong J. 2020. Seasonal variations in the surface energy and CO2 flux over a high-rise, high-population, residential urban area in the East Asian monsoon region. *International Journal of Climatology*, 40(10): 4384–4407. https://doi.org/10.1002/joc.6463.

Hsieh C-I, Katul G, Chi T. 2000. An approximate analytical model for footprint estimation of scalar fluxes in thermally stratified atmospheric flows. *Advances in Water Resources*, 23(7): 765–772. https://doi.org/10.1016/S0309-1708(99)00042-1.

Hu X-M, Xue M. 2016. Influence of Synoptic Sea-Breeze Fronts on the Urban Heat Island Intensity in Dallas–Fort Worth, Texas. *Monthly Weather Review*, 144(4): 1487–1507. https://doi.org/10.1175/MWR-D-15-0201.1.

Hu Y, Tan J, Grimmond S, Ao X, Yan Y, Liu D. 2022. Observed and Modeled Urban Heat Island and Sea-Breeze Circulation Interactions: A Shanghai Case Study. *Journal of Applied Meteorology and Climatology*. American Meteorological Society, 61(3): 239–259. https://doi.org/10.1175/JAMC-D-20-0246.1.

Huffman GJ, Stocker EF, Bolvin DT, Nelkin EJ, Tan J. 2019. GPM IMERG Final Precipitation L3 1 month 0.1 degree x 0.1 degree V06. NASA Goddard Earth Sciences Data and Information Services Center (GES DISC). https://gpm1.gesdisc.eosdis.nasa.gov/data/GPM_L3/GPM_3IMERGHH.06 (Accessed December 2, 2021).

IPCC (ed). 2014. *Climate Change 2013 - The Physical Science Basis: Working Group I Contribution to the Fifth*

Assessment Report of the Intergovernmental Panel on Climate Change. Cambridge University Press: Cambridge.

Jayakrishnan PR, Sivaprasad P, Nettukandy Chenoli S, Babu CA, Samah AA, Mohammedali NP. 2021. Sea breeze characteristics over a coastal station in peninsular Malaysia. *Journal of Earth System Science*, 130(3): 126. https://doi.org/10.1007/s12040-021-01632-z.

Jiang P, Wen Z, Sha W, Chen G. 2017. Interaction between turbulent flow and sea breeze front over urban-like coast in large-eddy simulation. *Journal of Geophysical Research: Atmospheres*, 122(10): 5298–5315. https://doi.org/10.1002/2016JD026247.

Jiménez PA, de Arellano JV-G, Dudhia J, Bosveld FC. 2016. Role of synoptic- and meso-scales on the evolution of the boundary-layer wind profile over a coastal region: the near-coast diurnal acceleration. *Meteorology and Atmospheric Physics*, 128(1): 39–56. https://doi.org/10.1007/s00703-015-0400-6.

Junnaedhi IDGA, Inagaki A, Ferdiansyah MR, Darmanto NS, Kanda M, Hadi TW, Trilaksono NJ. 2018. Annual Characteristics of Urban Micro Climate in Jakarta Based on a Flux-Observation Network. paper presented at the 10th International Conference on Urban Climate/14th Symposium on Urban Environment. International Association on Urban Climate: New York. https://ams.confex.com/ams/ICUC10/meetingapp.cgi/Paper/343150.

Junnaedhi IDGA, Inagaki A, Varquez ACG, Kanda M. 2021. Evaluation of Multiple Simulated Sea-Breeze Events in Tropical Megacity Using High-Temporal-Resolution Observation Data. *Journal of Japan Society of Civil Engineers, Ser. B1 (Hydraulic Engineering)*, 77(2): I_1309-I_1314. https://doi.org/10.2208/jscejhe.77.2_I_1309.

Kaimal JC, Wyngaard JC, Izumi Y, Coté OR. 1972. Spectral characteristics of surface-layer turbulence. *Quarterly Journal of the Royal Meteorological Society*, 98(417): 563–589. https://doi.org/10.1002/qj.49709841707.

Kanda M. 2007. Progress in Urban Meteorology: A Review. *Journal of the Meteorological Society of Japan. Ser. II*, 85B: 363–383. https://doi.org/10.2151/jmsj.85B.363.

Kanda M, Inagaki A, Miyamoto T, Gryschka M, Raasch S. 2013. A New Aerodynamic Parametrization for Real Urban Surfaces. *Boundary-Layer Meteorology*, 148(2): 357–377. https://doi.org/10.1007/s10546-013-9818-x.

Kanda M, Inoue Y, Uno I. 2001. Numerical Study on Cloud Lines Over an Urban Street in Tokyo. *Boundary-Layer Meteorology*, 98(2): 251–273. https://doi.org/10.1023/A:1026504904902.

Kanda M, Kanega M, Kawai T, Moriwaki R, Sugawara H. 2007. Roughness Lengths for Momentum and Heat Derived from Outdoor Urban Scale Models. *Journal of Applied Meteorology and Climatology*. American Meteorological Society, 46(7): 1067–1079. https://doi.org/10.1175/JAM2500.1.

Kanda M, Kawai T, Nakagawa K. 2005. A Simple Theoretical Radiation Scheme for Regular Building Arrays. *Boundary-Layer Meteorology*, 114(1): 71–90. https://doi.org/10.1007/s10546-004-8662-4.

Katsumata M, Mori S, Hamada J-I, Hattori M, Syamsudin F, Yamanaka MD. 2018. Diurnal cycle over a coastal area of the Maritime Continent as derived by special networked soundings over Jakarta during HARIMAU2010. *Progress in Earth and Planetary Science*, 5(1): 64. https://doi.org/10.1186/s40645-018-0216-3.

Kawai T, Ridwan MK, Kanda M. 2009. Evaluation of the Simple Urban Energy Balance Model Using Selected Data from 1-yr Flux Observations at Two Cities. *Journal of Applied Meteorology and Climatology*, 48(4): 693–715. https://doi.org/10.1175/2008JAMC1891.1.

Keeling CD, Piper SC, Bacastow RB, Wahlen M, Whorf TP, Heimann M, Meijer HA. 2001. Exchanges of

Atmospheric CO2 and 13CO2 with the Terrestrial Biosphere and Oceans from 1978 to 2000. I. Global Aspects. .

Kent CW, Grimmond S, Barlow J, Gatey D, Kotthaus S, Lindberg F, Halios CH. 2017. Evaluation of Urban Local-Scale Aerodynamic Parameters: Implications for the Vertical Profile of Wind Speed and for Source Areas. *Boundary-Layer Meteorology*, 164(2): 183–213. https://doi.org/10.1007/s10546-017-0248-z.

Khanh DN, Varquez ACG, Kanda M. 2023. Impact of urbanization on exposure to extreme warming in megacities. *Heliyon*. Elsevier, 9(4). https://doi.org/10.1016/j.heliyon.2023.e15511.

Kitada T. 1987. Turbulence structure of sea breeze front and its implication in air pollution transport - Application of k-ε turbulence model. *Boundary-Layer Meteorology*, 41(1): 217–239. https://doi.org/10.1007/BF00120440.

Kljun N, Calanca P, Rotach MW, Schmid HP. 2004. A Simple Parameterisation for Flux Footprint Predictions. *Boundary-Layer Meteorology*, 112(3): 503–523. https://doi.org/10.1023/B:BOUN.0000030653.71031.96.

Kljun N, Calanca P, Rotach MW, Schmid HP. 2015. A simple two-dimensional parameterisation for Flux Footprint Prediction (FFP). *Geoscientific Model Development*. Copernicus GmbH, 8(11): 3695–3713. https://doi.org/10.5194/gmd-8-3695-2015.

Kormann R, Meixner FX. 2001. An Analytical Footprint Model for Non-Neutral Stratification. *Boundary-Layer Meteorology*, 99(2): 207–224. https://doi.org/10.1023/A:1018991015119.

Kottayil A, Xavier P, Satheesan K, Mohanakumar K, Rakesh V. 2020. Vertical structure and evolution of monsoon circulation as observed by 205-MHz wind profiler radar. *Meteorology and Atmospheric Physics*, 132(4): 531–545. https://doi.org/10.1007/s00703-019-00695-4.

Kottek M, Grieser J, Beck C, Rudolf B, Rubel F. 2006. World Map of the Köppen-Geiger climate classification updated. *Meteorologische Zeitschrift*. Schweizerbart'sche Verlagsbuchhandlung, 259–263. https://doi.org/10.1127/0941-2948/2006/0130.

Kusuma WL, Chih-Da W, Yu-Ting Z, Hapsari HH, Muhamad JL. 2019. PM2.5 Pollutant in Asia—A Comparison of Metropolis Cities in Indonesia and Taiwan. *International Journal of Environmental Research and Public Health*. Multidisciplinary Digital Publishing Institute, 16(24): 4924. https://doi.org/10.3390/ijerph16244924.

Lee X, Massman W, Law B (eds). 2005. *Handbook of Micrometeorology*. Springer Netherlands: Dordrecht.

Lestari P, Arrohman MK, Damayanti S, Klimont Z. 2022. Emissions and spatial distribution of air pollutants from anthropogenic sources in Jakarta. *Atmospheric Pollution Research*, 13(9): 101521. https://doi.org/10.1016/j.apr.2022.101521.

Lin JC, Mitchell L, Crosman E, Mendoza DL, Buchert M, Bares R, Fasoli B, Bowling DR, Pataki D, Catharine D, Strong C, Gurney KR, Patarasuk R, Baasandorj M, Jacques A, Hoch S, Horel J, Ehleringer J. 2018. CO2 and Carbon Emissions from Cities: Linkages to Air Quality, Socioeconomic Activity, and Stakeholders in the Salt Lake City Urban Area. *Bulletin of the American Meteorological Society*. American Meteorological Society, 99(11): 2325–2339. https://doi.org/10.1175/BAMS-D-17-0037.1.

Lindberg F, Grimmond CSB, Gabey A, Huang B, Kent CW, Sun T, Theeuwes NE, Järvi L, Ward HC, Capel-Timms I, Chang Y, Jonsson P, Krave N, Liu D, Meyer D, Olofson KFG, Tan J, Wästberg D, Xue L, Zhang Z. 2018. Urban Multi-scale Environmental Predictor (UMEP): An integrated tool for city-based climate services. *Environmental Modelling & Software*, 99: 70–87. https://doi.org/10.1016/j.envsoft.2017.09.020.

Liu HZ, Feng JW, Järvi L, Vesala T. 2012. Four-year (2006–2009) eddy covariance measurements of CO_2 flux over an urban area in Beijing. *Atmospheric Chemistry and Physics*. Copernicus GmbH, 12(17): 7881–7892. https://doi.org/10.5194/acp-12-7881-2012.

Liu Y, Liu H, Du Q, Xu L. 2021. Multi-level CO2 fluxes over Beijing megacity with the eddy covariance method. *Atmospheric and Oceanic Science Letters*, 14(6): 100079. https://doi.org/10.1016/j.aosl.2021.100079.

Liu Z, He C, Zhou Y, Wu J. 2014. How much of the world's land has been urbanized, really? A hierarchical framework for avoiding confusion. *Landscape Ecology*, 29(5): 763–771. https://doi.org/10.1007/s10980-014-0034-y.

Lorenz EN. 1963. Deterministic Nonperiodic Flow. *Journal of the Atmospheric Sciences*, 20(2): 130–141. https://doi.org/10.1175/1520-0469(1963)020<0130:DNF>2.0.CO;2.

Lyons W. 1982. Turbulent Diffusion and Pollutant Transport in Shoreline Environments. , 136–208.

Marcotullio PJ, Keßler C, Quintero Gonzalez R, Schmeltz M. 2021. Urban Growth and Heat in Tropical Climates. *Frontiers in Ecology and Evolution*, 9.

Masouleh ZP, Walker DJ, Crowther JM. 2019. A Long-Term Study of Sea-Breeze Characteristics: A Case Study of the Coastal City of Adelaide. *Journal of Applied Meteorology and Climatology*. American Meteorological Society, 58(2): 385–400. https://doi.org/10.1175/JAMC-D-17-0251.1.

Massman W. 2005. Concerning the Measurement of Atmospheric Trace Gas Fluxes with Open- and Closed-Path Eddy Covariance System: The WPL Terms and Spectral Attenuation. In: Lee X, Massman W and Law B (eds) *Handbook of Micrometeorology: A Guide for Surface Flux Measurement and Analysis*. Springer Netherlands: Dordrecht, 133–160.

Matthews B, Schume H. 2022. Tall tower eddy covariance measurements of CO2 fluxes in Vienna, Austria. *Atmospheric Environment*, 274: 118941. https://doi.org/10.1016/j.atmosenv.2022.118941.

Mauder M, Cuntz M, Drüe C, Graf A, Rebmann C, Schmid HP, Schmidt M, Steinbrecher R. 2013. A strategy for quality and uncertainty assessment of long-term eddy-covariance measurements. *Agricultural and Forest Meteorology*, 169: 122–135. https://doi.org/10.1016/j.agrformet.2012.09.006.

Mauder M, Foken T. 2006. Impact of post-field data processing on eddy covariance flux estimates and energy balance closure. *Meteorologische Zeitschrift*. Schweizerbart'sche Verlagsbuchhandlung, 597–609. https://doi.org/10.1127/0941-2948/2006/0167.

McMillen RT. 1988. An eddy correlation technique with extended applicability to non-simple terrain. *Boundary-Layer Meteorology*, 43(3): 231–245. https://doi.org/10.1007/BF00128405.

McPherson RD. 1970. A Numerical Study of the Effect of a Coastal Irregularity on the Sea Breeze. *Journal of Applied Meteorology and Climatology*. American Meteorological Society, 9(5): 767–777. https://doi.org/10.1175/1520-0450(1970)009<0767:ANSOTE>2.0.CO;2.

Miao Y, Li J, Miao S, Che H, Wang Y, Zhang X, Zhu R, Liu S. 2019. Interaction Between Planetary Boundary Layer and PM2.5 Pollution in Megacities in China: A Review. *Current Pollution Reports*, 5(4): 261–271. https://doi.org/10.1007/s40726-019-00124-5.

Miller STK, Keim BD, Talbot RW, Mao H. 2003. Sea breeze: Structure, forecasting, and impacts. *Reviews of*

Geophysics, 41(3). https://doi.org/10.1029/2003RG000124.

Moncrieff J, Clement R, Finnigan J, Meyers T. 2005. Averaging, Detrending, and Filtering of Eddy Covariance Time Series. In: Lee X, Massman W and Law B (eds) *Handbook of Micrometeorology: A Guide for Surface Flux Measurement and Analysis*. Springer Netherlands: Dordrecht, 7–31.

Moncrieff JB, Massheder JM, de Bruin H, Elbers J, Friborg T, Heusinkveld B, Kabat P, Scott S, Soegaard H, Verhoef A. 1997. A system to measure surface fluxes of momentum, sensible heat, water vapour and carbon dioxide. *Journal of Hydrology*, 188–189: 589–611. https://doi.org/10.1016/S0022-1694(96)03194-0.

Moore III B, Braswell BH. 1994. The lifetime of excess atmospheric carbon dioxide. *Global Biogeochemical Cycles*, 8(1): 23–38. https://doi.org/10.1029/93GB03392.

Mori S, Hamada J-I, Hattori M, Wu P-M, Katsumata M, Endo N, Ichiyanagi K, Hashiguchi H, Arbain AA, Sulistyowati R, Lestari S, Syamsudin F, Manik T, Yamanaka MD. 2018. Meridional march of diurnal rainfall over Jakarta, Indonesia, observed with a C-band Doppler radar: an overview of the HARIMAU2010 campaign. *Progress in Earth and Planetary Science*, 5(1): 47. https://doi.org/10.1186/s40645-018-0202-9.

Moriwaki R, Kanda M. 2004. Seasonal and Diurnal Fluxes of Radiation, Heat, Water Vapor, and Carbon Dioxide over a Suburban Area. *Journal of Applied Meteorology and Climatology*. American Meteorological Society, 43(11): 1700–1710. https://doi.org/10.1175/JAM2153.1.

Moron V, Robertson AW, Boer R. 2009. Spatial Coherence and Seasonal Predictability of Monsoon Onset over Indonesia. *Journal of Climate*. American Meteorological Society, 22(3): 840–850. https://doi.org/10.1175/2008JCLI2435.1.

Neale R, Slingo J. 2003. The Maritime Continent and Its Role in the Global Climate: A GCM Study. *Journal of Climate*. American Meteorological Society, 16(5): 834–848. https://doi.org/10.1175/1520-0442(2003)016<0834:TMCAIR>2.0.CO;2.

Nemitz E, Hargreaves KJ, McDonald AG, Dorsey JR, Fowler D. 2002. Micrometeorological Measurements of the Urban Heat Budget and CO2 Emissions on a City Scale. *Environmental Science & Technology*. American Chemical Society, 36(14): 3139–3146. https://doi.org/10.1021/es010277e.

Nitta T, Sekine S. 1994. Diurnal Variation of Convective Activity over the Tropical Western Pacific. *Journal of the Meteorological Society of Japan. Ser. II*, 72(5): 627–641. https://doi.org/10.2151/jmsj1965.72.5_627.

Oke TR, Mills G, Christen A, Voogt JA. 2017. *Urban Climates*. Cambridge University Press: Cambridge.

OpenStreetMap contributor. 2023. OpenStreetMap. OpenStreetMap Foundation (OSMF). https://www.openstreetmap.org/ (Accessed June 5, 2023).

Orlanski I. 1975. A rational subdivision of scales for atmospheric processes. *Bulletin of the American Meteorological Society*, 56(5): 527–530.

Otsuka S, Trilaksono NJ, Yoden S. 2017. Comparing Simulated Size Distributions of Precipitation Systems at Different Model Resolution. *Sola*, 13: 130–134. https://doi.org/10.2151/sola.2017-024.

Page CM, Nicholls N, Plummer N, Trewin B, Manton M, Alexander L, Chambers LE, Choi Y, Collins DA, Gosai A, Della-Marta P, Haylock MR, Inape K, Laurent V, Maitrepierre L, Makmur EEP, Nakamigawa H, Ouprasitwong N, Mcgree S, Pahalad J, Salinger MJ, Tibig L, Tran TD, Vediapan K, Zhai P. 2004. Data Rescue in the Southeast Asia

and South Pacific Region: Challenges and Opportunities. *Bulletin of the American Meteorological Society*, 85(10): 1483–1489. https://doi.org/10.1175/BAMS-85-10-1483.

Park C, Jeong S, Park M-S, Park H, Yun J, Lee S-S, Park S-H. 2022. Spatiotemporal variations in urban CO2 flux with land-use types in Seoul. *Carbon Balance and Management*, 17(1): 3. https://doi.org/10.1186/s13021-022-00206-w.

Pawlak W, Fortuniak K, Siedlecki M. 2011. Carbon dioxide flux in the centre of Łódź, Poland—analysis of a 2-year eddy covariance measurement data set. *International Journal of Climatology*, 31(2): 232–243. https://doi.org/10.1002/joc.2247.

Peel MC, Finlayson BL, McMahon TA. 2007. Updated world map of the Köppen-Geiger climate classification. *Hydrology and Earth System Sciences*. Copernicus GmbH, 11(5): 1633–1644. https://doi.org/10.5194/hess-11-1633-2007.

Pielke RA. 1981. An overview of our current understanding of the physical interactions between the sea- and land-breeze and the coastal waters. *Ocean Management*, 6(2): 87–100. https://doi.org/10.1016/0302-184X(81)90030-5.

Pinandito M, Sugondo S, Sugimoto N, Matsui I. 2001. Long-term lidar observation and analysis of aerosol vertical profiles in Jakarta, Indonesia. *Lidar Remote Sensing for Industry and Environment Monitoring*. paper presented at the Lidar Remote Sensing for Industry and Environment Monitoring. SPIE Digital Library: Sendai, Japan, 191–198.

Prabha TV, Venkatesan R, Mursch-Radlgruber E, Rengarajan G, Jayanthi N. 2002. Thermal internal boundary layer characteristics at a tropical coastal site as observed by a mini-SODAR under varying synoptic conditions. *Journal of Earth System Science*, 111(1): 63–77. https://doi.org/10.1007/BF02702223.

Qian J-H. 2008. Why Precipitation Is Mostly Concentrated over Islands in the Maritime Continent. *Journal of the Atmospheric Sciences*, 65(4): 1428–1441. https://doi.org/10.1175/2007JAS2422.1.

Qian J-H, Robertson AW, Moron V. 2010. Interactions among ENSO, the Monsoon, and Diurnal Cycle in Rainfall Variability over Java, Indonesia. *Journal of the Atmospheric Sciences*. American Meteorological Society, 67(11): 3509–3524. https://doi.org/10.1175/2010JAS3348.1.

Qian T, Epifanio CC, Zhang F. 2012. Topographic Effects on the Tropical Land and Sea Breeze. *Journal of the Atmospheric Sciences*, 69(1): 130–149. https://doi.org/10.1175/JAS-D-11-011.1.

Ramage CS. 1968. Role of a tropical “maritime continent” in the atmospheric circulation. *Monthly Weather Review*, 96(6): 365–370. https://doi.org/10.1175/1520-0493(1968)096<0365:ROATMC>2.0.CO;2.

Raman S, Templeman B, Templeman S, Holt T, Murthy AB, Singh MP, Agarwaal P, Nigam S, Prabhu A, Ameenullah S. 1990. Structure of the Indian southwesterly pre-monsoon and monsoon boundary layers: Observations and numerical simulation. *Atmospheric Environment. Part A. General Topics*, 24(4): 723–734. https://doi.org/10.1016/0960-1686(90)90273-P.

Reddy TVR, Mehta SK, Ananthavel A, Ali S, Annamalai V, Rao DN. 2021. Seasonal characteristics of sea breeze and thermal internal boundary layer over Indian east coast region. *Meteorology and Atmospheric Physics*, 133(2): 217–232. https://doi.org/10.1007/s00703-020-00746-1.

Reible DD, Simpson JE, Linden PF. 1993. The sea breeze and gravity-current frontogenesis. *Quarterly Journal of*

the Royal Meteorological Society, 119(509): 1–16. https://doi.org/10.1002/qj.49711950902.

Renggono F, Hashiguchi H, Fukao S, Yamanaka MD, Ogino S-Y, Okamoto N, Murata F, Sitorus BP, Kudsy M, Kartasasmita M, Ibrahim G. 2001. Precipitating clouds observed by 1.3-GHz boundary layer radars in equatorial Indonesia. *Annales Geophysicae*. Copernicus GmbH, 19(8): 889–897. https://doi.org/10.5194/angeo-19-889-2001.

Ribeiro FND, Oliveira AP de, Soares J, Miranda RM de, Barlage M, Chen F. 2018. Effect of sea breeze propagation on the urban boundary layer of the metropolitan region of Sao Paulo, Brazil. *Atmospheric Research*, 214: 174–188. https://doi.org/10.1016/j.atmosres.2018.07.015.

Robinson FJ, Patterson MD, Sherwood SC. 2013. A Numerical Modeling Study of the Propagation of Idealized Sea-Breeze Density Currents. *Journal of the Atmospheric Sciences*. American Meteorological Society, 70(2): 653–668. https://doi.org/10.1175/JAS-D-12-0113.1.

Robinson FJ, Sherwood SC, Gerstle D, Liu C, Kirshbaum DJ. 2011. Exploring the Land–Ocean Contrast in Convective Vigor Using Islands. *Journal of the Atmospheric Sciences*. American Meteorological Society, 68(3): 602–618. https://doi.org/10.1175/2010JAS3558.1.

Roth M. 2007. Review of urban climate research in (sub)tropical regions. *International Journal of Climatology*, 27(14): 1859–1873. https://doi.org/10.1002/joc.1591.

Roth M, Jansson C, Velasco E. 2017. Multi-year energy balance and carbon dioxide fluxes over a residential neighbourhood in a tropical city. *International Journal of Climatology*, 37(5): 2679–2698. https://doi.org/10.1002/joc.4873.

Roth M, Oke TR. 1993. Turbulent transfer relationships over an urban surface. I. Spectral characteristics. *Quarterly Journal of the Royal Meteorological Society*, 119(513): 1071–1104. https://doi.org/10.1002/qj.49711951311.

Roth M, Sanchez B, Li R, Velasco E. 2022. Spatial and temporal characteristics of near-surface air temperature across local climate zones in a tropical city. *International Journal of Climatology*, 42(16): 9730–9752. https://doi.org/10.1002/joc.7862.

Ruppert JH, Zhang F. 2019. Diurnal Forcing and Phase Locking of Gravity Waves in the Maritime Continent. *Journal of the Atmospheric Sciences*. American Meteorological Society, 76(9): 2815–2835. https://doi.org/10.1175/JAS-D-19-0061.1.

Sandeep A, Rao TN, Ramkiran CN, Rao SVB. 2014. Differences in Atmospheric Boundary-Layer Characteristics Between Wet and Dry Episodes of the Indian Summer Monsoon. *Boundary-Layer Meteorology*, 153(2): 217–236. https://doi.org/10.1007/s10546-014-9945-z.

Schlichting (Deceased) H, Gersten K. 2016. *Boundary-Layer Theory*. Springer Berlin Heidelberg.

Schmutz M, Vogt R, Feigenwinter C, Parlow E. 2016. Ten years of eddy covariance measurements in Basel, Switzerland: Seasonal and interannual variabilities of urban CO2 mole fraction and flux. *Journal of Geophysical Research: Atmospheres*, 121(14): 8649–8667. https://doi.org/10.1002/2016JD025063.

Schoenberger LM. 1984. Doppler Radar Observation of a Land-Breeze Cold Front. *Monthly Weather Review*. American Meteorological Society, 112(12): 2455–2464. https://doi.org/10.1175/1520-0493(1984)112<2455:DROOAL>2.0.CO;2.

Schotanus P, Nieuwstadt FTM, De Bruin HAR. 1983. Temperature measurement with a sonic anemometer and its application to heat and moisture fluxes. *Boundary-Layer Meteorology*, 26(1): 81–93. https://doi.org/10.1007/BF00164332.

Schwandner FM, Gunson MR, Miller CE, Carn SA, Eldering A, Krings T, Verhulst KR, Schimel DS, Nguyen HM, Crisp D, O'Dell CW, Osterman GB, Iraci LT, Podolske JR. 2017. Spaceborne detection of localized carbon dioxide sources. *Science*. American Association for the Advancement of Science, 358(6360): eaam5782. https://doi.org/10.1126/science.aam5782.

Seibert P, Beyrich F, Gryning S-E, Joffre S, Rasmussen A, Tercier P. 2000. Review and intercomparison of operational methods for the determination of the mixing height. *Atmospheric Environment*, 34(7): 1001–1027. https://doi.org/10.1016/S1352-2310(99)00349-0.

Seidel DJ, Zhang Y, Beljaars A, Golaz J-C, Jacobson AR, Medeiros B. 2012. Climatology of the planetary boundary layer over the continental United States and Europe. *Journal of Geophysical Research: Atmospheres*, 117(D17). https://doi.org/10.1029/2012JD018143.

Seto KC, Dhakal S, Bigio A, Blanco H, Delgado GC, Dewar D, Huang L, Inaba A, Kansal A, Lwasa S, McMahon J, Müller DB, Murakami J, Nagendra H, Ramaswami A. 2014. Chapter 12 - Human settlements, infrastructure and spatial planning. Cambridge University Press.

Shen L, Zhao C, Ma Z, Li Z, Li J, Wang K. 2019. Observed decrease of summer sea-land breeze in Shanghai from 1994 to 2014 and its association with urbanization. *Atmospheric Research*, 227: 198–209. https://doi.org/10.1016/j.atmosres.2019.05.007.

Shen L, Zhao C, Yang X. 2021. Insight Into the Seasonal Variations of the Sea-Land Breeze in Los Angeles with Respect to the Effects of Solar Radiation and Climate Type. *Journal of Geophysical Research: Atmospheres*, 126(6): e2020JD033197. https://doi.org/10.1029/2020JD033197.

Shi Y, Zhang Y, Li R. 2019. Local-Scale Urban Energy Balance Observation under Various Sky Conditions in a Humid Subtropical Region. *Journal of Applied Meteorology and Climatology*. American Meteorological Society, 58(7): 1573–1591. https://doi.org/10.1175/JAMC-D-18-0273.1.

Simpson JE. 1969. A comparison between laboratory and atmospheric density currents. *Quarterly Journal of the Royal Meteorological Society*, 95(406): 758–765. https://doi.org/10.1002/qj.49709540609.

Simpson JE, Britter RE. 1979. The dynamics of the head of a gravity current advancing over a horizontal surface. *Journal of Fluid Mechanics*. Cambridge University Press, 94(3): 477–495. https://doi.org/10.1017/S0022112079001142.

Simpson JE, Britter RE. 1980. A laboratory model of an atmospheric mesofront. *Quarterly Journal of the Royal Meteorological Society*, 106(449): 485–500. https://doi.org/10.1002/qj.49710644907.

Siswanto S, Oldenborgh GJ van, Schrier G van der, Jilderda R, Hurk B van den. 2016. Temperature, extreme precipitation, and diurnal rainfall changes in the urbanized Jakarta city during the past 130 years. *International Journal of Climatology*, 36(9): 3207–3225. https://doi.org/10.1002/joc.4548.

Siswanto S, Schrier G van der, Hurk B van den. 2022. Observed Increase of Urban Extreme Rainfall as Surface Temperature Rise: The Jakarta Case. *Journal of the Meteorological Society of Japan. Ser. II*, advpub. https://doi.org/10.2151/jmsj.2022-023.

Sofyan A, Kitada T, Kurata G. 2007. Characteristics of Air Pollution Transport in Jakarta Area in Dry Season. *Proceedings of the Symposium on Global Environment*, 15: 89–94. https://doi.org/10.2208/proge.15.89.

Sorbjan Z, Grachev AA. 2010. An Evaluation of the Flux–Gradient Relationship in the Stable Boundary Layer. *Boundary-Layer Meteorology*, 135(3): 385–405. https://doi.org/10.1007/s10546-010-9482-3.

State of The Tropics. 2020. *State of the Tropics 2020 Report*. Text. James Cook University: Townsville, Australia. https://www.jcu.edu.au/state-of-the-tropics/publications/state-of-the-tropics-2020-report (Accessed June 3, 2023).

Stull RB. 1988. *An introduction to boundary layer meteorology*. Kluwer Academic Publishers: Dordrecht ; Boston.

Stull RB. 2020. Practical Meteorology. *LibreText Geoscience - Meteorology & Climate Science*. LibreTexts: online. https://geo.libretexts.org/Bookshelves/Meteorology_and_Climate_Science/Practical_Meteorology_(Stull) (Accessed June 19, 2023).

Sugawara H, Ishidoya S, Terao Y, Takane Y, Kikegawa Y, Nakajima K. 2021. Anthropogenic CO2 Emissions Changes in an Urban Area of Tokyo, Japan, Due to the COVID-19 Pandemic: A Case Study During the State of Emergency in April–May 2020. *Geophysical Research Letters*, 48(15): e2021GL092600. https://doi.org/10.1029/2021GL092600.

Sugimoto N, Matsui I, Shimizu A, Pinandito M, Sugondo S. 2000. Climatological characteristics of cloud distribution and planetary boundary layer structure in Jakarta, Indonesia revealed by lidar observation. *Geophysical Research Letters*, 27(18): 2909–2912. https://doi.org/10.1029/2000GL011544.

Sumner GN. 1977. Sea Breeze Occurrence in Hilly Terrain. *Weather*, 32(6): 200–208. https://doi.org/10.1002/j.1477-8696.1977.tb04556.x.

Suwarman R, Ichiyanagi K, Tanoue M, Yoshimura K, Mori S, Yamanaka MD, Kurita N, Syamsudin F. 2013. The Variability of Stable Isotopes and Water Origin of Precipitation over the Maritime Continent. *Sola*, 9: 74–78. https://doi.org/10.2151/sola.2013-017.

Takashima H, Hara K, Nishita-Hara C, Fujiyoshi Y, Shiraishi K, Hayashi M, Yoshino A, Takami A, Yamazaki A. 2019. Short-term variation in atmospheric constituents associated with local front passage observed by a 3-D coherent Doppler lidar and in-situ aerosol/gas measurements. *Atmospheric Environment: X*, 3: 100043. https://doi.org/10.1016/j.aeaoa.2019.100043.

Talbot C, Augustin P, Leroy C, Willart V, Delbarre H, Khomenko G. 2007. Impact of a sea breeze on the boundary-layer dynamics and the atmospheric stratification in a coastal area of the North Sea. *Boundary-Layer Meteorology*, 125(1): 133–154. https://doi.org/10.1007/s10546-007-9185-6.

Tanaka M. 1994. The Onset and Retreat Dates of the Austral Summer Monsoon over Indonesia, Australia and New Guinea. *Journal of the Meteorological Society of Japan. Ser. II*, 72(2): 255–267. https://doi.org/10.2151/jmsj1965.72.2_255.

Tokairin T, Sofyan A, Kitada T. 2010. Effect of land use changes on local meteorological conditions in Jakarta, Indonesia: toward the evaluation of the thermal environment of megacities in Asia. *International Journal of Climatology*, 30(13): 1931–1941. https://doi.org/10.1002/joc.2138.

TomTom International BV. 2022. *Jakarta traffic report | TomTom Traffic Index*. *Jakarta traffic report | TomTom Traffic Index*. https://www.tomtom.com/traffic-index/jakarta-traffic/ (Accessed June 5, 2022).

Trenberth KE, Stepaniak DP, Caron JM. 2000. The Global Monsoon as Seen through the Divergent Atmospheric Circulation. *Journal of Climate*. American Meteorological Society, 13(22): 3969–3993. https://doi.org/10.1175/1520-0442(2000)013<3969:TGMAST>2.0.CO;2.

Trilaksono NJ, Otsuka S, Yoden S. 2011. A Time-Lagged Ensemble Simulation on the Modulation of Precipitation over West Java in January–February 2007. *Monthly Weather Review*, 140(2): 601–616. https://doi.org/10.1175/MWR-D-11-00094.1.

Ueyama M, Ando T. 2016. Diurnal, weekly, seasonal, and spatial variabilities in carbon dioxide flux in different urban landscapes in Sakai, Japan. *Atmospheric Chemistry and Physics*. Copernicus GmbH, 16(22): 14727–14740. https://doi.org/10.5194/acp-16-14727-2016.

Ueyama M, Takano T. 2022. A decade of CO2 flux measured by the eddy covariance method including the COVID-19 pandemic period in an urban center in Sakai, Japan. *Environmental Pollution*, 304: 119210. https://doi.org/10.1016/j.envpol.2022.119210.

UN DESA. 2018. *World Urbanization Prospects - Population Division*. *United Nation Department of Economic and Social Affairs*. https://population.un.org/wup/maps/ (Accessed June 30, 2023).

United Nations. 2018a. *2018 Revision of World Urbanization Prospects*. *United Nations Department of Economic and Social Affairs*. United Nations. https://www.un.org/en/desa/2018-revision-world-urbanization-prospects (Accessed June 1, 2023).

United Nations. 2018b. *The World's Cities in 2018*. United Nations.

Varquez ACG, Darmanto N, Kawano N, Takakuwa S, Kanda M, Xin Z. 2017. Representative Urban Growing Scenarios for Future Climate Models. *土木学会論文集 b1（水工学）*, 73(4): I_103-I_108. https://doi.org/10.2208/jscejhe.73.I_103.

Varquez ACG, Kiyomoto S, Khanh DN, Kanda M. 2021. Global 1-km present and future hourly anthropogenic heat flux. *Scientific Data*. Nature Publishing Group, 8(1): 64. https://doi.org/10.1038/s41597-021-00850-w.

Varquez ACG, Nakayoshi M, Kanda M. 2015. The Effects of Highly Detailed Urban Roughness Parameters on a Sea-Breeze Numerical Simulation. *Boundary-Layer Meteorology*, 154(3): 449–469. https://doi.org/10.1007/s10546-014-9985-4.

Velasco E. 2021. Impact of Singapore's COVID-19 confinement on atmospheric CO2 fluxes at neighborhood scale. *Urban Climate*, 37: 100822. https://doi.org/10.1016/j.uclim.2021.100822.

Velasco E, Pressley S, Allwine E, Westberg H, Lamb B. 2005. Measurements of CO2 fluxes from the Mexico City urban landscape. *Atmospheric Environment*, 39(38): 7433–7446. https://doi.org/10.1016/j.atmosenv.2005.08.038.

Velasco E, Pressley S, Grivicke R, Allwine E, Coons T, Foster W, Jobson BT, Westberg H, Ramos R, Hernández F, Molina LT, Lamb B. 2009. Eddy covariance flux measurements of pollutant gases in urban Mexico City. *Atmospheric Chemistry and Physics*. Copernicus GmbH, 9(19): 7325–7342. https://doi.org/10.5194/acp-9-7325-2009.

Velasco E, Roth M. 2010. Cities as Net Sources of CO2: Review of Atmospheric CO2 Exchange in Urban Environments Measured by Eddy Covariance Technique. *Geography Compass*, 4(9): 1238–1259. https://doi.org/10.1111/j.1749-8198.2010.00384.x.

Velasco E, Roth M, Tan SH, Quak M, Nabarro SDA, Norford L. 2013. The role of vegetation in the CO_2 flux from a tropical urban neighbourhood. *Atmospheric Chemistry and Physics*. Copernicus GmbH, 13(20): 10185–10202. https://doi.org/10.5194/acp-13-10185-2013.

Venturi S, Randazzo A, Tassi F, Gioli B, Buccianti A, Gualtieri G, Capecchiacci F, Cabassi J, Brilli L, Carotenuto F, Santi R, Vagnoli C, Zaldei A, Vaselli O. 2021. Unveiling the changes in urban atmospheric CO2 in the time of COVID-19 pandemic: A case study of Florence (Italy). *Science of The Total Environment*, 795: 148877. https://doi.org/10.1016/j.scitotenv.2021.148877.

Vickers D, Mahrt L. 1997. Quality Control and Flux Sampling Problems for Tower and Aircraft Data. *Journal of Atmospheric and Oceanic Technology*. American Meteorological Society, 14(3): 512–526. https://doi.org/10.1175/1520-0426(1997)014<0512:QCAFSP>2.0.CO;2.

Vitale D, Fratini G, Bilancia M, Nicolini G, Sabbatini S, Papale D. 2020. A robust data cleaning procedure for eddy covariance flux measurements. *Biogeosciences*. Copernicus GmbH, 17(6): 1367–1391. https://doi.org/10.5194/bg-17-1367-2020.

Wang C, Wang Z-H, Yang J, Li Q. 2018. A Backward-Lagrangian-Stochastic Footprint Model for the Urban Environment. *Boundary-Layer Meteorology*, 168(1): 59–80. https://doi.org/10.1007/s10546-018-0338-6.

Wang Q, Wang Y, Fan Y, Hang J, Li Y. 2019. Urban heat island circulations of an idealized circular city as affected by background wind speed. *Building and Environment*, 148: 433–447. https://doi.org/10.1016/j.buildenv.2018.11.024.

Wati T, Nasution RI. 2018. Evaluation of urban pollution and bio-climate using total suspended particles and discomfort index in Jakarta City. *IOP Conference Series: Earth and Environmental Science*. IOP Publishing, 203: 012003. https://doi.org/10.1088/1755-1315/203/1/012003.

Webb EK, Pearman GI, Leuning R. 1980. Correction of flux measurements for density effects due to heat and water vapour transfer. *Quarterly Journal of the Royal Meteorological Society*, 106(447): 85–100. https://doi.org/10.1002/qj.49710644707.

Wikipedia. 2023. *Atmosphere of Earth*. *Wikipedia*. https://en.wikipedia.org/w/index.php?title=Atmosphere_of_Earth&oldid=1160034842 (Accessed June 22, 2023).

Wu P, Hamada J-I, Yamanaka MD, Matsumoto J, Hara M. 2009. The Impact of Orographically-Induced Gravity Waves on the Diurnal Cycle of Rainfall over Southeast Kalimantan Island. *Atmospheric and Oceanic Science Letters*. Taylor & Francis, 2(1): 35–39. https://doi.org/10.1080/16742834.2009.11446773.

Wu P, Hara M, Fudeyasu H, Yamanaka MD, Matsumoto J, Syamsudin F, Sulistyowati R, Djajadihardja YS. 2007. The Impact of Trans-equatorial Monsoon Flow on the Formation of Repeated Torrential Rains over Java Island. *SOLA*, 3: 93–96. https://doi.org/10.2151/sola.2007-024.

Yamanaka MD. 2016. Physical climatology of Indonesian maritime continent: An outline to comprehend observational studies. *Atmospheric Research*, 178–179: 231–259. https://doi.org/10.1016/j.atmosres.2016.03.017.

Yamanaka MD, Ogino S-Y, Wu P-M, Jun-Ichi H, Mori S, Matsumoto J, Syamsudin F. 2018. Maritime continent coastlines controlling Earth's climate. *Progress in Earth and Planetary Science*, 5(1): 21. https://doi.org/10.1186/s40645-018-0174-9.

Yang G-Y, Slingo J. 2001. The Diurnal Cycle in the Tropics. *Monthly Weather Review*. American Meteorological Society, 129(4): 784–801. https://doi.org/10.1175/1520-0493(2001)129<0784:TDCITT>2.0.CO;2.

Yoden S, Otsuka S, Joko Trilaksono N, Wahyu Hadi T. 2016. Recent Progress in Research on the Maritime Continent Monsoon. *The Global Monsoon System*. World Scientific, 63–77.

Yoshikado H. 1992. Numerical Study of the Daytime Urban Effect and Its Interaction with the Sea Breeze. *Journal of Applied Meteorology*, 31(10): 1146–1164. https://doi.org/10.1175/1520-0450(1992)031<1146:NSOTDU>2.0.CO;2.

Yoshikado H. 1994. Interaction of the Sea Breeze with Urban Heat Islands of Different Sizes and Locations. *Journal of the Meteorological Society of Japan. Ser. II*, 72(1): 139–143. https://doi.org/10.2151/jmsj1965.72.1_139.

Yoshikado H, Kondo H. 1989. Inland penetration of the sea breeze over the suburban area of Tokyo. *Boundary-Layer Meteorology*, 48(4): 389–407. https://doi.org/10.1007/BF00123061.

Yulihastin E, Hadi TW, Abdillah MR, Fauziah IR, Ningsih NS. 2022. Propagation of Convective Systems Associated with Early Morning Precipitation and Different Northerly Background Winds over Western Java. *Journal of the Meteorological Society of Japan. Ser. II*, advpub. https://doi.org/10.2151/jmsj.2022-005.

Yulihastin E, Wahyu Hadi T, Sari Ningsih N, Ridho Syahputra M. 2020. Early morning peaks in the diurnal cycle of precipitation over the northern coast of West Java and possible influencing factors. *Annales Geophysicae*. Copernicus GmbH, 38(1): 231–242. https://doi.org/10.5194/angeo-38-231-2020.